

Modelling the Long-Term Fate and Transport Pathways of Pollutant in the Canadian Arctic

by

Ran Tao

A thesis submitted in partial fulfillment of the requirements for the degree of

Master of Science

Department of Earth and Atmospheric Sciences
University of Alberta

© Ran Tao, 2020

Abstract

Sea ice in the Arctic Ocean has been declining at an accelerated rate over the last few decades. From a shipping perspective, it results in larger open water for a longer period. Since 1990's, ship traffic in the Canadian Arctic has nearly tripled, and it will continue to increase in the future. However, the declining sea ice also resulted in more mobile multi-year ice in the complex waterways of the Canadian Arctic, which presents significant risk to maritime operations. Due to its remoteness, harsh environment, and insufficient supportive infrastructures, if an accidental spill occurred, the pollutant would not be recovered within the same operating season. Therefore, I am motivated to study the long-term fate and transport pathways of pollutant spilt along the two major shipping routes in the Canadian Arctic (Northwest Passages and Arctic Bridge). I used a high-resolution numerical model, NEMO (Nucleus for European Modelling of the Ocean) in the regional configuration, ANHA12 (Arctic and Northern Hemisphere Atlantic). The pollutants are represented by a Lagrangian particle tracking tool, ARIANE. The particles are released along the Northwest Passages and Arctic Bridge every 10 days during the operating season (1st June ~ 31st October) for 12 years (2004 ~ 2015). By analysing the circulation pathway of particles, the role of oceanic advection in the spread of pollutant is highlighted. More importantly, I computed the spreading area covered by particles, distances particles travelled, percentage of deep spread (depth exceeding 90 m), and the probability of particles, so that the 'worse-case' scenario can be illuminated. This study

provides an oceanographic overview to the commercially opening of the Canadian Arctic, especially in the role of oceanic advection in the spread of pollutant. By determining when and over which region the spill of pollutant could have the most severe consequence, this research can aid in the future development and regulation in the Canadian Arctic, and highlights the need for more detailed case studies.

Preface

Chapter 4 and Chapter 5 of this thesis are being prepared to become publications with authorships of Ran Tao and Paul G Myers. I am responsible for the data analysis and the writing of the manuscript and Paul G. Myers kindly provided advice and manuscript edits.

Acknowledgments

I would like to thank my supervisor, Prof. Dr. Paul G Myers, for giving me the opportunity to pursue this subject which has been the only thing that I want to do since adolescence. Only with his knowledge, guidance, and kindness, this is possible. I would also like thank my parents for their unconditional support through the years, without them I would not be here.

Thank you, Laura C Gillard, for helping me get started with my experiments. Thank you, my dearest friend, it has been a privilege. Thank you, Alex Turner, Conor McGregor, and Corey Taylor, for the inspiration and company till the end of the line, Charles and Jan, for chasing the rabbits with me; Jodie Heinrichs, without you I would not be who I am today.

Lastly, I wish to thank my committee member, Prof. Dr. Andrew B.G. Bush and Prof. Dr. Bruce Sutherland, it is a privilege to share the last steps with you.

Hold Fast.

Table of Contents

Chapter 1 Motivation	1
1.1. Interests in the Arctic Ocean	1
1.2. Shipping in the Canadian Arctic.....	2
1.3. Challenges in the Canadian Arctic	7
1.4. Oil Spills in the Arctic Ocean.....	8
1.5. Motivation	10
References	12
Chapter 2 Background.....	15
2.1. Introduction	15
2.2. The Arctic Ocean Circulation.....	15
2.3. The Canadian Arctic Circulation.....	17
2.3.1. The Canadian Beaufort Sea	17
2.3.2. The Canadian Arctic Archipelago.....	18
2.3.3. Baffin Bay and Labrador Sea.....	19
2.3.4. Hudson Bay Complex.....	20
2.4. Sea Ice Dynamics	22
References	23
Chapter 3 Methodology.....	27
3.1. NEMO (Nucleus for European Modelling of the Ocean) Frame Work	27
3.2. Arctic and Northern Hemisphere Atlantic (ANHA).....	33
3.3. Trajectory Calculation	35
3.4. Experiment Design and Analysis	36
References	43

Chapter 4 Modelling the Long-term Fate and Transport Pathways of Pollutant in the Hudson Bay Complex due to Oceanic Advection.....45

Abstract45

4.1. Introduction46

4.2. Methodology51

4.3. Circulation Pathways, Time Scales, and Accumulation Regions.....57

 4.3.1. Eastern Hudson Strait Releases60

 4.3.2. Western Hudson Strait Releases63

 4.3.3. Foxe Basin, Foxe Channel, and Hudson Bay Releases66

4.4. Discussion69

 4.4.1. Horizontal Spreading Area.....69

 4.4.2. Distances72

 4.4.3. Deep Spread76

 4.4.4. Variability and Sensitivity.....80

4.5. Conclusion.....85

Acknowledgement.....86

Bibliography87

Chapter 5 The Role of Oceanic Advection and Circulation Pathways in the Spread of Pollutant in the Canadian Northwest Passages92

Abstract92

5.1. Introduction93

5.2. Methodology100

5.3. Circulation Pathways and Long-term Fate of Particles.....103

 5.3.1. Canadian Beaufort Sea Releases.....107

 5.3.2. CAA Releases.....111

 5.3.2.1. Parry Channel Releases.....111

 5.3.2.2. Southern CAA Releases.....116

 5.3.2.3. Circulation Pathways of the CAA Releases.....121

 5.3.3. Baffin Bay Releases123

5.4. Discussion129

5.4.1. Horizontal Spreading Area.....	129
5.4.2. Distances.....	135
5.4.3. Deep Spreading.....	138
5.4.4. Sensitivity and Limitations.....	143
5.5. Conclusion.....	147
Bibliography.....	148
Chapter 6 Summary and Conclusion.....	154
References.....	157
Bibliography.....	158

List of Figures

Figure 1.1: Shipping routes in the Arctic Ocean.	5
Figure 1.2: The Northwest Passages and Arctic Bridge.	6
Figure 2.1: Geography of the Canadian Arctic.	21
Figure 3.1: Mesh grid of the Arakawa C-grid cell.	32
Figure 3.2: ANHA12 horizontal mesh grid.	34
Figure 3.3: Locations of release sites.	42
Figure 4.1-a: Geography and oceanic circulation of Hudson Bay Complex and its surrounding seas.	48
Figure 4.1-b: Arctic Bridge and the southern route of Northwest Passages.	49
Figure 4.2-a: Average June sea ice concentration integrated by ANHA12.	53
Figure 4.2-b: Average June sea ice concentration observed from passive microwave satellite observation.	54
Figure 4.3: Advective pathways of particles from each of the release sites in Hudson Bay Complex (released on June 1st, 2010).	59
Figure 4.4: Advective pathway of particles from Hudson Strait East (time elapsed: every 2 weeks).	62
Figure 4.5: Advective pathways of particles released from Hudson Strait Northwest.	65
Figure 4.6: Advective pathways of particles released from Foxe Basin.	68
Figure 4.7: Average horizontal spreading area, envelope area, variability and uncertainty of Hudson Bay Complex releases.	70
Figure 4.8: Average direct distance and full trajectory of Hudson Bay releases.	74
Figure 4.9: Strength of recirculation of Hudson Bay Complex releases.	75
Figure 4.10: Average percentage of particles with depth exceeding 90 m of Hudson Bay Complex release.	77
Figure 4.11: Particle depth at the end of two year simulation of Hudson Bay Complex Releases.	79

Figure 4.12: Inter-annual average horizontal spreading area of Hudson Bay Complex releases.....	82
Figure 4.13: Yearly averages of horizontal spreading area of Hudson Bay Complex releases.....	83
Figure 5.1-a: Geography and oceanic circulation of the Canadian Arctic. ...	95
Figure 5.1-b: The approximate location of the release sites in the Canadian Arctic.	96
Figure 5.2: Propagation of particles released on the 1st June, 2010 in the Canadian Arctic.	106
Figure 5.3: Circulation pathways of particles released in the Canadian Beaufort Sea.	108
Figure 5.4: Average probability of all simulations from the Canadian Beaufort Sea.	110
Figure 5.5: Circulation pathways of particles released in Parry Channel. ..	115
Figure 5.6: Circulation pathways of particles released in southern CAA. ...	120
Figure 5.7: Average probability of all CAA releass.	122
Figure 5.8: Circulation pathways of Baffin Bay releases.....	126
Figure 5.9: Average probability all Baffin Bay releases.....	128
Figure 5.10: Regional average horizontal spreading area of NWP releases.	132
Figure 5.11: Average spreading area of all releases from Parry Channel....	133
Figure 5.12: Average spreading area of all releases from southern CAA. ...	134
Figure 5.13: Regional average direct distance, full trajectory, and rate of recirculation for all releases from the Canadian Arctic.....	137
Figure 5.14: Regional average of deep spread of particles released from the Canadian Arctic.	139
Figure 5.15: Depth of particles released in the Canadian Arctic on June 1st 2010.	142
Figure 5.16: Sensitivity of the circulation pathways of particles to the initial seeded location.	146

List of Tables

Table 3.1: Simulation sites.	38
Table 4.1: The approximate location of release sites in the Hudson Bay Complex.	56
Table 5.1: The approximate location and their regional group of release sites in the Canadian Arctic.	102

Abbreviations and Acronyms

AG	Amundsen Gulf
ANHA	Arctic and Northern Hemisphere Atlantic
AO	Arctic Oscillation
BB	Baffin Bay
BBN	Northern Baffin Bay
BBS	Southern Baffin Bay
BFS	Beaufort Sea
BG	Beaufort Gyre
BI.	Bank Island
BRW	Barrow Strait
BS*	Ballantyne Strait
CAA	Canadian Arctic Archipelago
CBF	Canadian Beaufort Sea
CFI	Chesterfield Inlet
CG	Coronation Gulf
CGRF	Canadian Meteorological Centre's Global Deterministic Prediction System Reforecasts
CHL	Churchill
CI.	Coats Island
CMC	Canadian Meteorological Centre
CPC	Climate Prediction Centre
CS	Cumberland Sound
DS	Davis Strait
DSE	Eastern Davis Strait
DSW	Western Davis Strait

EHS	Eastern Hudson Strait
EI.	Ellesmere Island
EPC	Eastern Parry Channel
ESCAA	Southeastern CAA
FB	Foxe Basin
FC	Foxe Channel
FHS	Fury and Hecla Strait
FMC	Flemish Cap
FMP	Flemish Pass
FS	Frosbisher Sound
GB	Gulf of Boothia
GDPS	Global Deterministic Prediction System
GLORYS	Global Ocean ReanalYSIS
GrIS	Greenland Ice Sheet
GSL	Gulf of St Lawrence
HB.	Hamilton Bank
HBC	Hudson Bay Complex
HS	Hudson Strait
HSE	Hudson Strait East
HSNW	Hudson Strait Northwest
HSSW	Hudson Strait Southwest
JB	James Bay
JS	Jones Sound
LIM	Louvain la-neuve Ice Model
LS	Lancaster Sound
LSS	Larson Sound
LSE	Lancaster Sound East

LSW	Lancaster Sound West
MB.	Makkovik Bank
MCC	M’Clintock Channel
MCLE	Eastern M’Clure Strait
MCLW	Western M’Clure Strait
MCLS	M’Clure Strait
MCLS*	M’Clure Sound
MI.	Mansel Island
MVI.	Melville Island
MS	M’Clure Strait
MS*	M’Clure Sound
MYI	Multi-Year Ice
NAO	North Atlantic Oscillation
NCDC	National Climatic Data Center
NEMO	Nuclues for European Modelling of the Ocean
NEP	Northeast Passages
NS	Nares Strait
NWP	Northwest Passages
OPA	Ocean Parallelise
PG	Prince Gustav Adolf Strait
PS	Peel Sound
PW	Pacific Water
PWI	Prince of Wales Island
PWS	Prince of Wales Strait
QEI	Queen Elizabeth Islands
QMG	Queen Maud Gulf
RWS	Roes Welcome Sound

SBI	Strait of Belle Isle
SI.	Southampton Island
SRB	St Roch Basin
SS.	Scotian Shelf
TPD	Transpolar Drift
UB	Unvaga Bay
VI.	Victoria Island
VMS	Viscount Melville Sound
VMSE	Eastern Viscount Melville Sound
WHS	Western Hudson Strait
WPC	Western Parry Channel
WSCAA	Southwestern CAA

Chapter 1

Motivation

1.1. Interests in the Arctic Ocean

The Land of the Midnight Sun has been longed by mankind since the first explorer Pytheas of Massalia reached a frozen sea in the ancient Greek era. Since then, great explorers have attempted to conquer the rough ice-covered seas for colonisation and trade. As the Norsemen sailed as far as Ellesmere Island of the Canadian Arctic in the Middle Ages, Russian settlers and traders were exploring part of the Northeast Passages (NEP). Exploration to the High North continued in the Age of Discovery, driven by the rediscovery of Ptolemy's *Geographia* and other Classics, and the quest for commercial expansion. Following the discovery of the American continent, exploration continued around its northern edge for a promising route to the Orient. With little knowledge and preparation for the harsh conditions of the Arctic Ocean, many quests for the Northwest Passages (NWP) ended in darkness and terror. It was only in the beginning of the 20th century that the Norwegian explorer Roald Amundsen completed the first successful traverse of the NWP, heralding the beginning of the modern exploration era to the Arctic Ocean (Mills, 2003).

Attributed to the warming climate, Arctic sea ice exhibits an accelerated decline in its concentration, thickness, and strength (*e.g.* Cosmo, 2012; Kwok *et al.*, 2013; Stroeve *et al.*, 2007). The retreat of sea ice promotes trans-Arctic shipping, which provides considerable advantage in time and distance between the Pacific and Atlantic ports, as compared to using the

Suez and Panama Canals. This results in reduced fuel consumed, which is particularly important for general cargo vessels with large quantity of goods. Another participator in the NWP and NEP is cruise ships. There are three systems of trans-Arctic shipping routes: 1) the Northeast Passages along the coast of Russia and Norway; 2) the Northwest Passages along the coast of Canada and U.S. Alaska; and 3) the Transpolar Sea Route directly traversing the international waters of the Central Arctic (figure 1.1). In recent years, the NWP and NEP have been used with the assistance of icebreakers, and both are expected to have increasing demands in the coming decades (Østreng *et al.*, 2013).

The Arctic Ocean not only provides shorter transit options between several economic poles, but itself also contains great wealth of natural resources. The Arctic contains approximately 22% of the world's undiscovered hydrocarbon resources, and is among the last frontiers in terms of her mineral resources (Shasby *et al.*, 2015). Other natural resources in the Arctic Ocean and lands includes forests and fish. Forests in the Arctic consist of less than 10% of the forests in the world's total amount, and the production of woods in the Arctic is mostly prohibited. The seas of the High North are irreplaceable for the global fishery markets, and the Arctic Ocean contains great ecological resources. However, the commercial exploitation of the fishery in the High Arctic is prohibited among the international community for ecological conservation against the warming climate (Østreng *et al.*, 2013).

1.2. Shipping in the Canadian Arctic

Canada has the longest coastline of all countries, stretching more than 200,000 km and connecting three major oceans: the Pacific, Arctic, and Atlantic Oceans. Domestically, the Canadian Arctic is dependent on maritime transport as the complexity and remoteness of her chain of islands is thus only accessible by sea or air (Brigham *et al.*, 2009). For the international market, making use of the trans-Arctic shipping route can significantly reduce the distance that vessels travel between ports in the Pacific and Atlantic Oceans. For instance, the distance between London and Yokohama via the NWP is around 15,700 km, which is significantly shorter

than the distance if taking the Suez Canal (21,200 km) or the Panama Canal (23,300 km) (Østreng *et al.*, 2013). Furthermore, the deep Arctic straits and channels allow vessels to carry more cargo than that via the shallower routes of the Panama or Suez Canals, where freighters must sail higher. The resultant reduced fuel consumption, time and salaries, appear as major interests for participators in bulk shipping (McGarrity and Gloystein, 2013; Stueck, 2013).

Therefore, thanks to the retreat of sea ice, increasing investments in ice-strengthening vessels, expanding exploration to Arctic resources, population growth and more demands in the Arctic communities, the shipping traffic in the Canadian Arctic has been increasing remarkably, especially at the beginning of this century. The total distance that vessels travelled in the Canadian Arctic had almost tripled in the past 25 years, and significant increase is found after 2010 (Dawson *et al.*, 2017).

Since 1990, general cargo vessels and government icebreakers have been consistently the largest contributor to the distance travelled in the Canadian Arctic. A significant increase for general cargo activity is found beginning in 2007, which is a year of record low sea ice. By 2010, the distance travelled by cargo vessels has increased by over 150% compared the 1990's (Dawson *et al.*, 2017). Another turning point for commercial shipping in the NWP was the successful transit of *MS Nordic Orion* in 2013. She was the first sea freighter, carrying 15,000 metric tons of coal and travelling with a Canadian Coast Guard icebreaker, *Louis S. St-Laurent*. *MS Nordic Orion*'s route allowed her to load 25% more cargo and shorten four days of travel, saving approximately USD \$80,000 worth of fuel (McGarrity and Gloystein, 2013). The successive traverse of *MS Nordic Orion* opens a new era for commercial shipping in the NWP and the Canadian Arctic. The distance travelled in 2014 reached to a record high (Dawson *et al.*, 2018).

The Canadian Arctic consist of two systems of shipping routes (figure 1.2). The NWP provides a trans-Arctic shipping route connecting the Atlantic and Pacific Oceans Baffin Bay in the Eastern Arctic and the Beaufort Sea in the Western Arctic through the straits and sounds of the Canadian Arctic Archipelago (CAA). The Arctic Bridge connects Europe and Eurasia to the Port of Churchill, Manitoba, through Hudson Strait and into Hudson Bay (Østreng *et al.*, 2013).

The NWP consists of seven different routes via the waterways of the CAA. Beside one that takes the direct Parry Cannel, the other six start in the western part of Parry Channel, and then turn southward at various points. The routes are used with respect to the best sea ice conditions at any one time and place, as the CAA provides an area of the most complex geography and harsh climate. Sea ice conditions within the CAA varies dramatically both annually and seasonally, providing unpredictability to any surface operation (Østreng *et al.*, 2013).

The Arctic Bridge is a sub-Arctic waterway connecting Churchill in Hudson Bay to the Russian port of Murmansk via the Hudson Strait (Østreng *et al.*, 2013). Although strong tidal currents present navigational challenges in Fury and Hecla Strait, the reduced sea ice in Foxe Basin and Hudson Bay promotes the use of the Arctic Bridge. The longer operating season and promotion by the government will encourage shipping via the Port of Churchill through Hudson Bay (Prowse *et al.*, 2009).

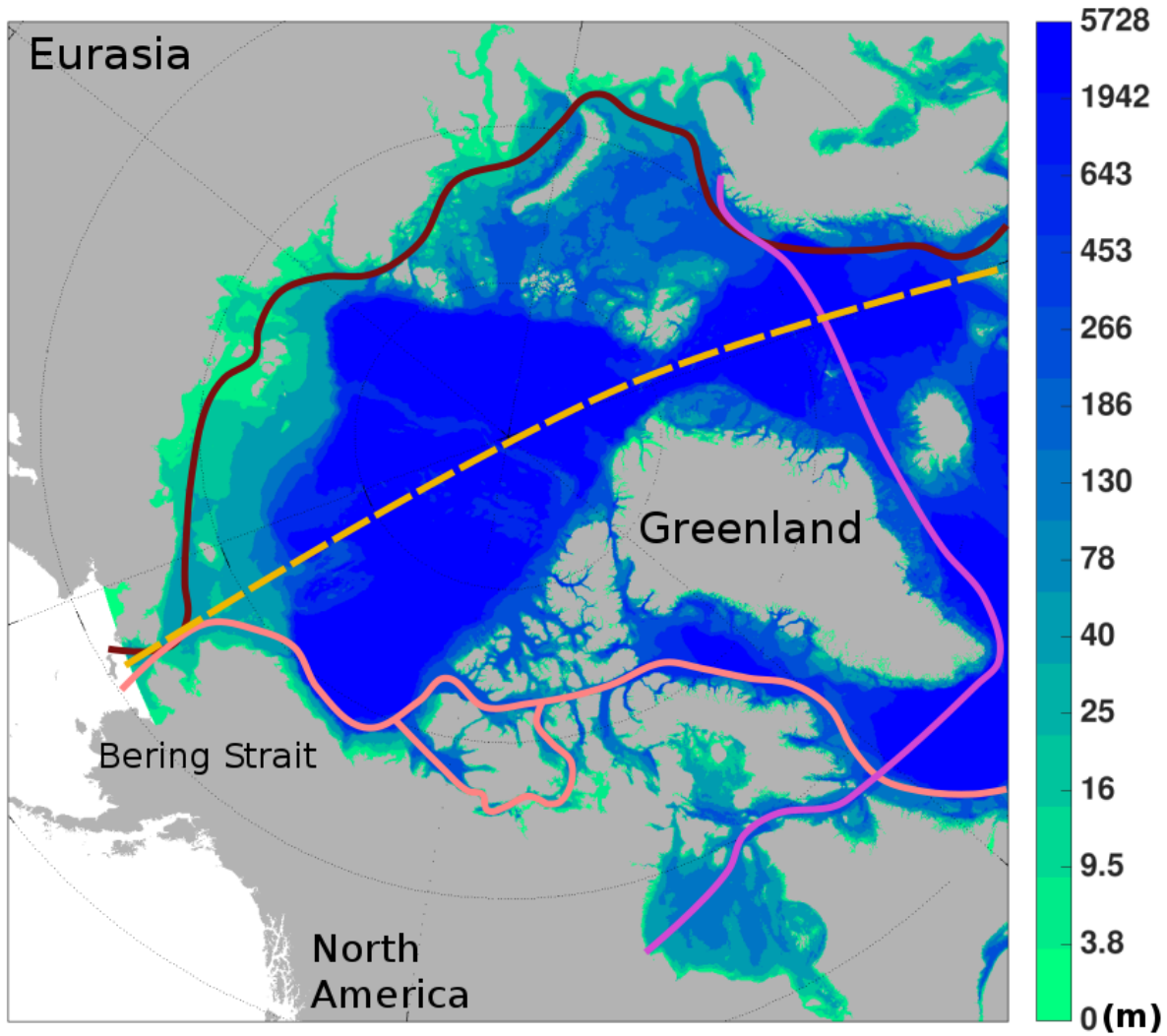


Figure 1.1: Shipping routes in the Arctic Ocean (Northeast Passages in dark red, Transpolar Sea Route in yellow, and the Northwest Passages in coral) and the Arctic Bridge in purple. Note that they are illustrated as the approximate routes, as in practice, vessels do not follow one defined route but take precautions due the ice conditions. Colour bar indicates bathymetry in metres.

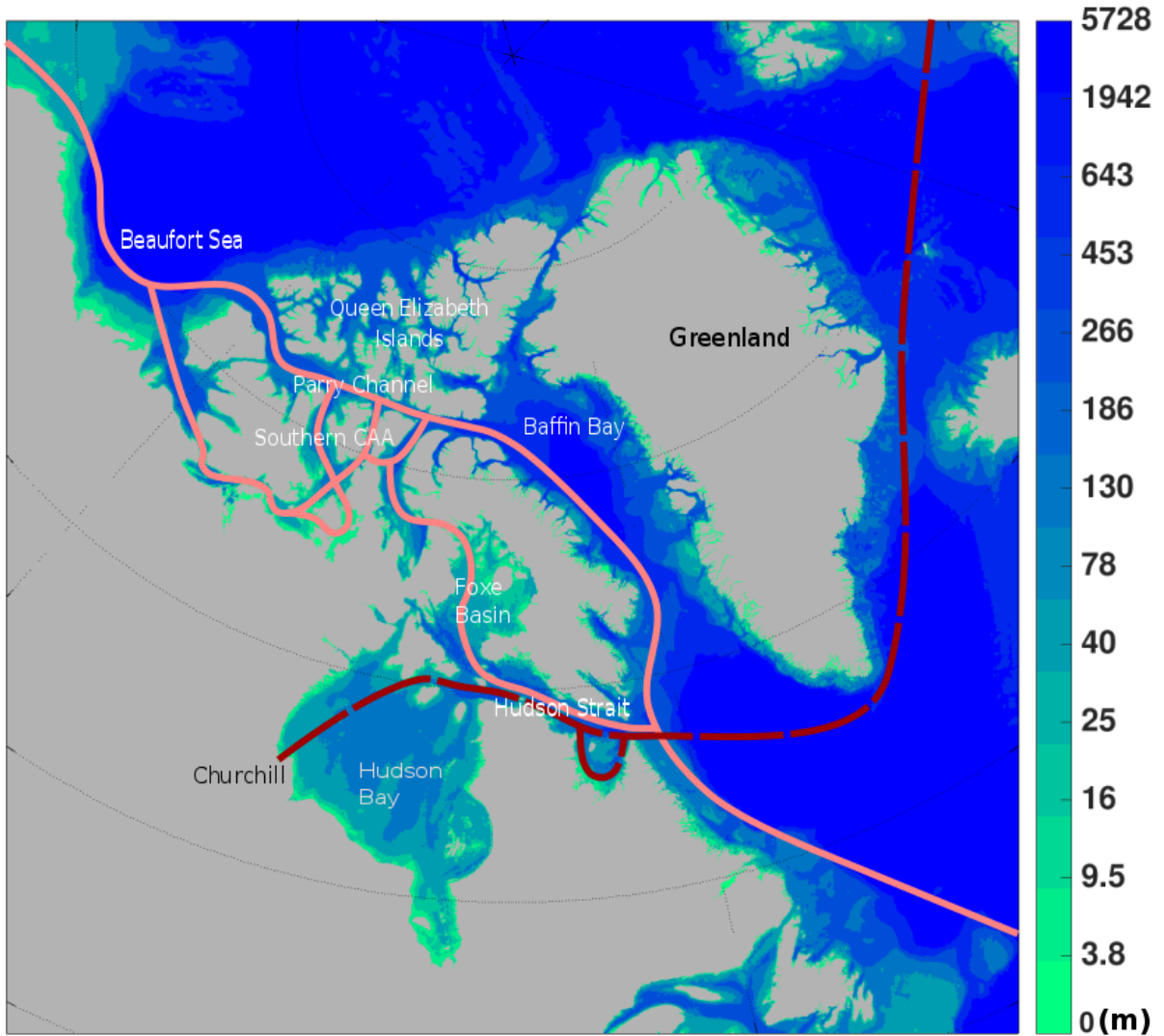


Figure 1.2: the shipping routes of the NWP (in coral) and Arctic Bridge (dashed maroon). Note that only the main geographic features are indicated here; the detailed geography of the Canadian Arctic is introduced in Chapter 2.

1.3. Challenges in the Canadian Arctic

The retreat of sea ice has been a clear trend for the Arctic Ocean, and it is significantly and positively correlated with shipping activities in the Canadian Arctic, especially those areas that are dominated by multiyear ice that survived the summer (Pizzolato *et al.*, 2016). However, transiting or operating in the Canadian Arctic is still both difficult and dangerous for its natural challenges and lack of supportive facilities. The Canadian Arctic faces particularly harsh environment due to the atmospheric forcing and complex geography (Lackenbauer and Lajeunesse, 2014). From a mariner's standpoint, the Canadian Arctic does not provide sufficient support to safely operate in its challenging waters, in terms of its lack of icebreaking support services, search-and-rescue capability, marine-traffic surveillance, control, and enforcement, coastal facilities for fuelling and loading cargo, and deepwater ports (Østreng *et al.*, 2013; Prowse *et al.*, 2009).

The warming temperature in the Arctic Ocean is changing the characteristics and distribution of sea ice. As more open water is present and the strength of sea ice decreases, the thick multiyear ice (MYI) is shifted by the atmospheric forcing. The drifting ice movement exhibits significant annual and inter-annual variability, which is extremely hard to predict (Guy and Lasserre, 2016). In addition to its high variability, the predicted longer operating season does not imply consecutive weeks of open water (Lackenbauer and Lajeunesse, 2014).

The invasion of MYI into the CAA creates major pitfall for navigation, known as 'chokepoints', clogging the narrow straits (Guy and Lasserre, 2016). From the Canadian Basin, Queen Elisabeth Islands (QEI), and the Greenland Ice Sheet, the small growlers (icebergs) are barely detectable, and presents serious hazards for shipping: in November 2007, the cruise ship *MS Explorer* sank in Antarctica after hitting a growler, although it had an ice-strengthened hull (Stewart *et al.*, 2009).

As for the fully operational mines that engage in year-round shipping in the Canadian Arctic, unsurprisingly, the harsher winter months (January, February, and March) exhibit the highest percentage of shipping accidents, due to the presence of consolidated ice. It is one of the

most hazardous navigational challenges as it is difficult to detect until a ship is in contact. Being beset in the ice can result in significant loss in revenue and operational expenses (Mussells *et al.*, 2017). The Canadian Arctic only has five weather stations at Eureka, Resolute Bay, Isachsen, Mould Bay, and Alert. The shortage of meteorological stations in the Canadian North is problematic as they cannot confidently predict the increasing dynamic and unpredictable nature of Arctic weather.

The inadequate charting of the Canadian Arctic presents another challenge to operators. Only 12% of the Canadian Arctic has been charted to the modern international standards. This is a deficiency that was dramatically demonstrated by the grounding of two vessels in the southern NWP (Lackenbauer and Lajeunesse, 2014). Another example is when *CCGS Amundsen* transited Bellot Strait in 2006. Marine tables stated she would have the tide against her; in fact, the reverse proved to be the case (Guy and Lasserre, 2016).

The increasing ship tracks and higher risk of accidents highlight the demand for icebreaking support, coastal facilities, and search-and-rescue capabilities in the Canadian Arctic (Prowse *et al.*, 2009). For most of the NWP, there are limited navigation aid and in-time rescue operations that are not intended for trans-Arctic shippings but for local communities. There are no deepwater ports located in the Canadian Arctic, besides the Port of Churchill in Hudson Bay. Along the NWP, there are very few ports adequate for international shipping standards (Østreng *et al.*, 2013). The lack of major infrastructure in the Canadian Arctic will further increase the risks of accidents and any resultant spill of pollutant.

1.4. Oil Spills in the Arctic Ocean

For this study, we consider the source of pollutant to be fuel spilt by shipping accidents. Once spilt into the ocean, oil is transported by advection, spreading, sedimentation, dispersion, and encapsulation with the presence of sea ice. Its weathering processes include evaporation, emulsification, photooxidation, biodegradation and dissolution. The rate of these processes reflects the complex dynamics between the environmental parameters and the physical and

chemical characteristics of the pollutant (Afenyo *et al.*, 2016). Its physical properties, such as volatility, insolubility, spreadability, and the tendency, are of most importance when considering its emulsion dynamics (rate and behaviour when mixing with seawater). For instance, the presence of natural surfactants in the right proportions creates the condition for emulsion formation (Buist *et al.*, 2009; Reed *et al.*, 1999).

Furthermore, the presence of sea ice in the Arctic Ocean creates another layer of complexity. Various types of ice would interact with oil differently: the encapsulation of oil within ice becomes an additional process (Sørstrøm *et al.*, 2010; Drozdowski *et al.*, 2011). The role of sea ice in the fate and transport of oil is determined by the nature of sea ice, such as its type, concentration, structural anomalies, roughness *etc.* (DeCola *et al.*, 2006).

For response to oil spills in the Arctic Ocean, containment and recovery methods consists of in-situ burning and dispersant. In-situ burning can remove large fractions of an oil slick on water or ice, provided the water content in the oil is less than $\square 25\%$ and the slick is at least 1-2mm thick. Slick thickness is increased in cold temperatures and aided by herding between ice floes, however booms may be required to obtain necessary slick thicknesses in areas of low ice coverage. Burning does not remove all of the oil and adverse environmental impacts are to be expected from the residue, as well as the smoke emitted from the burn (Transport Canada and Canadian Coast Guard, 2010).

Dispersant application has been shown to work reasonably well for breaking up oil slicks in ice-covered waters, provided adequate mixing energy is available. This may present an issue in dense ice conditions, since the ice damps wave action which has traditionally provided this mixing energy. Additional energy may need to be added, for example using ship props (Sørstrøm *et al.*, 2010). However dispersant application results in large volumes of oil drifting at depth (Drozdowski *et al.*, 2011). Natural degradation processes are slowed in the cold Arctic environment and this oil at depth may resurface.

1.5. Motivation

Due to the remoteness of and insufficient facilities in the Canadian Arctic, it is likely that the pollutant cannot be recovered within the operating season of its spill, before the formation of sea ice makes it inaccessible during the following winter. Therefore, we are motivated to examine the transport and fate of pollutant if spilt into the Canadian Arctic along the Northwest Passages and the Arctic Bridge, in order to provide comprehensive data and scientific guidance for future regulations and development.

From this research, I will be able to answer the following research questions:

- 1) Over which site and when would the spill of pollutant have the most severe outcome?
- 2) Over which area would the pollutant mostly accumulate?
- 3) How does the pollutant propagate over a long-term period?

In order to answer these questions, I will use the state-of-art ocean/sea-ice numerical framework to simulate the spread of pollutant with oceanic advection. Passive particles representing pollutant will be released at various locations along the shipping routes within the Canadian Arctic during the projected extended operating season from June to November. I will analyse the location and trajectory of the pollutant at four crucial cutoffs: at the beginning and end of the following operating season, and after one and two years after the release. The first research question will be answered by analysing the area particles occupied and distances they travelled over one and two years. The second question will highlight the practicality of this research, illustrate the most probable location for recovery operations. In order to answer the third research question, I will analysis the spatial distribution and spreading area one and two years after the release, thus to determine the propagation of pollutant over a two year period.

As the focus of this study is to determine the role of advection in the spread of pollutant over various sites during a long experiment period, therefore, the pollutant is represented by passive particles. This presents a major limitation. Although most of the weathering reactions occur within the first weeks after the release, there are processes (*e.g.* sedimentation and

emulsification) can take place months after the spill (Afenyo *et al.*, 2016). Another limitation of this work is the lack of encapsulation, *i.e.* oil trapped with sea ice. Under encapsulation, oil would travel with sea ice drifts and be released where sea ice melt. Whether oil drifts with oceanic advection or sea ice movement depends on the sea ice concentration: if sea ice concentration is in excess of 60%, the transport pathways of oil would travel with the drift of sea ice instead of oceanic advection (Venkatesh *et al.*, 1990).

This thesis is split into three sections, beginning with a literature review. In Chapter 2, I will review the characteristic of ocean, and atmosphere, and sea ice of the Arctic Ocean and the dynamics in channels and straits of the Canadian Arctic. Chapter 3 provides the modelling background for my experiments and details of experiment design. Chapter 4 and 5 are independently written to answer the research question in focusing on the NWP and Arctic Bridge, respectively. Both are prepared to become publications Chapter 6 provides a summary to this research, and its significance both scientifically and for future development of the Canadian Arctic.

References

- Afenyo, M., Veitch, B., & Khan, F. (2016). A State-of-the-Art Review of Fate and Transport of Oil Spills in Open and Ice-Covered Water. *Ocean Engineering*, *119*, 233-248. Doi:10.1016/J.Oceaneng.2015.10.014
- Brigham, L. W., Ellis, B., Arctic Council, & Arctic Council Protection of the Arctic Marine Environment Working Group. (2009). *Arctic Marine Shipping Assessment 2009 Report*. Akureyri, Iceland: Arctic Council, PAME, Protection of the Arctic Marine Environment.
- Buist, I., Belore, R., Dickins, D., Hackenberg, D., Guarino, A., & Wang, Z. (2009). Empirical Weathering Properties of Oil in Ice and Snow. Paper Presented at the *Proceedings Arctic and Marine Oilspill Program Technical Seminar*, , 32 67-107.
- Comiso, J. C. (2012). Large Decadal Decline of the Arctic Multiyear Ice Cover. *Journal of Climate*, *25*(4), 1176-1193. doi:10.1175/JCLI-D-11-00113.1
- Dawson, J., Pizzolato, L., Howell, S. E. L., Copland, L., & Johnston, M. E. (2018). Temporal and Spatial Patterns of Ship Traffic in the Canadian Arctic From 1990 to 2015. *Arctic: Journal of the Arctic Institute of North America*, *71*, 15-26. <https://doi.org/10.14430/arctic4698>
- DeCola, Robertson, Fletcher, Susan Harvey, 2006. Offshore Oil Spill Response in Dynamic Ice Conditions: A Report to WWF on Considerations for the Sakhalin II Project. *Nuka Research and Planning Group*.
- Drozdowski, A., Nudds, S., Hannah, C. G., Niu, H., Peterson, I., & Perrie, W. (2011). *Review of Oil Spill Trajectory Modelling in the Presence of Ice*. Canada
- Guy, E., & Lasserre, F. (2016). Commercial Shipping in the Arctic: New Perspectives, Challenges and Regulations. *Polar Record*, *52*(3), 294-304. Doi:10.1017/S0032247415001011

- Kwok, R., Spreen, G., & Pang, S. (2013). Arctic Sea Ice Circulation and Drift Speed: Decadal Trends and Ocean Currents. *Journal of Geophysical Research: Oceans*, 118(5), 2408-2425. Doi:10.1002/Jgrc.20191
- Lackenbauer, W., Lajeunesse, A., Canadian Defence and Foreign Affairs Institute, & University of Calgary School of Public Policy. (2014). On Uncertain Ice: the Future of Arctic Shipping and the Northwest Passage.
- McGarrity, J., & Gloystein, H. (2013, September 27). Big Freighter Traverses Northwest Passage for 1st Time. *Reuters Environment*
- Mills, W. J. (2003). *Exploring Polar Frontiers: a Historical Encyclopedia*. Santa Barbara, Calif.: Abc-Clio.
- Mussells, O., Dawson, J., & Howell, S. (2017). Navigating Pressured Ice: Risks and Hazards for Winter Resource-Based Shipping in the Canadian Arctic. *Ocean and Coastal Management*, 137, 57-67. Doi:10.1016/J.Ocecoaman.2016.12.010
- Offshore Oil Spill Response, & in Dynamic Ice Conditions. *Offshore Oil Spill Response in Dynamic Ice Conditions*
- Østreng, W., Eger, K. M., Fløistad, B., Jørgensen-Dahl, A., Lothe, L., Mejlænder-Larsen, M., . . . Wergeland, T. (2013). *Shipping In Arctic Waters: A Comparison Of The Northeast, Northwest And Trans Polar Passages*. Dordrecht ; New York: Springer.
- Pizzolato, L., Howell, S. E. L., Dawson, J., Laliberté, F., & Copland, L. (2016). The Influence of Declining Sea Ice on Shipping Activity in the Canadian Arctic. *Geophysical Research Letters*, 43(23), 12-12,154
- Prowse, T. D., Furgal, C., Chouinard, R., Melling, H., Milburn, D., & Smith, S. L. (2009). Implications of Climate Change for Economic Development in Northern Canada: Energy, Resource, and Transportation Sectors. *Royal Swedish Academy of Sciences*, 38(Ambio: Climate Impacts on Northern Canada), 272-281.

- Reed, M., Johansen, Ø, Brandvik, P. J., Daling, P., Lewis, A., Fiocco, R., . . . Prentki, R. (1999). *Oil Spill Modeling Towards the Close of the 20th Century: Overview of the State of the Art*
- Shasby, Mark, and Smith, Durelle, 2015, USGS Arctic science strategy, 2015–2020: U.S. Geological Survey Fact Sheet 2015-3049, 2 p., <https://dx.doi.org/10.3133/fs20153049>.
- Sørstrøm, S. E., Brandvik, P. J., Buist, I., Daling, P., Dickins, D., Faksness, L., . . . Singaas, I. (2010). *Joint Industry Program On Oil Spill Contingency For Arctic And Ice-Covered Waters : Summary Report*. (). Trondheim
- Stewart, E. J., Howell, S. E. L., Draper, D., Yackel, J., & Tivy, A. (2009). Sea Ice in Canada's Arctic: Implications for Cruise Tourism. *Arctic*, 60(4) Doi:10.14430/Arctic194
- Stroeve, J., Holland, M. M., Meier, W., Scambos, T., & Serreze, M. (2007). Arctic Sea Ice Decline: Faster Than Forecast. *Geophysical Research Letters*, 34(9)
- Stueck, W. (2013, September 19). Danish Firm Seeks To Be First To Bring Bulk Carrier Through Northwest Passage. *The Globe and Mail*
- Transport Canada and Canadian Coast Guard. Assessment of Proposals Related to Oil Spill Risk for the South Coast of Newfoundland
- Venkatesh, S., El-Tahan, H., Comfort, G., & Abdelnour, R. (1990). Modelling the Behaviour of Oil Spills in Ice-Infested Waters. *Atmosphere-Ocean*, 28(3), 303-329. Doi:10.1080/07055900.1990.9649380

Chapter 2

Background

2.1. Introduction

The Arctic Ocean receives relatively cold and fresh water from the Pacific Ocean via the Bering Strait. The Pacific Water propagates with the Transpolar Drift, mixes with the cold and fresh Arctic Water, then exits the Arctic Ocean via the Fram Strait, Nares Strait, or waterways of the Canadian Arctic Archipelago, eventually entering the North Atlantic Ocean via the Labrador Sea. This chapter will firstly review the large scale processes in the Arctic Ocean, and then focus on the regional dynamics in the Canadian Arctic (figure 2.1).

Furthermore, considering the pan-Arctic trend in the retreat of sea ice and the narrow straits of the CAA, there are many ice chokepoints along the NWP. In the last section of this chapter, I will review the dynamics of sea ice and the projected future of the accessibility of the NWP.

2.2. The Arctic Ocean Circulation

The synoptic circulation in the Arctic Ocean is driven by the difference in sea-level gradient and atmospheric features. In the Arctic Ocean, the different sea-level gradient is mainly attributed to the spatial variability in salinity, correlated to the proximity of freshwater input and

associated reservoirs (Aagaard and Carmack, 1989). The sea surface pressure is driven by the four pressure centres: the Icelandic Low in the southern Nordic Seas, the Aleutian Low of the Bering Sea, the Siberian High in central Eurasia, and the North Atlantic High; all exhibit significant seasonal, annual, and decadal variations (Serreze and Barry, 2014).

The Arctic Ocean has three main freshwater sources: river runoff, Pacific inflow via Bering Strait, and excessive precipitation over evaporation. River runoff is the largest freshwater source of the Arctic Ocean. There are significant annual and inter-annual variations in these flows with the maximum in the melting season (Aagaard and Carmack, 1989). The Pacific Water inflows into the Arctic Ocean via Bering Strait, propagates into the Chukchi Shelf. The Pacific Water turns east along the Alaskan coast or the Chukchi Sea shelf. Whilst some joins the anti-cyclonic circulation, the majority enters the Arctic Ocean following the Transpolar Drift (Hu *et al.*, 2019). The outflow of Arctic water follows two pathways: the eastern route via Fram Strait or western route via the Davis Strait. The majority of the polar export with the Transpolar Drift propagates through Fram Strait into the Nordic Seas, circumnavigates Greenland, and reaches the Labrador Sea (Yang *et al.*, 2016). However, a branch of the TPD recirculates eastward along the northern coast of Greenland before passing Fram Strait, then enters Nares Strait or propagates further south and turns east at the gates of the northern CAA (at the Queen Elisabeth Islands) (Hu *et al.*, 2019). Compared to the shallow and complex CAA of the western route, the eastern route allows more export of sea ice and intermediate water (Aksenov *et al.*, 2010).

The fluctuation between the atmospheric pressure centres over the Arctic Ocean is described by the Arctic Oscillation (AO). A band of upper-level winds circulates around the Arctic basin, forming the polar vortex. Its strength and shift are described by the AO index. From which, a positive AO implies a lower pressure over the Arctic resulting in cyclonic winds, whereas negative and neutral values correspond to high pressure, resulting in anticyclonic winds. When the AO index shifts to the negative value, the most visible results are the pathways of Atlantic and Pacific originated water and the strength and freshwater content of the Beaufort Gyre (Karcher *et al.*, 2012) . The continuous yet shifting sea-level pressure induces Ekman transport, which is one of the most important processes for examining the velocity of ocean surface waters and ice. Its convergence or divergence can induce upwelling, linking subsurface

oceanic processes with the surface mixed layer. When considering the effects of its variability, strong seasonality should be considered in terms of the existence of ice. In the ice-covered Arctic Ocean, the surface momentum flux comes from both air–water and ice–water stresses (Yang, 2009).

2.3. The Canadian Arctic Circulation

2.3.1. The Canadian Beaufort Sea

The Canadian Beaufort Sea is the open water in the southeast of the Arctic Ocean, consisting of the eastern portion of the Beaufort Sea. The oceanographic circulation is dominated by the Pacific inflow and Mackenzie River runoff along the coast, propagating eastward into the CAA, and the anti-cyclonic Beaufort Gyre offshore, which dominates the large-scale circulation of sea ice and surface water. During summer months, the Mackenzie River runoff dominates the surface property distribution. The freshwater from river runoff and ice melt are mixed into the top 10~20 metres of the water column due to frequent storms throughout summer and early autumn. During winter with the formation of sea ice, density-driven flows dominate due to brine rejection (Carmack and MacDonald, 2002). The Beaufort Gyre drives the circulation of sea ice and ocean anti-cyclonically offshore, attributed to the Beaufort High, whose strength exhibits a clear seasonality: the sea level pressure is high from spring to autumn and weak during winter months (Yang, 2009). The long-term variability of the Beaufort Gyre is characterised by the AO index: the negative phase of AO results strong persistent Beaufort High, promotes the recirculation in the Arctic whilst the positive AO index reduces its strength and size (Serreze and Barry, 2014).

2.3.2. The Canadian Arctic Archipelago

The CAA is a triangle of shallow basins and narrow straits that connects the Arctic Ocean to Baffin Bay and North Atlantic. It consists of two regions: the Queen Elizabeth Islands (QEI) in the north, which is an area with relatively small islands surrounded by the larger Ellesmere, Devon, Cornwallis, Bathurst, Melville, and Prince Patrick Islands; and the southern CAA with larger islands (Bank, Victoria, and Prince of Wales Islands). Between the two regions, Parry Channel directly connects the Beaufort Sea to Baffin Bay via the M'Clure Strait, Melville Sound, Barrow Strait, and Lancaster Sound. Among the QEI, Nares Strait and Jones Sound are the other two exits .

The general oceanic circulation is an eastward polar outflow, whose volume and strength is subjected to its upstream source, the Beaufort Sea, during summer and autumn. During winter and spring months, the volume transport is controlled by the evolution of Baffin Bay and the Labrador Sea, as the ice friction increases in the Beaufort Sea (Lu *et al.*, 2014).

However, the polar outflow via the CAA does not follow a direct path via the Parry Channel. Smaller scale drifts are mostly induced by the local bathymetric features. In Melville Sound, a significant portion flows southward into the M'Clintock Channel, travelling northward via the Peel Sound and returns to the Barrow Strait. This is caused by the enhancement of ageostrophic acceleration due to the change of coastline and a sharp decrease in the bathymetry (Wang *et al.*, 2012). Barrow Strait is a key region of water modification due to its shallow bathymetry and location which hosts various water masses, such as those from the southern Beaufort Sea, northeastern Canadian Basin, and Baffin Bay (Wang *et al.*, 2012). At the eastern end of the Parry Channel, Lancaster Sound is the gateway entering Baffin Bay. Lancaster Sound exhibits strong easterly flux towards the Baffin Bay from the Arctic Ocean due to the difference in sea-level difference (Hughes *et al.*, 2017). However, at the mouth of the Lancaster Sound, a westerly recirculation is present due to the strong coastal current from Baffin Bay, which is induced by the increased glacier runoff. The westward flux only circulates in the mouth of the

Sound rather than penetrating further into the Barrow Strait due to its strong stratification and bathymetry (Hughes *et al.*, 2017).

2.3.3. Baffin Bay and Labrador Sea

Baffin Bay receives freshwater from the Arctic Ocean via the CAA and Nares Strait, Greenland Ice Sheet runoff via various pathways, and polar outflow from the Nordic Seas (Gillard *et al.*, 2016). The accelerated melting, especially from the northwestern coast of the Greenland Ice Sheet (GrIS), results in a decrease in surface salinity, thus an increase in its steric height, which is more prominent along the boundary currents, within the channels of the CAA, and along the Greenland Shelf. As the gradient between the coast and interior steepens, the eastern branch of the cyclonic gyre in Baffin Bay strengthens, leading to more freshwater import via the Davis Strait, ultimately leading to an even larger steric height. As the downstream source of the Arctic outflow via the CAA, the increase in Baffin Bay's steric height would suppress its export volume, which is balanced by the increase in the outflow via the Fram Strait (Dukhovskoy *et al.*, 2016).

The Arctic water exits the Canadian Arctic via Nares Strait, the waterways of the CAA and HBC, then enters the Labrador Sea (Dukhovskoy *et al.*, 2016). The Arctic water forms the Baffin Island Current (Münchow *et al.*, 2015) and the Labrador Current above the East Canadian Shelf (Lazier and Wright, 1993). The Labrador Sea also receives polar water exiting Fram Strait, which circumnavigates Greenland and mixes with the glacial runoff from the GrIS (Yang *et al.*, 2016). Exiting Fram Strait, the Arctic water is mixed with the extension of the North Atlantic Current in the Nordic Seas. It circumnavigates the coast of Greenland, and then forms the West Greenland Current, flowing into the Labrador Sea (Münchow *et al.*, 2015).

One of the consequences of the decreasing Arctic outflow via the CAA is the decreasing heat exchange due to stronger density stratification and increasing energy content in the Baffin Bay. The energy content is enhanced by the further penetration of the West Greenland Irminger Water, caused by the stronger Ekman pumping due to strengthened cyclonic gyre. Such surplus

of energy could accelerate the melting of GrIS (Castro de la Guardia *et al.*, 2015). From the surface layer, Greenland Ice Sheet runoff spreads to the lower latitudes and is mixed downwards by convection, then laterally advected to distant basins, eventually penetrating into the deep layers in the convective areas (Dukhovskoy *et al.*, 2016).

2.3.4. Hudson Bay Complex

The Hudson Bay Complex (HBC) connects the Canadian Arctic Archipelago via the Fury and Hecla Strait and the Labrador Sea of the North Atlantic Ocean via the Hudson Strait. The HBC is a large system of isolated sea that consists of the Foxe Basin, Hudson Bay, James Bay, and Ungava Bay.

The Arctic Water enters the HBC via the Fury and Hecla Strait, propagates southward along the western coast of Foxe Basin (Straneo and Saucier, 2008). The surface circulation in Foxe Basin is mainly cyclonic and stronger on the western side. Upon reaching the northern coast of Southampton Island, the water forms two branches: whilst some continues into Hudson Bay through Roes Welcome Sound, the other branch propagates eastward into Hudson Strait (Saucier *et al.*, 2004). The circulation in Foxe Basin exhibits a strong inter-annual variability, with summer months surface velocity larger than that of the winter. The seasonal variability is caused by the formation of sea ice, as the circulation of the surface water is affected by the friction and shielding of the sea ice cover (Defossez *et al.*, 2012).

The overall circulation in Hudson Bay is cyclonic with a strong coastal current. There is a strong seasonal variability due to the large river runoff in its southwestern coast, as during spring and summer months, a weak anti-cyclonic flow exists on the eastern side (Ridenour *et al.*, 2019). Water from Hudson Bay and Foxe Basin travels along the southern coast of Hudson Strait. Some mixes with the coastal current from Baffin Bay and recirculates at the mouth of Hudson Strait and Ungava Bay. Along the northern side of Hudson Strait, the Baffin Inland Current enters Hudson Strait from the Labrador Sea and propagates into Foxe Basin (Straneo and Saucier, 2008).

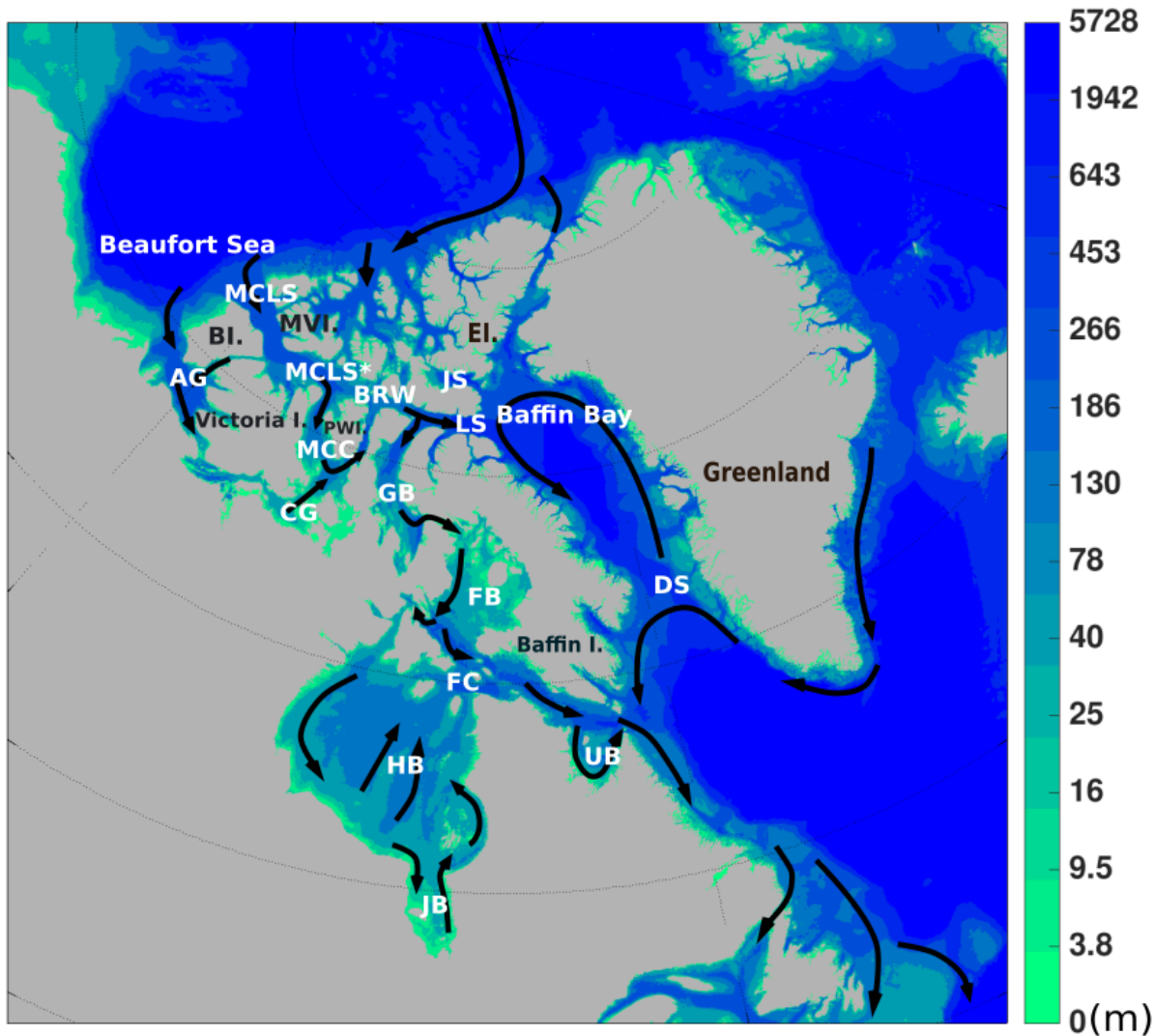


Figure 2.1: geography of the Canadian Arctic. The general circulation schematics are illustrated by black arrows. MCLS: M'Clure Strait, MCLS*: M'Clure Sound, BRW: Barrow Strait, LS: Lancaster Sound, DS: Davis Strait; AG: Amundsen Gulf, CG: Coronation Gulf; MCC: M'Clintock Channel, GB: Gulf of Boothia, FB: Foxe Basin, FC: Foxe Channel, HS: Hudson Strait, UB: Ungava Strait; HB: Hudson Bay, JB: James Bay

2.4. Sea Ice Dynamics

Over the past decades, the Arctic sea ice has experienced an accelerated decline with an increasing rate (Stroeve *et al.*, 2007). The most significant decline is found within the month with minimum sea ice concentration, September, in the CAA and the HBC (Tivy *et al.*, 2011). The accumulation of more energy over the summer prohibits the formation of first-year ice, thus creating more open water for the drift of multi-year ice (Kwok *et al.*, 2013).

With the thinner and weaker seasonal ice cover, the sea ice is more responsive to oceanic currents and geostrophic wind. In the Arctic Ocean, the mean annual drift of ice consists of two primary features: the anticyclonic motion with the Beaufort Gyre and the Transpolar Drift (TPD) characterising the motion of ice away from Siberian coast and export via Fram Strait. During winter, sea ice motion follows the strong Beaufort Gyre and the TPD. Whilst in summer, sea ice retreats with the Beaufort Gyre south into the Beaufort Sea, and is then transported into the CAA via M'Clure Strait and the QEI (Howell *et al.*, 2013; Serreze and Barry, 2014).

In the CAA, sea ice is a mix of first year ice and multiyear ice (MYI). MYI can make up more than half of the total ice covered area. The majority of the MYI is located in the QEI, Western Parry Channel, and M'Clintock Channel where ice concentration often remains high even at the end of the melt season. During the winter, sea ice in the CAA is almost entirely land-fast. When the sea ice breaks up in July, it is exchanged with the Arctic Ocean to the north and west, which provides the CAA an additional source of MYI (Howell *et al.*, 2013). Therefore, the decline in sea ice cover is not yet significant in the CAA when compared to other regions in the Canadian Arctic (Tivy *et al.*, 2011).

The MYI from the Arctic Ocean accumulates in the Western Parry Channel: M'Clure Strait, Viscount Melville Sound, M'Clintock Channel, and Peel Sound, creating ice chokepoints (Howell *et al.*, 2008 and Fissel *et al.*, 2011). In order to avoid such navigation hazard, vessels could consider the southern alternative routes, however, difficulties are still present due to their shallow depths or the accumulated MYI in the vicinity of the Victoria Strait (Steward *et al.*, 2009).

References

- Aagaard, K., & Carmack, E. C. (1989). The Role of Sea Ice and Other Fresh Water in the Arctic Circulation. *Journal of Geophysical Research: Oceans*, 94, 14485-14498. Doi:10.1029/JC094iC10p14485
- Aksenov, Y., Bacon, S., Coward, A. C., & Holliday, N. P. (2010). Polar Outflow From the Arctic Ocean: a High Resolution Model Study Doi://Doi.Org/10.1016/J.Jmarsys.2010.06.007
- Carmack, E. C., & MacDonald, R. W. (2002). Oceanography of the Canadian Shelf of the Beaufort Sea: a Setting for Marine Life. *Arctic*, 55(2), S29.
- Castro De, L. G., Hu, X., & Myers, P. G. (2015). Potential Positive Feedback Between Greenland Ice Sheet Melt and Baffin Bay Heat Content on the West Greenland Shelf. *Geophysical Research Letters*, 42(12), 4922-4930. Doi:10.1002/2015GL064626
- Defossez, M., Saucier, F. J., Myers, P. G., Caya, D., & Dumais, J. -. (2012). Comparing Winter and Summer Simulated Estuarine Circulations in Foxe Basin, Canada. *Atmosphere-Ocean*, 50(3), 386-401. Doi:10.1080/07055900.2012.693256
- Dukhovskoy, D. S., Myers, P. G., Platov, G., Timmermans, M., Curry, B., Proshutinsky, A., . . . Somavilla, R. (2016). Greenland Freshwater Pathways In The Sub-Arctic Seas From Model Experiments With Passive Tracers. *Journal Of Geophysical Research: Oceans*, 121(1), 877-907. Doi:10.1002/2015JC011290
- Fissel, D. B., De, M., Álvarez, S., Kulan, N., Mudge, T., & Marko, J. R. (2011). Long-Term Trends for Sea Ice in the Western Arctic Ocean: Implications for Shipping and Offshore Oil and Gas Activities
- Gillard, L. C., Hu, X., Myers, P. G., & Bamber, J. L. (2016). Meltwater Pathways From Marine Terminating Glaciers of the Greenland Ice Sheet. *Geophysical Research Letters*, 43(20), 10,873-10,882. Doi:10.1002/2016GL070969
- Howell, S. E. L., Wohlleben, T., Daboor, M., Derksen, C., Komarov, A., & Pizzolato, L. (2013). Recent Changes in the Exchange of Sea Ice Between the Arctic Ocean and the Canadian

- Arctic Archipelago. *Journal of Geophysical Research: Oceans*, 118(7), 3595-3607.
Doi:10.1002/Jgrc.20265
- Howell, S. E. L., Tivy, A., Yackel, J. J., & McCourt, S. (2008). Multi-Year Sea-Ice Conditions in the Western Canadian Arctic Archipelago Region of the Northwest Passage: 1968-2006. *Atmosphere-Ocean*, 46(2), 229-242. Doi:10.3137/Ao.460203
- Hu, X., Myers, P. G., & Lu, Y. (2019). Pacific Water Pathway in the Arctic Ocean and Beaufort Gyre in Two Simulations With Different Horizontal Resolutions. *Journal of Geophysical Research: Oceans*, 124(8), 6414-6432. Doi:10.1029/2019JC015111
- Hughes, K. G., Klymak, J. M., Hu, X., & Myers, P. G. (2017). Water Mass Modification and Mixing Rates in a 1/12° Simulation of the Canadian Arctic Archipelago. *Journal of Geophysical Research: Oceans*, 122(2), 803-820. Doi:10.1002/2016JC012235
- Karcher, M., Smith, J. N., Kauker, F., Gerdes, R., & Smethie Jr., W. M. (2012). Recent Changes in Arctic Ocean Circulation Revealed by Iodine-129 Observations and Modeling. *Journal of Geophysical Research: Oceans*, 117 Doi:10.1029/2011JC007513
- Kwok, R., Spreen, G., & Pang, S. (2013). Arctic Sea Ice Circulation and Drift Speed: Decadal Trends and Ocean Currents. *Journal of Geophysical Research: Oceans*, 118(5), 2408-2425. Doi:10.1002/Jgrc.20191
- Lazier, J. R. N., & Wright, D. G. (1993). Annual Velocity Variations in the Labrador Current. *Journal of Physical Oceanography*, 23(4), 659-678.
- Lu, Y., Higginson, S., Nudds, S., Prinsenber, S., & Garric, G. (2014). Model Simulated Volume Fluxes Through the Canadian Arctic Archipelago and Davis Strait: Linking Monthly Variations to Forcing in Different Seasons. *Journal of Geophysical Research: Oceans*, 119(3), 1927-1942. Doi:10.1002/2013JC009408
- Münchow, A., Falkner, K. K., & Melling, H. (2015). Baffin Island and West Greenland Current Systems in Northern Baffin Bay Doi:10.1016/J.Pocean.2014.04.001

- Ridenour, N. A., Hu, X., Sydor, K., Myers, P. G., & Barber, D. G. (2019). Revisiting the Circulation of Hudson Bay: Evidence for a Seasonal Pattern. *Geophysical Research Letters*, *46*(7), 3891-3899. Doi:10.1029/2019GL082344
- Saucier, F. J., Senneville, S., Prinsenber, S., Roy, F., Smith, G., Gachon, P., . . . Laprise, R. (2004). Modelling the Sea Ice-Ocean Seasonal Cycle in Hudson Bay, Foxe Basin and Hudson Strait, Canada. *Climate Dynamics*, *23*(3), 303-326. Doi:10.1007/S00382-004-0445-6
- Serreze, M. C., & Barry, R. G. (2014). *The Arctic Climate System* (Second Ed.). Cambridge: Cambridge University Press.
- Stewart, E. J., Howell, S. E. L., Draper, D., Yackel, J., & Tivy, A. (2009). Sea Ice in Canada's Arctic: Implications for Cruise Tourism. *Arctic*, *60*(4) Doi:10.14430/Arctic194
- Straneo, F., & Saucier, F. (2008). The Outflow From Hudson Strait and its Contribution to the Labrador Current. *Deep Sea Research Part I: Oceanographic Research Papers*, *55*(8), 926-946.
- Stroeve, J., Holland, M. M., Meier, W., Scambos, T., & Serreze, M. (2007). Arctic Sea Ice Decline: Faster Than Forecast. *Geophysical Research Letters*, *34*(9) Doi:10.1029/2007GL029703
- Tivy, A., Howell, S. E. L., Alt, B., McCourt, S., Chagnon, R., Crocker, G., . . . Yackel, J. J. (2011). Trends and Variability in Summer Sea Ice Cover in the Canadian Arctic Based on the Canadian Ice Service Digital Archive, 1960–2008 and 1968–2008. *Journal of Geophysical Research: Oceans*, *116* Doi:10.1029/2009JC005855
- Wang, Q., Myers, P. G., Hu, X., & Bush, A. B. G. (2012). Flow Constraints on Pathways Through the Canadian Arctic Archipelago. *Atmosphere-Ocean*, *50*(3), 373-385. Doi:10.1080/07055900.2012.704348
- Yang, J. (2009). Seasonal and Interannual Variability of Downwelling in the Beaufort Sea. *Journal of Geophysical Research*, *114* Doi:10.1029/2008JC005084

Yang, Q., Dixon, T. H., Myers, P. G., Bonin, J., Chambers, D., Van, D. B., . . . Mortensen, J. (2016). Recent Increases in Arctic Freshwater Flux Affects Labrador Sea Convection and Atlantic Overturning Circulation. *Nature Communications*, 7(1), 10525. Doi:10.1038/Ncomms10525

Chapter 3

Methodology

3.1. NEMO (Nucleus for European Modelling of the Ocean) Frame Work

I used the numerical model, Nucleus for European Modelling of the Ocean (NEMO) version 3.4 to describe the dynamics of the ocean. NEMO utilises the ocean engine, Ocean Parallelise (OPA) on a three dimensional Arakawa C-type staggered grid. It is coupled with the sea ice implementation, the Louvain la-neuve Ice Model (LIM2), which interfaces with sea ice thermodynamic and dynamic numerical model (Fichefet and Morales Maqueda, 1997; Madec and NEMO System Team, 2013).

NEMO describes the physics of the ocean by the fluid dynamic primitive equations and a non-linear equations of state, which describes temperature and salinity to fluid density. It adapted six mathematical assumptions:

1) Spherical Earth Approximation:

Earth is considered as a sphere rather than a ellipsoid, therefore, the acceleration of gravity is aligned with the Earth's radius at any given points;

2) Thin-shell Approximation:

The ocean depth is negligible comparing the Earth's radius;

3) Hydrostatic Hypothesis:

The vertical momentum equation is reduced to a balance between the vertical pressure gradient and the buoyancy, removing the explicit resolution of the convective processes from the Navier-Stoke's equations;

4) Boussinesq Approximation:

Density differences are neglected except as they influence buoyancy force. Thus, the difference in inertia is neglected whilst gravity is strong enough to make the specific weight appreciably different as the fluid properties changes;

5) Incompressibility Hypothesis:

At an infinitesimal scale, the flow density is constant when following the flow motion. Combined with the continuity equation, the three dimensional divergence of the velocity vector is zero; and

6) Turbulent Closure Hypothesis:

Turbulent fluxes that represent the small-scale processes are expressed in terms of large-scale features as they can affect the large-scale processes.

NEMO uses a curvilinear z -coordinate system with vertical levels fixed at given depths. Based on the spherical and thin layer approximations, the upward vector k is defined as the z -axis, and the horizontal plane is chosen with the unit vectors (i, j) orthogonal to k . The i and j origin are defined at the bottom left boundary of the domain, with indices increasing eastwards for i and northwards for j . At the convergence of the meridians in the standard geographical latitude-longitude grid system a singularity appears (Madec and Imbard, 1996). Therefore, a tri-polar grid transformation is used by the model, which consists of a grid rotated and re-projected to displace the singularity to land instead of at the North Pole (*e.g.* Murray (1996); Madec and Imbard (1996)). Therefore, the i -axis and j -axis are not aligned with longitude and latitude.

With the mathematical assumptions, seven primitive equations describe the model ocean physics: the momentum balance, hydrostatic equilibrium, the incompressibility equation, the heat and salt conversion equation, and an equation of state:

$$\frac{\delta U_h}{\delta t} = \left(\nabla \times U_h \right) \times U_h + \frac{1}{2} \nabla U_h^2 - f k \times U_h - \frac{1}{\rho_0} \nabla_h p + D^U + F^U \quad (3.1)$$

$$\nabla \cdot U = 0 \quad (3.2)$$

$$\frac{\delta S}{\delta t} = -\nabla \cdot (SU) + D^S + F^S \quad (3.3)$$

$$\frac{\delta T}{\delta t} = -\nabla \cdot (TU) + D^T + F^T \quad (3.4)$$

$$\rho = \rho(T, S, p) \quad (3.5)$$

$$\frac{\delta p}{\delta z} = -\rho g \quad (3.6)$$

Where the three-dimensional velocity is $U = U_h + w\hat{k}$, and U_h is the horizontal velocity defined on the plane (i, j) , w the vertical velocity. The potential temperature is defined as T , salinity S , in-situ density ρ , reference density ρ_0 , and pressure p . The gravitational acceleration is defined as g , Coriolis parameter f is defined as: $f = 2\Omega \sin \varphi$, where Ω is Earth's angular velocity and φ latitude. The parameterisation of sub-grid scale diffusion for momentum, potential temperature, and salinity are defined as D^U , D^T , and D^S , respectively. Lastly, the surface forcing terms for momentum, potential temperature, and salinity are defined as F^U , F^T , and F^S , respectively.

The boundary conditions are set at the bottom of sea floor and surface where the sea interacts with the atmosphere or sea ice. At the bottom, the depth of the sea floor is defined as H , therefore: $z = -H(i, j)$; and at the surface of sea-air or sea-ice interface, the sea surface height is defined as η : $z = \eta(i, j, k, t)$. The reference value is $z = 0.22 \text{ m}$.

Between the land and ocean, there are two types of interfaces. Between the continental margins and ocean, river runoff creates a mass exchange which results in the change of sea

surface salinity. Via the sea floor, the solid earth and ocean interface exchange heat and fluxes, which are usually small and negligible in the model. However, the geothermal heating associated with solid earth cooling might have the impact on the thermohaline circulation of the ocean (Madec and NEMO System Team, 2013). The boundary condition is set to no flux exchange of heat or salt through the solid boundaries, and bottom velocity parallel to the solid boundaries. The kinematic boundary conditions are thus expressed as:

$$w = -U_h \cdot \nabla h(H) \quad (3.7)$$

Between the atmosphere and ocean, there are exchanges of heat, horizontal momentum of wind stress, and mass flux of freshwater, which is resulted from excess precipitation than evaporation. Therefore, the kinematic surface condition and mass flux is expresses as equation (3.12). At this dynamic boundary, the capillary waves from the surface is removed by neglecting surface tension. Applying a continuity of pressure across the interface $z=\eta$ gives:

$$w = \frac{\delta\eta}{\delta t} + U_h \Big|_{(z=\eta)} \cdot \nabla h(\eta) + P - E \quad (3.8)$$

Between the sea ice and ocean, there are exchanges of heat, salt, freshwater, and momentum. At this interface, the sea surface temperature is set to be at the freezing point, whilst the sea ice salinity is set to be lower than that of the ocean.

The total pressure at any depth z is calculated from the surface pressure p_s a reference geopotential surface ($z=0$) and a hydrostatic pressure p_h . The free surface formation for the surface pressure is used in this study. The free-surface elevation, η , is used to describe the atmosphere-ocean interface, which is associated with the external gravity waves.

The configuration for this study also involves time-splitting and short barotropic time steps due to the high phase speed of surface gravity waves. This is attributed to the barotropic flow and the surface as restoring forces as it moves vertically.

The smaller scale dynamics are represented in terms of the larger-scale patterns in order to complete the equation. The smaller scale processes are important in balancing the kinetic energy and heat over the long-term simulations. The effects of small scale processes are presented in the primitive equations as the divergence of turbulent fluxes in the form of eddies. The configuration used in this study applied a second order operator.

The model's stability is increased from the sub-grid scale processes by dissipating the energy towards to the grid scale and not interfering with the solved mesoscale activities. The Arakawa C-type staggered grid used allows the arrangement of variables in all directions consistently. As the vector points (u, v, w) are defined in the centre of each cells, the scalar points (t, S, p, ρ) are located on the centre of cells (figure 3.1).

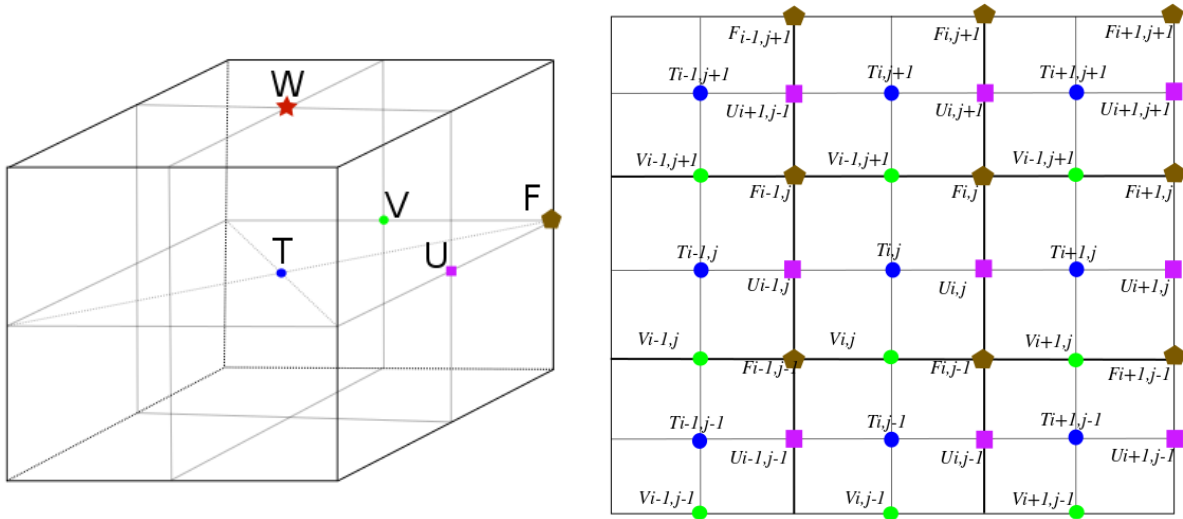


Figure 3.1: 3D (left) and 2D over the horizontal plane (right) mesh grid of the Arakawa C-grid cell with the position of each quantity.

3.2. Arctic and Northern Hemisphere Atlantic (ANHA)

The regional configuration used for this study, ANHA (Arctic and Northern Hemisphere Atlantic), provides a high resolution at 1/12 degree (ANHA12 hereinafter). ANHA12 is a sub-domain of the global ORCA12 mesh. The highest horizontal resolution (~ 1.93 km) is in Dease Strait (in the Canadian Arctic) (figure 3.2). There are 50 vertical levels with layer thickness smoothly increasing from 1.05 metres at the surface to 453.13 metres at the last level. Enhanced resolution is applied to the surface layer, providing the vertical resolution of less than 2 metres for the layers in the top 10 metres.

Partial steps are used to better resolve the bathymetry, which is derived from the 1 minute-arc global relief model of Earth's surface ETOPO1 (Amante and Eakins, 2009). Two open boundaries are present in the Bering Sea and at 20°S in the Atlantic Ocean. Open boundary conditions consisting of temperature, salinity, and horizontal velocities are obtained from the GLobal Ocean ReanalYSis 2 version 3 (GLORYS2v3; Mercator Ocean (2017)). Surface forcing consists of the 10 m winds, 2 m temperature and specific humidity, surface down-welling short and long wave radiative fluxes. These variables are obtained from the high temporal and spatial resolution atmospheric forcing from the Canadian Meteorological Centre's (CMC) Global Deterministic Prediction System (GDPS) ReForcasts (CGRF) (Smith *et al.*, 2014). The initial conditions consisting of ocean temperature, salinity, horizontal velocities, and sea surface height are obtained from GLORYS2v3.

Runoff in this configuration consists of two sources: river discharge and glacial melt. River discharge data is mapped based on Dai *et al.* (2009), which provides monthly $1^{\circ} \times 1^{\circ}$ data until 2007. The source of Greenland meltwater is mapped based on Bamber *et al.* (2012), providing a resolution of $5 \text{ km} \times 5 \text{ km}$ until 2010. After each end date, the data from the last year is repeated until the end of the simulation.

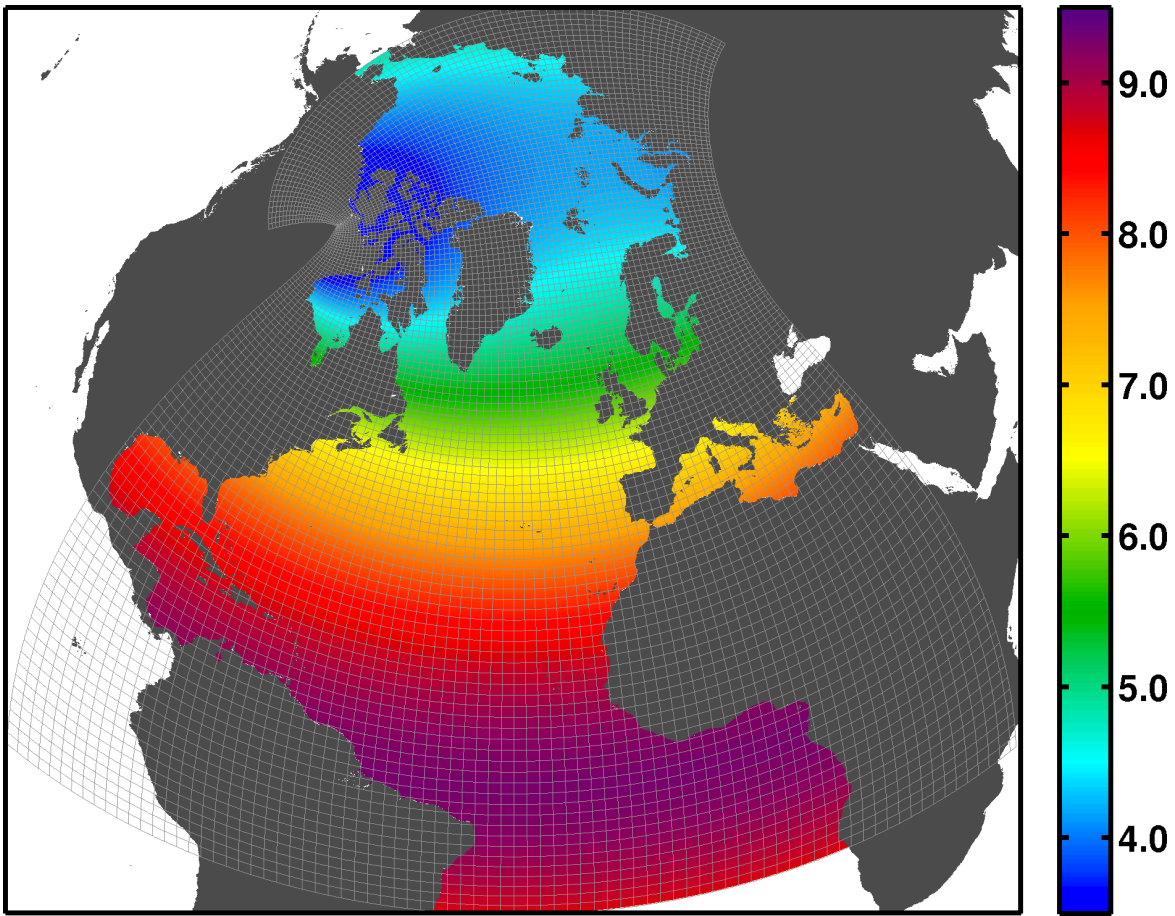


Figure 3.2: ANHA12 horizontal mesh grid (every 20 grids, colour shows the resolution in kilometres)

3.3. Trajectory Calculation

I apply the offline Lagrangian tool, ARIANE, to the model output velocity fields to calculate the three-dimensional trajectories of particles based on oceanic advection (Blanke and Raynaud, 1997). The particles are homogeneously distributed in time and space. The offline manner of calculating the transport of particles avoids running multiple oceanic model simulations, thus provides an effective approach to examine the transport of particles to oceanic advection.

ARIANE consists of two modes: quantitative and qualitative. Via the qualitative mode, the calculation provides the distribution of particles for each grid cell and the mass exchange; whilst via the quantitative mode, ARIANE calculates the three-dimensional trajectory of each particle released. In this release, I applied the qualitative mode to calculate the three-dimensional position of particles at each time step of the model integration (Blanke and Grima, 2008).

ARIANE is a well-tested powerful tool that has been extensively used to study the circulation pathways of a highlighted water mass (*e.g.* Gillard *et al.* (2016); Feucher *et al.* (2019) or specific particles (*e.g.* Popova *et al.* (2013); Kelly *et al.* (2018)). Its performance is optimised when coupling with the volume continuity equation expressed on an Arakawa C-grid model. It thus provides several advantages to the analytical calculation in terms of successive time intervals (van Sebille *et al.*, 2018).

Although the passive particles tracking scheme provided great efficiency and is adequate to present the transport of pollutant due to oceanic advection, there were some limitations induced by the misassumption of its neutral buoyancy. Using a passive representation, the pollutant was considered to be neutrally buoyant particles essentially marking the pollutant infested seawater. Thus, the vertical entrainment of the pollutant would be more significant if the density difference was properly accounted for, especially in the area of deep convection (Blanke *et al.*, 1997). Another limitation in the vertical component is from the integration approach. From the ocean bottom, where the vertical velocity is zero, an upward integration is applied to the

surface. It results in the erroneous surface values, causing the particles to enter the atmosphere (Blanke and Grima, 2008).

When working with offline schemes, temporal interpolation is usually required due to the interval between consecutive stored velocity fields generally being longer than the time-step. This temporal interpolation of the velocity fields can be a large source of error, particularly when the interval with which velocity fields are stored becomes longer than a few days (van Sebille *et al.*, 2018). This results in the unrepresented parameterised mixing processes of small time scales, so we can only consider the effects of advection but not diffusion. The individual particles effectively represent large quantities of pollutant molecules. This can be compensated for by using many particles over an ensemble of releases (Kelly *et al.*, 2018).

The transport of particles is governed by the averaged current velocity field (advection) and the presence of the random chaotic component in the velocity field (diffusion). Turbulence in the ocean is determined by the current velocity gradients, surface and deep perturbations, and seawater stratification. It plays an important role in the intensity of the diffusion processes and thus the pollutant's spatial distribution (Baumert *et al.*, 2005). However, the Lagrangian calculation that ARAINE applies cannot resolve certain processes such as diffusion and convection. As the particles evolve on the Eulerian output fields, these processes are parameterised in the ocean tracers and dynamic fields. The Lagrangian calculation of ARIANE is capable to confidently integrate the large-scale diagnostics.

3.4. Experiment Design and Analysis

I have a total number of 35 stations distributed along the NWP and the Arctic Bridge. Their locations were assigned with consideration to their oceanographic dynamics (strong currents and sea ice accumulation), geographic features (narrow straits), and the density of ship traffic over the past 30 years based on the data provided by Dawson *et al.* (2018). At each station, I released 5,000 particles over a 5 km by 5 km grid, to simulate the condition of spilt oil days after the spill. With consideration to the different types of fuel that vessels might use, I also have

an initial area of 10 km by 10 km within each station. In the area where open water presents more dynamic ice conditions, such as the Canadian Beaufort Sea and Baffin Bay, I have considered the alternative route that vessels might take. Table 3.1 provides the name and location of these locations, and their location are visualised in figure 3.3.

I released the virtual particles at each site of each station every 10 days during the extent operating season for the Arctic Ocean: from June 1st to November 1st. All simulations are repeated for 12 available model integration years from 2004 to 2015 (last simulation output ends in 2017). Within the simulation period of two years, I examine the propagation of particles with respect to the time elapsed. The probability of particle distribution was calculated at two cutoffs: (1) at the beginning of the next operating season (June 1st of the next year of release year); and (2) at the end of the next year (November 1st of the next year of release year). The regions of high probabilities were evaluated for recovery operations.

In order to examine the severity of the spill in terms of the time and location, I calculated the following parameters at one and two years after the release date of each simulation: (1) horizontal spreading area, which is based on the number of grid cells that particles occupied after one and two years of integration were calculated. Then, it was converted into kilometres with respect to the model mesh grid; (2) direct distance from the location of particles at one / two years after the release to their initial locations; (3) full trajectory that particles travelled throughout the integration at every time step; and (4) percentage of particles with depth exceeding 90 metres.

Table 3.1: simulation sites

<u>Station ID</u>	<u>Description</u>	<u>Range (Longitude)</u>	<u>Range (Latitude)</u>
<u>Canadian Beaufort Sea</u>			
CBF	Canadian Beaufort Sea (5 km by 5 km grid)	-132.1883 -131.5387	70.9712 71.2208
CBF_10	10 km by 10 km grid (same centre as CBF)	-132.1883 -130.8892	70.9712 71.4704
CBF_c	1/2 distance to shore (to CBF)	-132.2388 -132.1097	70.3526 70.3980
CBF_c_10	10 km by 10 km grid (same centre as CBF_c)	-132.3040 -132.0472	70.3256 70.4213
<u>Canadian Arctic Archipelago</u>			
LSE	Lancaster Sound East	-80.8059 -80.6315	74.0931 74.1397
LSE_10		-80.8849 -80.5560	74.0718 74.1611
LSW	Lancaster Sound West	-85.9200 -86.0821	74.0829 74.1286
LSW_10		-86.1597 -85.8328	74.0597 74.1478
BRW	Barrow Strait	-92.3532 -92.1863	74.3294 74.3754
BRW_10		-92.4322 -92.1046	74.3096 74.4005
VMSE	Viscount Merville Sound East	-100.2908 -100.1116	74.1951 74.2414
VMSE_10		-100.3739 -100.0320	74.1728 74.2621
VMS	Viscount Merville Sound	-104.7932 -104.6181	74.0651 74.1099
VMS_10		-104.8721 -104.5419	74.0431 74.1332
MCLE	M'Clure Strait East	-114.5466 -114.3760	73.9738 74.0197
MCLE_10		-114.6301 -114.2991	73.9504 74.0435
MCLW	M'Clure West	-125.3265 -125.1370	75.0836 75.1312
MCLW_10		-125.3979 -125.0436	75.0648 75.1583

<u>Station ID</u>	<u>Description</u>	<u>Range (Longitude)</u>	<u>Range (Latitude)</u>
<u>Canadian Arctic Archipelago (cont.)</u>			
GB	Gulf of Boothia	-90.8771 -90.7257	70.9947 71.0383
GB_10		-90.9403 -90.6629	70.9683 71.0581
PS	Peel Sound	-95.8525 -95.6974	72.4901 72.5330
PS_10		-95.9198 -95.6205	72.4652 72.5559
SRB	St Roch Basin	-94.9613 -94.8246	69.1358 69.1846
SRB_10		-95.0247 -94.7528	69.1152 69.2065
MCC	M'Clintock Channel	-102.5981 -102.4533	71.7939 71.8416
MCC_10		-102.6675 -102.3736	71.7715 71.8611
LSS	Larsen Sound	-98.7211 -98.5872	70.3978 70.4429
LSS_10		-98.7836 -98.5130	70.3706 70.4629
QMG	Queen Maud Gulf	-101.2132 -101.0879	68.7514 68.7968
QMG_10		-101.2781 -101.0309	68.7289 68.8174
CG	Coronation Gulf	-113.4663 -113.3412	68.2969 68.3438
CG_10		-113.5252 -113.2808	68.2715 68.3628
AG	Amundsen Gulf	-122.0819 -121.9442	70.5042 70.5493
AG_10		-122.1485 -121.8766	70.4799 70.5717
<u>Hudson Bay Complex</u>			
HSE	Hudson Strait East	-64.8286 -64.7373	60.9326 60.9776
HSE_10		-64.8739 -64.6892	60.9116 61.0003
UB	Ungava Bay	-67.0951 -67.0046	59.8556 59.8997
UB_10		-67.1392 -66.9613	59.8321 59.9233
HSNW	Hudson Strait Northwest	-76.4525 -76.3488	63.8161 63.8653
HSNW_10		-76.5074 -76.3062	63.7918 63.8836

<u>Station ID</u>	<u>Description</u>	<u>Range (Longitude)</u>	<u>Range (Latitude)</u>
<u>Hudson Bay Complex (cont.)</u>			
HSSW	Hudson Strait Southwest	-77.9497 -77.8493	62.7752 62.8225
HSSW_10		-78.0038 -77.7988	62.7491 62.8434
FB	Foxe Basin	-79.3915 -79.2748	67.3737 67.4181
FB_10		-79.4533 -79.2205	67.3481 67.4384
FC	Foxe Channel	-81.5833 -81.4738	65.2581 65.3037
FC_10		-81.6310 -81.4164	65.2366 65.3275
SI	(South of) Southampton Island	-83.1309 -83.0285	63.7128 63.7566
SI_10		-83.1856 -82.9824	63.6876 63.7786
CFI	Chesterfield Inlet	-90.1296 -90.0273	63.3342 63.3847
CFI_10		-89.9806 -90.1794	63.3128 63.4021
CHL	Port of Churchill	-93.8795 -93.7909	59.0936 59.1390
CHL_10		-93.9224 -93.7463	59.0683 59.1579
<u>Baffin Bay</u>			
BBN	Baffin Bay North	-68.4309 -69.2895	72.3539 72.3982
BBN_10		-68.5050 -68.2166	72.3293 72.4181
BBN_c		-70.5724 -70.4307	71.7314 71.7785
BBN_c_10		-70.6463 -70.3593	71.7077 71.7983
BBS	Baffin Bay South	-63.1796 -63.0566	69.1643 69.2061
BBS_10		-63.2427 -63.0031	69.1404 69.2292
BBS_c		-65.1845 -65.0588	68.5144 68.5588
<u>Baffin Bay (cont.)</u>			
BBS_c_10		-65.2401 -64.9963	68.4895 68.5804

<u>Station ID</u>	<u>Description</u>	<u>Range (Longitude)</u>	<u>Range (Latitude)</u>
DSW	Davis Strait West	-61.4178 -61.3104	65.2184 65.2641
DSW_10		-61.4690 -61.2561	65.1950 65.2833
DSE		-54.2299 -54.1228	65.2430 65.2890
DSE_10		-54.2875 -54.0754	65.2196 65.3091
CS	Cumberland Sound	-66.2277 -66.1172	65.4677 65.5136
CS_10		-66.2872 -66.0716	65.4451 65.5371
FS	Frobisher Bay	-67.3631 -67.2631	63.1272 63.1717
FS_10		-67.4101 -67.2890	63.1045 63.1935
<u>End of Table</u>			

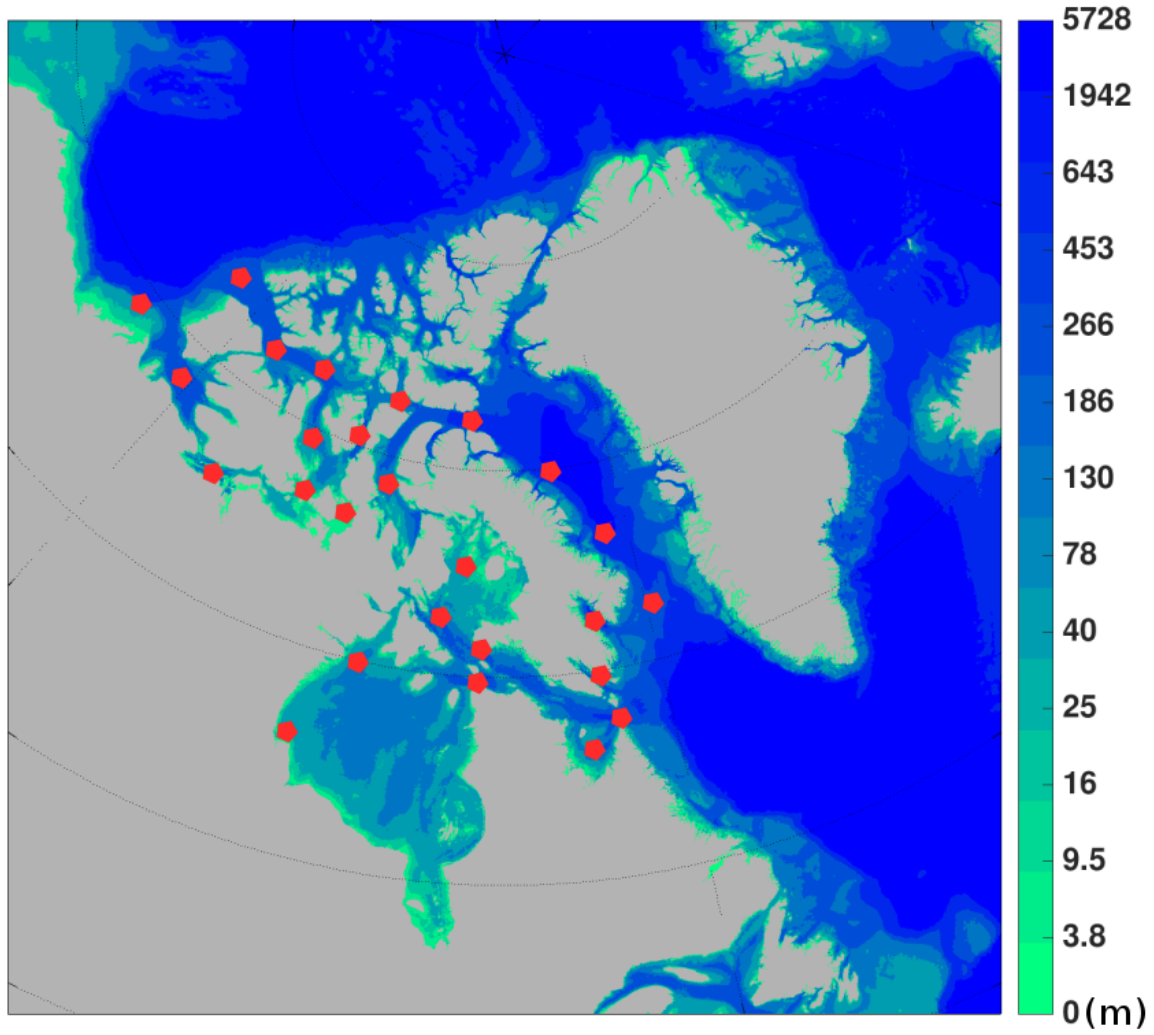


Figure 3.3: red stars are the approximate locations of simulation sites

References

- Amante, C., & Eakins, B. W. (2009). ETOPO1 global relief model converted to PanMap layer format. Retrieved from <https://doi.org/10.1594/PANGAEA.769615>
- Bamber, J., van, d. B., Ettema, J., Lenaerts, J., & Rignot, E. (2012). Recent large increases in freshwater fluxes from greenland into the north atlantic. *Geophysical Research Letters*, 39(19) doi:10.1029/2012GL052552
- Baumert, H., Simpson, J., Sundermann, J., 2005. Marine turbulence: Theories, Observations, and Models. Cambridge University Press, New York.
- Blanke, B. & Grima, N. (2008) Tutorial: first steps with ARIANE, sequential version.
- Blanke, B., & Raynaud, S. (1997). Kinematics of the pacific equatorial undercurrent: An eulerian and lagrangian approach from GCM results. *Journal of Physical Oceanography*, 27(6), 1038-1053. doi:KOTPEU>2.0.CO;2
- Dai A, Qian T, Trenberth K, Milliman J (2009) Changes in continental freshwater discharge from 1948–2004. *J Clim* 22:2773–2791
- Dawson, J., Pizzolato, L., Howell, S. E. L., Copland, L., & Johnston, M. E. (2018). Temporal and spatial patterns of ship traffic in the canadian arctic from 1990 to 2015. *Arctic*, 71(1), 15-26. doi:10.14430/arctic4698
- Feucher, C., Garcia-Quintana, Y., Yashayaev, I., Hu, X., & Myers, P. G. (2019). Labrador sea water formation rate and its impact on the local meridional overturning circulation. *Journal of Geophysical Research: Oceans*, 124(8), 5654-5670. doi:10.1029/2019JC015065
- Fichefet, T., & Maqueda, M. A. M. (1997). Sensitivity of a global sea ice model to the treatment of ice thermodynamics and dynamics. *Journal of Geophysical Research: Oceans*, 102, 12609-12646. doi:10.1029/97JC00480

- Gillard, L. C., Hu, X., Myers, P. G., & Bamber, J. L. (2016). Meltwater pathways from marine terminating glaciers of the greenland ice sheet. *Geophysical Research Letters*, *43*(20), 10,873-10,882. doi:10.1002/2016GL070969
- Kelly, S., Popova, E., Aksenov, Y., Marsh, R., & Yool, A. (2018). Lagrangian modeling of arctic ocean circulation pathways: Impact of advection on spread of pollutants. *Journal of Geophysical Research: Oceans*, *123*(4), 2882-2902. doi:10.1002/2017JC013460
- Madec, G., & Imbard, M. (1996). A global ocean mesh to overcome the north pole singularity. *Climate Dynamics*, *12*(6), 381-388. doi:10.1007/BF00211684
- Madec Gurvan, Romain Bourdallé-Badie, Pierre-Antoine Bouttier, Clément Bricaud, Diego Bruciaferri, Daley Calvert, ... Martin Vancoppenolle. (2013, February 11). NEMO ocean engine (Version v3.4-patch). *Notes Du Pôle De Modélisation De L'institut Pierre-simon Laplace (IPSL)*. Zenodo. <http://doi.org/10.5281/zenodo.1475234>
- Mercator Ocean (2017): Mercator Ocean GLORYS2V3 Reanalysis - Forcing dataset (for MARVL). Australian Ocean Data Network.dataset.
- Murray, R. J. (1996). Explicit generation of orthogonal grids for ocean models doi://doi.org/10.1006/jcph.1996.0136
- Popova, E. E., Yool, A., Aksenov, Y., & Coward, A. C. (2013). Role of advection in arctic ocean lower trophic dynamics: A modeling perspective. *Journal of Geophysical Research: Oceans*, *118*(3), 1571-1586. doi:10.1002/jgrc.20126
- Smith, G. C., Roy, F., Mann, P., Dupont, F., Brasnett, B., Lemieux, J., . . . Bélair, S. (2014). A new atmospheric dataset for forcing ice–ocean models: Evaluation of reforecasts using the canadian global deterministic prediction system. *Quarterly Journal of the Royal Meteorological Society*, *140*(680), 881-894. doi:10.1002/qj.2194
- van Sebille, E., Griffies, S. M., Abernathey, R., Adams, T. P., Berloff, P., Biastoch, A., . . . Zika, J. D. (2018a). *Lagrangian ocean analysis: Fundamentals and practices* doi:<https://doi.org/10.1016/j.ocemod.2017.11.008>

Chapter 4

Modelling the Long-term Fate and Transport Pathways of Pollutant in the Hudson Bay Complex due to Oceanic Advection

This chapter is independently written and is prepared to become a publication with authorship of Ran Tao and Paul G Myers.

Abstract

In Canadian Arctic, ship traffic has nearly tripled over the past 25 years, especially in Hudson Bay Complex (HBC), attributed to declining sea ice and increasing maritime investments. We are motivated to evaluate the circulation pathways and spreading of possible pollutant spilt in the HBC, in order to determine over which region and when the spill of pollutant could pose the most severe consequence. In this study, we used a high-resolution numerical model, NEMO (Nucleus for European Modelling of the Ocean) in the regional configuration, ANHA (Arctic and Northern Hemisphere Atlantic) and a Lagrangian particle tracking tool, ARIANE, to model the transport of pollutant with oceanic advection. We analysed the circulation pathways of pollutant and compared the spreading in terms of area, distances

particles travelled, and percentage of deep spread. By determining the ‘worst-case scenario’, we expect this study to provide an oceanographic overview to the general circulation pathways of pollutant and to illuminate a focus for more detailed case studies in the future.

4.1. Introduction

The sea ice extent in the Arctic Ocean and sub-polar seas is experiencing a downward trend with the largest decline in September (Tivy *et al.*, 2011). The retreat of sea ice is especially significant after 1997, as its rate accelerated four times from 36,000 km² per year (1979-1996) to 130,000 km² per year (1997-2014) (Serreze and Stroeve, 2015). Sea ice in the Hudson Bay Complex exhibited significant decline amongst other regions in the Canadian Arctic as its geographical isolation limits the input of any drifting sea ice from the Arctic Ocean (Tivy *et al.*, 2011).

The Hudson Bay Complex (HBC) connects the Canadian Arctic Archipelago (CAA) via Fury and Hecla Strait and the Labrador Sea of North Atlantic Ocean via Hudson Strait. The HBC is a large isolated system surrounded by land, that consists of the Foxe Basin, Foxe Channel, Hudson Bay, James Bay, Hudson Strait, and Ungava Bay (figure 4.1-a). Arctic Water enters HBC via Fury and Hecla Strait, propagates southward along the western coast of Foxe Basin, and then branches off when reaching Southampton Island (Prinsenberg, 1986). Whilst some flow continues into Hudson Bay through Roes Welcome Sound, the other branch turns eastward into Hudson Strait (Jones and Anderson, 1994). The overall circulation in Hudson Bay is cyclonic with a strong boundary current. There is a strong seasonal variability due to the large river runoff in its southwestern coast: during spring and summer months, a weak anti-cyclonic flow exists on the eastern side (Ridenour *et al.*, 2019b). After circumnavigating Hudson Bay, water exits the complex along the southern coast of Hudson Strait. Along the northern side of Hudson Strait, water from the Baffin Island Current enters Hudson Strait. Whilst the majority of it propagates into Foxe Basin, some is mixed with the outflow and recirculates at the mouth of Hudson Strait and Ungava Bay (Straneo and Saucier, 2008b). After exiting Hudson Strait, the relatively fresh

water merges with the southward Baffin Island Current into Labrador Current (Mertz *et al.*, 1993). The Labrador Current propagates in the southeastern direction following the coast of the Labrador, mixing with the North Atlantic Current around the Grand Banks (Fratantoni and McCartney, 2010).

The sea ice cycle in the HBC is dominated by seasonal first-year ice. Therefore, the warming surface temperature is strongly correlated with the negative trend in sea ice concentration, thickness, and duration (Tivy *et al.*, 2011). In the HBC, the duration of sea ice coverage has a significant negative trend of 10~20 days per decade since 1979 (Parkinson, 2014). The longer sea ice-free season greatly promotes shipping accessibility, as the HBC provides a direct sea route connecting North America to Europe: the Arctic Bridge (Østreng *et al.*, 2013).

The Arctic Bridge is a sub-Arctic waterway connecting Churchill in Hudson Bay to the Russian port of Murmansk via Hudson Strait. Since 1990, ship traffic in the Canadian Arctic has increased dramatically (~300%), which is especially significant in HBC, as most vessels traversing the Arctic Bridge are not ice-strengthened (Dawson *et al.*, 2018, Tivy *et al.*, 2007). Furthermore, Foxe Basin also serves as an alternative southern route of the Northwest Passages (NWP) via Fury and Hecla Strait (Østreng *et al.*, 2013) (figure 4.1-b).

(a)

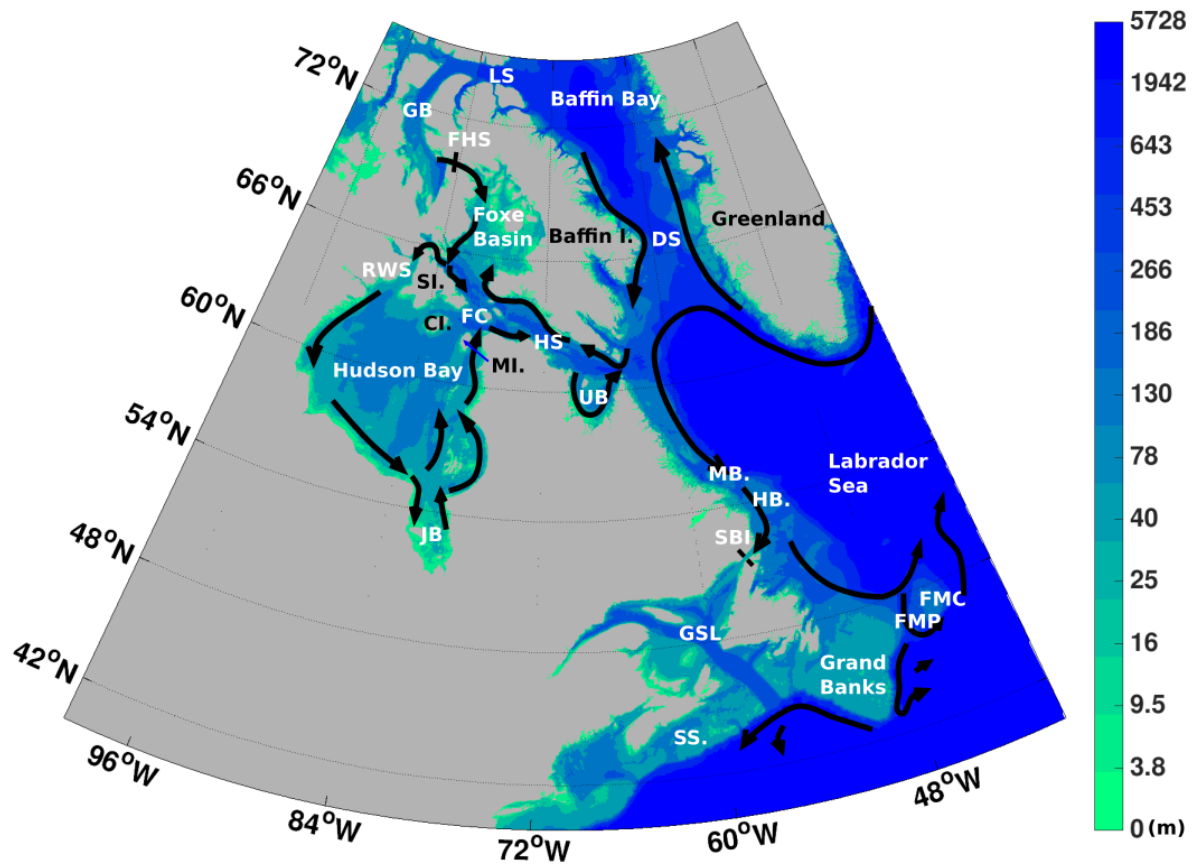


Figure 4.1-a: Geography and oceanic circulation of Hudson Bay Complex and its surrounding seas, black arrows illustrate the general circulation schemes and colour bar indicates bathymetry in metres. Oceanic features are labelled in white: GB: Gulf of Boothia, LS: Lancaster Sound, FHS: Fury and Hecla Strait, RWS: Roes Welcome Sound, FC: Foxe Channel, JB: James Bay, HS: Hudson Strait, UB: Ungava Bay, DS: Davis Strait, MB.: Makkovik Bank, HB.: Hamilton Bank, SBI: Strait of Belle Isle, GSL: Gulf of Saint Lawrence, FMP: Flemish Pass, FMC: Flemish Cap, and SS.: Scotian Shelf. Land features are labelled in black: SI.: Southampton Island, CI.: Coats Island, MI.: Mansel Island.

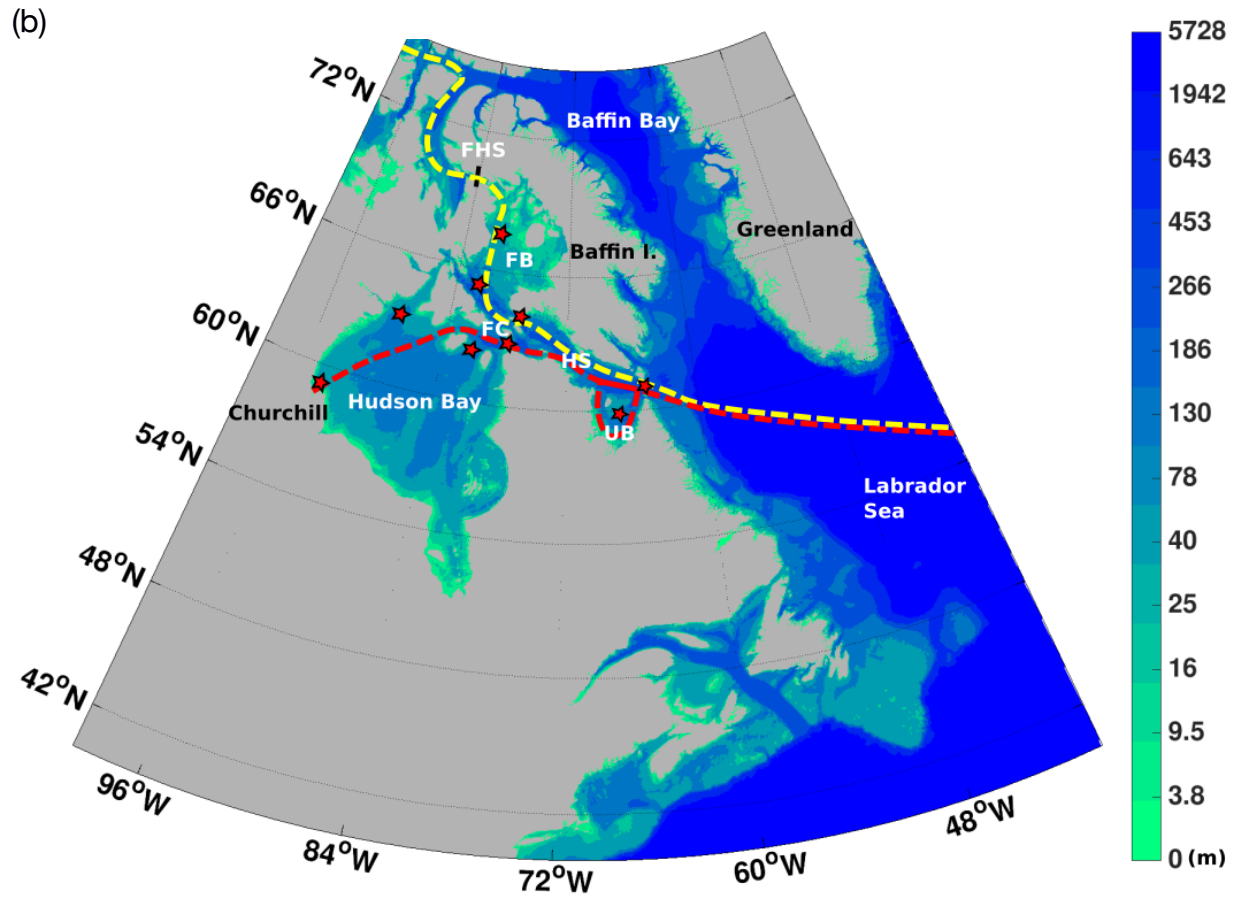


Figure 4.1-b: Arctic Bridge is showed with the red dashed line, and the southern route of NWP with the yellow dashed line. The experiment locations are approximately illustrated by red stars.

Although the sea ice cycle in the HBC exhibits a clear seasonal trend with an ice-free operating season, maritime challenges still arise from the strong tidal currents in Hudson Strait and Ungava Bay (Straneo and Saucier, 2008a; Prowse *et al.*, 2009). Due to the general lack of supportive facilities and adequate charting, operating in the HBC is still difficult (Østreg *et al.*, 2013; Prowse *et al.*, 2009). Therefore, increasing ship traffic in the HBC will increase the risk of accidents and resultant spills of pollutant, especially in the northern components of Foxe Basin due to its remoteness and harsher environment (Andrews *et al.*, 2018).

Once spilt into the ocean, oil is subjected to weathering and transportation. The weathering processes, such as evaporation, emulsification, photo-oxidation, biodegradation, and dissolution, have different rates of reaction under different environmental factors, such as salinity, temperature, the composition of pollutant and seawater. However, most of these processes needs days to weeks to complete after a spill in the Arctic environment. After the initial spreading, oil is transported mainly by advection and encapsulation (Afenyo *et al.*, 2016). Spilt in the Arctic Ocean, containment and recovery methods consist of in-situ burning and dispersant. In-situ burning can remove large fractions of an oil slick on water or ice, however, it is not an effective approach because burning cannot remove all oil and will result in environmental impacts from the residue (Transport Canada and Canadian Coast Guard, 2010). On the other hand, dispersant application is an effective way of breaking up oil slicks in ice-covered waters with adequate mixing energy (Sørstrøm *et al.*, 2010). However, dispersant application results in large volumes of oil drifting at depth (Drozdowski *et al.*, 2011), which is extremely difficult to recover (Kelly *et al.*, 2018).

Due to the remoteness and harsh environment, it is likely that the pollutant cannot be fully recovered within the same operating season of its spill, before the formation of sea ice makes it inaccessible during the following winter (Kelly *et al.*, 2018). Furthermore, the fate of HBC water after exiting the Hudson Strait is to join to Labrador Current spreading in the North Atlantic (Straneo and Saucier, 2008a). It is of particular importance to study the long-time fate and transport pathways of pollutant if spilt in the HBC in terms of its accumulation. Therefore, the most probable locations can be illustrated for recovery operations before it spreads into the open ocean. Furthermore, high concentrations of pollutants are extremely threatening for the

sensitive ecology of the region. By determining the most probable location where the pollutant will accumulate, this study provides aid to designing Marine Protected Areas in the future, with respect to the increasing ship traffic.

Therefore, we are motivated to examine the transport and fate of spilt oil due to oceanic advection in Hudson Bay Complex along the Arctic Bridge and the southern route of the NWP using a high-resolution numerical model, the Nucleus for European Modelling of the Ocean (NEMO) in the Arctic and Northern Hemisphere Atlantic (ANHA) configuration at $1/12^\circ$. The Lagrangian particle tracking tool, ARIANE, is used to calculate the transport pathways of the pollutant. From this study, we will examine the transport pathways and time-scales of particles to oceanic advection, and determine at which sites and when the accidental spill would have the most severe consequence in terms of the horizontal spreading area, distances and full trajectory, percentage of deep spread, level of variabilities and uncertainties. This paper is organised as follows. In section 2, we review the model configuration, evaluation, and experiment design. The circulation pathways, propagation time-scales, and most probable site of accumulation are analysed in section 3. In section 4, the simulation results are numerically discussed in their horizontal spread, distances, deep spread, their uncertainties, variabilities and sensitivities spatially and temporally. Lastly, we discuss the limitations and future directions of this study, and outline the worst-case scenario of the pollutant spills in the HBC.

4.2. Methodology

For this study, we used the well-evaluated ocean-sea ice coupled model NEMO (Nucleus for European Modelling of the Ocean) in the regional configuration of ANHA12, the Arctic and Northern Hemisphere Atlantic at $1/12^\circ$. ANHA12 consists of the Arctic Ocean, North Atlantic Ocean, and part of South Atlantic Ocean with two open boundaries at the Bering Strait and 20°S . Its mesh grid is based on the global tripolar grid, ORCA (DRAKKAR *et al.*, 2007). ANHA12 provides a $1/12^\circ$ resolution, with the highest resolution of ~ 1.93 km at the Dease Strait in Canadian Arctic. It has 50 vertical layers from 1.05 m at the surface smoothly increasing to

453.13 m at the bottom layer. The open boundary conditions and initial conditions are obtained from the GLObal Ocean ReanalYSIS 2 version 3 (GLORYS2v3; Mercator Ocean, 2017). Surface forcing is from the high temporal and spatial resolution atmospheric forcing from the Canadian Meteorological Centre's (CMC) Global Deterministic Prediction System (GDPS) ReForcasts (CGRF) (Smith *et al.*, 2014). The river runoff is implemented from Dai *et al.* (2009) monthly at $1^\circ \times 1^\circ$ resolution, whose dataset ends in 2007. Then the runoff data from 2007 is repeated till the end of the simulation. Discharge from the Greenland Ice Sheet is provided by Bamber *et al.* (2012) at $5 \text{ km} \times 5 \text{ km}$ until 2010, and then the data from 2010 are repeated.

The model configuration, ANHA12, is capable of representing the dynamics of the ocean and sea ice in the Arctic Ocean (*e.g.* Hughes *et al.* (2017), Grivault *et al.* (2018), Hu *et al.* (2018), and Hu *et al.* (2019)). In Hughes *et al.* (2017) and Grivault *et al.* (2018), the model was used to study the CAA. They found that the model's resolution was capable to represent the complex circulation with the CAA, and compared well with observational data. ANHA12 has also been used to simulate the freshwater exchange and deep convection in the Labrador Sea (*e.g.* Feucher *et al.* (2019) and Pennelly *et al.* (2019)). Both studies have found strong correspondence with observations in the mean geostrophic velocities and the depth of convection (Feucher *et al.*, 2019 and Pennelly *et al.*, 2019). Ridenour *et al.* (2019a) used simulations from ANHA12 and satellite observation to examine the circulation of the Hudson Bay Complex. Their work has found a strong correspondence in the mean geostrophic velocities between the model integration and satellite observation. We investigated the freshwater transport and volume flux via Davis Strait, which compared well with the observational data reported by Curry *et al.* (2011). Furthermore, the surface temperature and salinity fields from the model along the Labrador Sea compared well with satellite observations, indicating the model's capacity to represent the circulation over the study region. In terms of sea ice concentration and thickness, Ridenour *et al.* (2019a) showed that model's sea ice velocity and thickness compared well with satellite observations over the HBC. An example is provided in figure 4.2, illustrating the comparison in sea ice concentration between model integration and integrated satellite passive microwave data (available via: <https://nsidc.org/data/G02202/versions/3>).

(a)

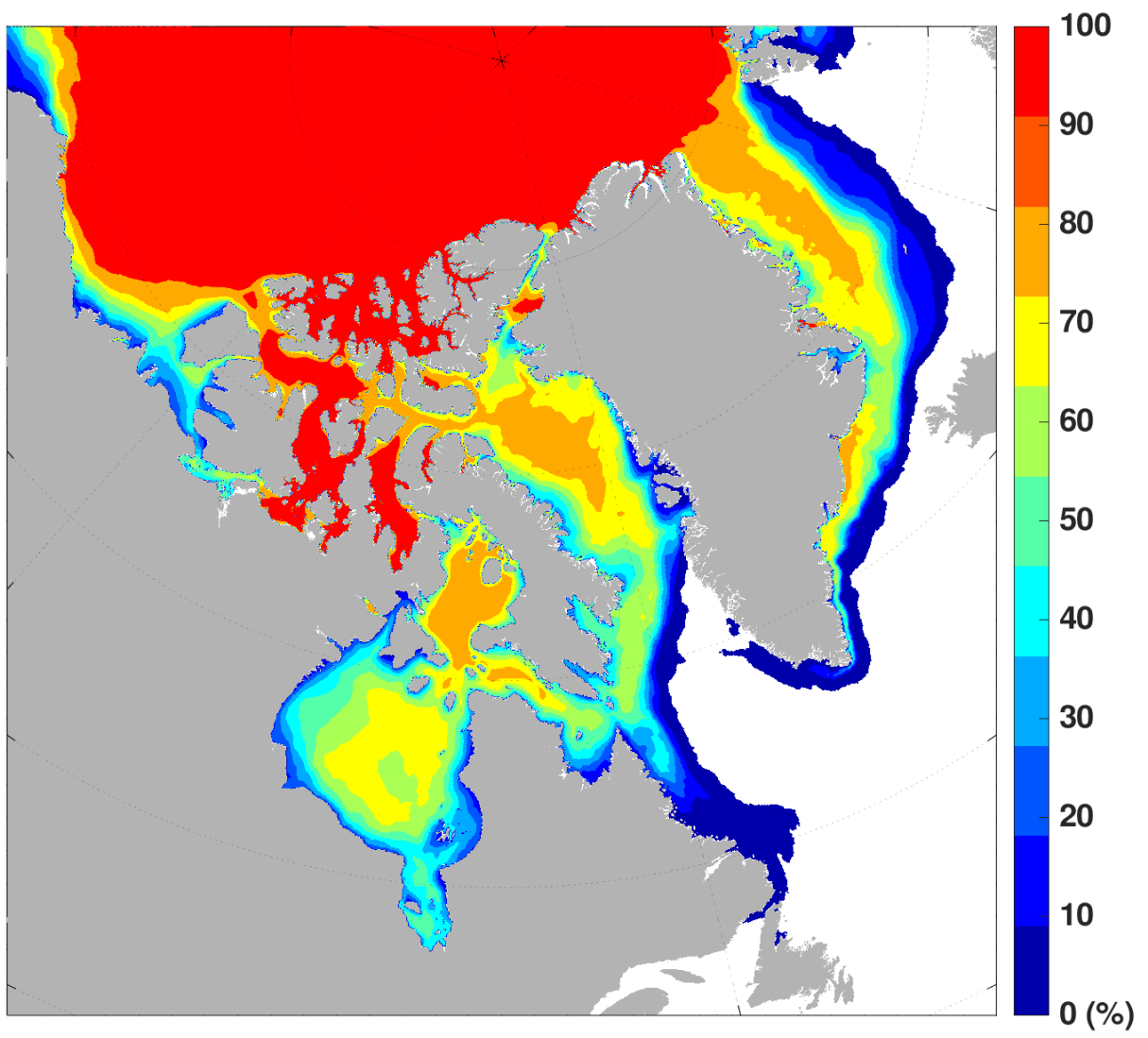


Figure 4.2-a: Average June sea ice concentration derived from the 5-day model output from ANHA12 (2011~2015);

(b)

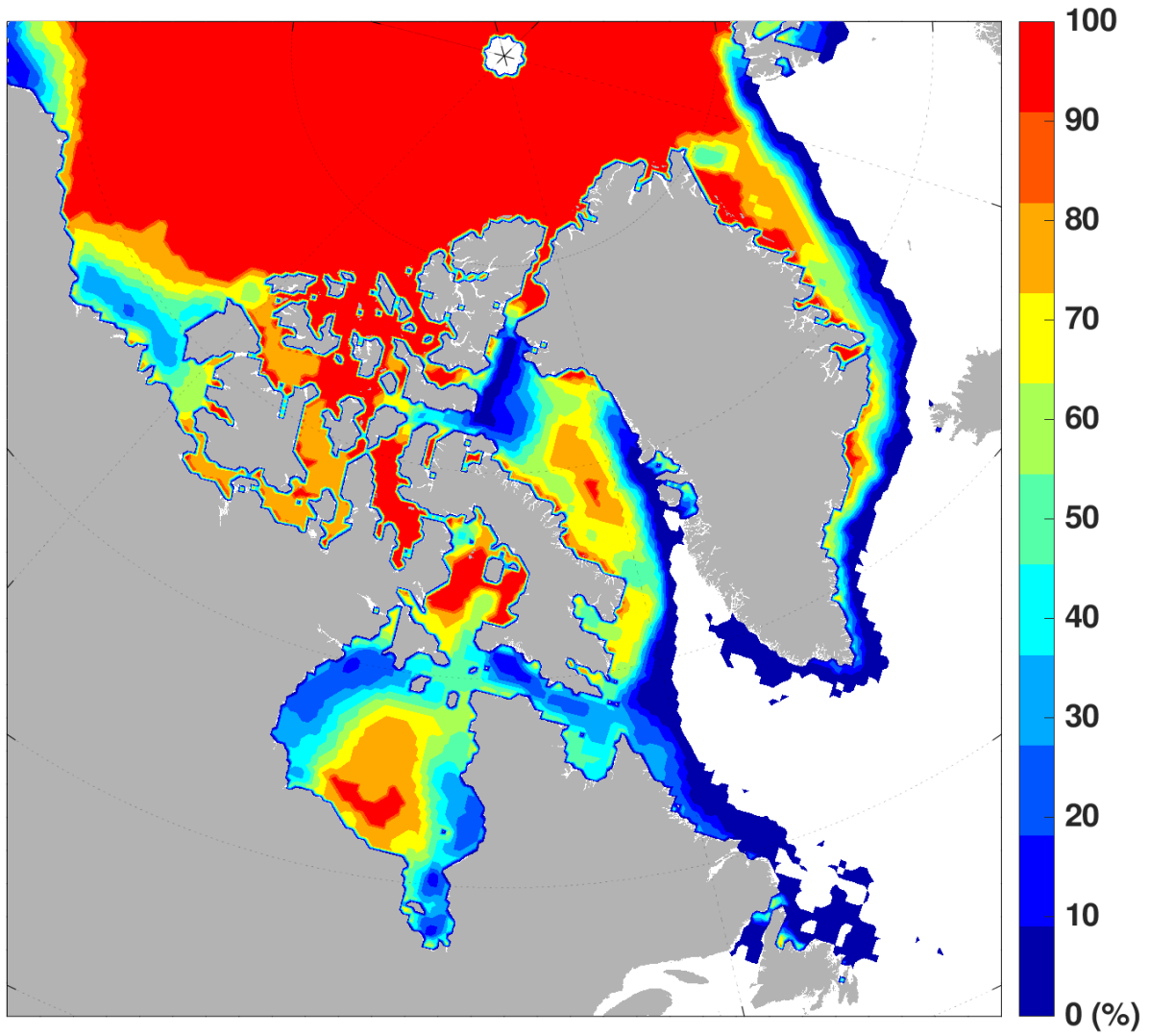


Figure 4.2-b: Average June sea ice concentration, calculated from the daily output provided by the Climate Data Record (satellite observations).

The three-dimensional velocity fields from the model outputs are implemented to drive the offline Lagrangian particle tracking tool, ARIANE. ARIANE is a well-tested tool (e.g. Gillard *et al.* (2016) and Feucher *et al.* (2019)) commonly used to examine the fate and transport pathways of a highlighted water mass (Blanke & Raynaud, 1997). However, the Lagrangian calculation that ARIANE applies cannot resolve diffusion and convection processes, which are instead parameterised in the ocean tracers and dynamic fields. By deploying sufficient amount of particles, the results from the Lagrangian offline calculation are comparable to the advective-diffusive tracer schemes (Wagner *et al.*, 2019).

For each simulation, we deploy 5,000 virtual particles over a primary initial area of 5 km by 5 km. Additionally, particles were released over an alternative initial area of 10 km by 10 km, centred at the same coordinates to the primary initial area, in order to determine if the transport of particles was sensitive to the initial area (table 4.1). The locations are chosen based on the ship traffic densities in the HBC over the last 25 years (Dawson *et al.*, 2018). The three-dimensional advection of these particles is integrated for 2 years starting from their release date. The simulations are repeated for 12 years from 2004 to 2015, with the end of the last simulation in 2017. Within each year, the particles are released every 10 days during the extended operating season from June 1st to Nov 1st. By evaluating the propagation of particles of each release, we can determine over which site and when the spill of the pollutant would have the most severe outcome.

<u>Release Site</u>	<u>Description</u>	<u>Longitude</u>	<u>Latitude</u>
HSE	Hudson Strait	-64.78	60.95
UB	Ungava Bay	-67.05	59.87
HSNW	Hudson Strait Northwest	-76.40	63.84
HSSW	Hudson Strait Southwest	-77.90	62.79
FB	Foxe Basin	-79.35	67.39
FC	Foxe Channel	-81.53	65.28
SI	Southampton Island	-83.07	63.73
CFI	Chesterfield Inlet	-90.07	63.36
CHL	Churchill	-93.83	59.11

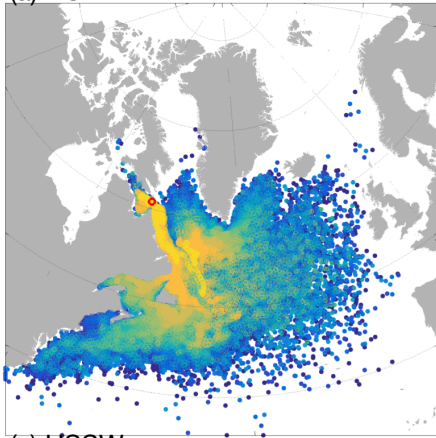
Table 4.1: the approximate location of release sites in the Hudson Bay Complex.

4.3. Circulation Pathways, Time Scales, and Accumulation Regions

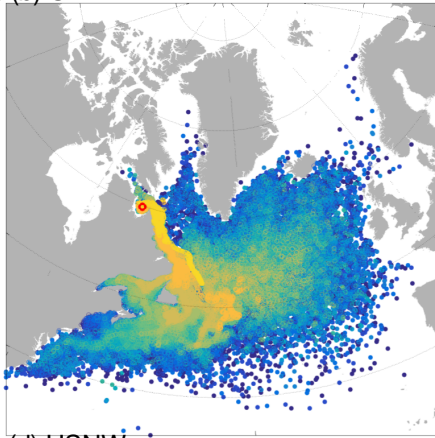
We first analyse the pathways of particles with respect to their propagation time scale to determine the role of oceanic advection in the spread of particles at the different release sites. Furthermore, the regions with the highest probability were computed in order to illustrate the most probable regions for accumulation.

The particles followed three main pathways: (1) eastward outflow via the southern side of Hudson Strait into the Labrador Current; (2) westward inflow via the northern side of Hudson Strait into Foxe Basin and Hudson Bay; and (3) cyclonic circulation within Foxe Basin and Hudson Bay. In figure 4.3, we arbitrarily visualised typical simulation output of all depth from each release site, released in June 1st, 2008, to illustrate how the circulation pathways of particles differs from different initial seeded location. Released in the Eastern Hudson Strait (HSE: Hudson Strait East and UB: Ungava Bay) (fig. 4.3-a and 4.3-b), particles mostly followed the outflow into Labrador Current, and then were mixed with the North Atlantic Current. The western Hudson Strait releases (HSSW: Hudson Strait Southwest and HSNW: Hudson Strait Northwest) (fig. 4.3-c and 4.3-d) show fewer particles following the eastward outflow, with more propagating westward with the inflow along the northern side of Hudson Strait into the interior of the HBC. The particles released in the interior of the HBC show two nodes of propagation. When released in Foxe Channel (FC) or northern Hudson Bay (SI: Southampton Island), the particles followed a mixed regime with propagation into Hudson Bay and Foxe Basin, all three circulation regimes in the HBC, propagated into the Hudson Bay and Foxe Basin, and export via Hudson Strait into the Labrador Current (fig. 4.3-e and 4.3-f). On the other hand, for releases in the interior of Foxe Basin (FB) and Hudson Bay (CFI: Chesterfield Inlet and CHL: Churchill), the particles were mostly constrained to the waterbodies of their release (fig. 4.3-g, 4.3-h, and 4.3-i).

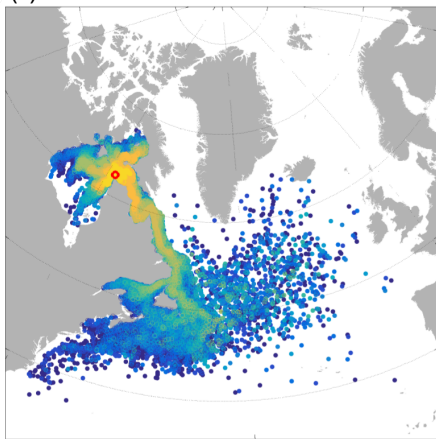
(a) HSE



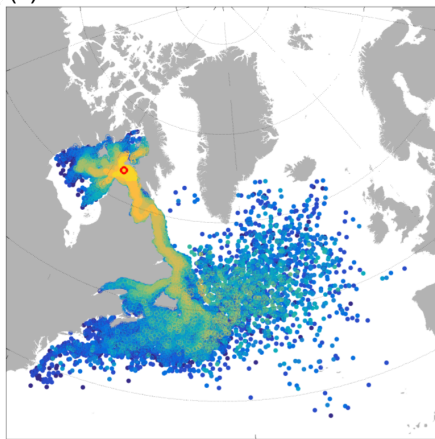
(b) UB



(c) HSSW



(d) HSNW



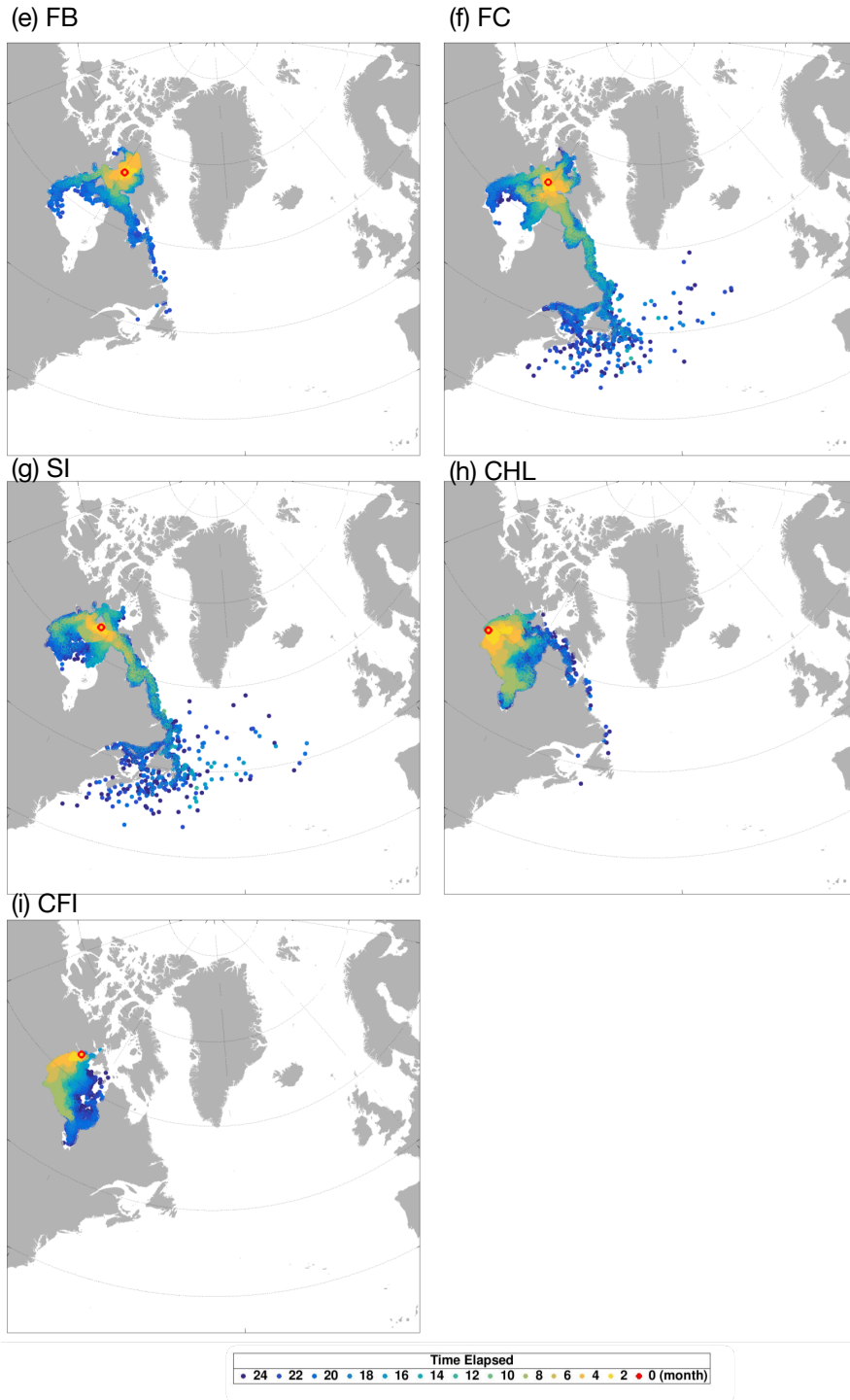


Figure 4.3: advective pathways of particles from each of the release sites marked by the red star, all released from June 1st, 2010 . Colour map indicated elapsed time in months. (a) Hudson Strait East, (b) Ungava Bay, (c) Hudson Strait Southwest, (d) Hudson Strait Northwest, (e) Foxe Basin, (f) Foxe Channel, (g) Southampton Island, (h) Churchill, and (i) Chesterfield Inlet.

4.3.1. Eastern Hudson Strait Releases

The particles released at the two sites in eastern Hudson Strait (HSE and UB) mostly followed the outflow via Hudson Strait (fig. 4.3-a, 4.3-b). There was some recirculation at the mouth of the Hudson Strait, but few particles were found in the interior of the HBC by the end of the simulations. The majority joined the southward Labrador Current immediately after release. Upon reaching Makkovik and Hamilton Banks, the particles were divided into a western branch following the inshore Labrador Current and an eastern branch on the Labrador Shelf before being mixed offshore. When the western coastal branch reaches Newfoundland, some particles turned westward into Gulf of Saint Lawrence via Strait of Belle Isle, while others flowed eastward along the eastern coast of Newfoundland. The latter then divided into several branches upon reaching the Grand Banks. The pathways of these branches were distinctive in the first four months after the release, then they exhibited stronger mixing associated with the North Atlantic Current (Yashayaev and Greenan, 2010). The particles spread into Labrador Sea eight months after release. After two years, particles were found over most of the North Atlantic and had recirculated into Baffin Bay and the Nordic Seas.

The spreading of particles released in the Eastern Hudson Strait is strongly linked to the strength of the North Atlantic Oscillation (NAO). The NAO index describes the strength of fluctuation in the sea level pressure between the Icelandic Low and the Azores High. During a positive year (NAO+), an increased pressure gradient is found over the North Atlantic Ocean (Hurrell *et al.*, 2003), resulting in a larger spread of particles, such as those released in 2008. Vice versa, NAO- limits the spread of particles.

The intra-annual variability is more subtle, exhibited in the manner of propagation, rather than the resultant spreading area, especially comparing to the annual variability. A typical example is fig. 4.3-a, the propagation of particles released from HSE in 2008 June 1st. Two to four months after the release, some particles are found east of Makkovik and Hamilton Banks. They have shown a clear northward flow before spreading into the Labrador Sea. Therefore, we explicitly investigated the propagation of the particles of this simulation during the first six months with a more detailed breakdown of elapsed time every 15 days (figure 4.4). Immediately

after exiting Hudson Strait, the particles formed two branches before propagating southward along the coast of Labrador. The two branches travelled with the Labrador Current parallel to each other until reaching Hamilton Bank when the eastern branch drifts further east. The signal of these two branches is only clear in June and July among all simulations of particles released in 2008. When examining all the June simulations throughout the simulation years, we have found that this did not always occur. For the simulations that did not show the immediate two branches, the particles would follow the eastern path along Labrador Shelf, *i.e.* the main pathway of the Labrador Current.

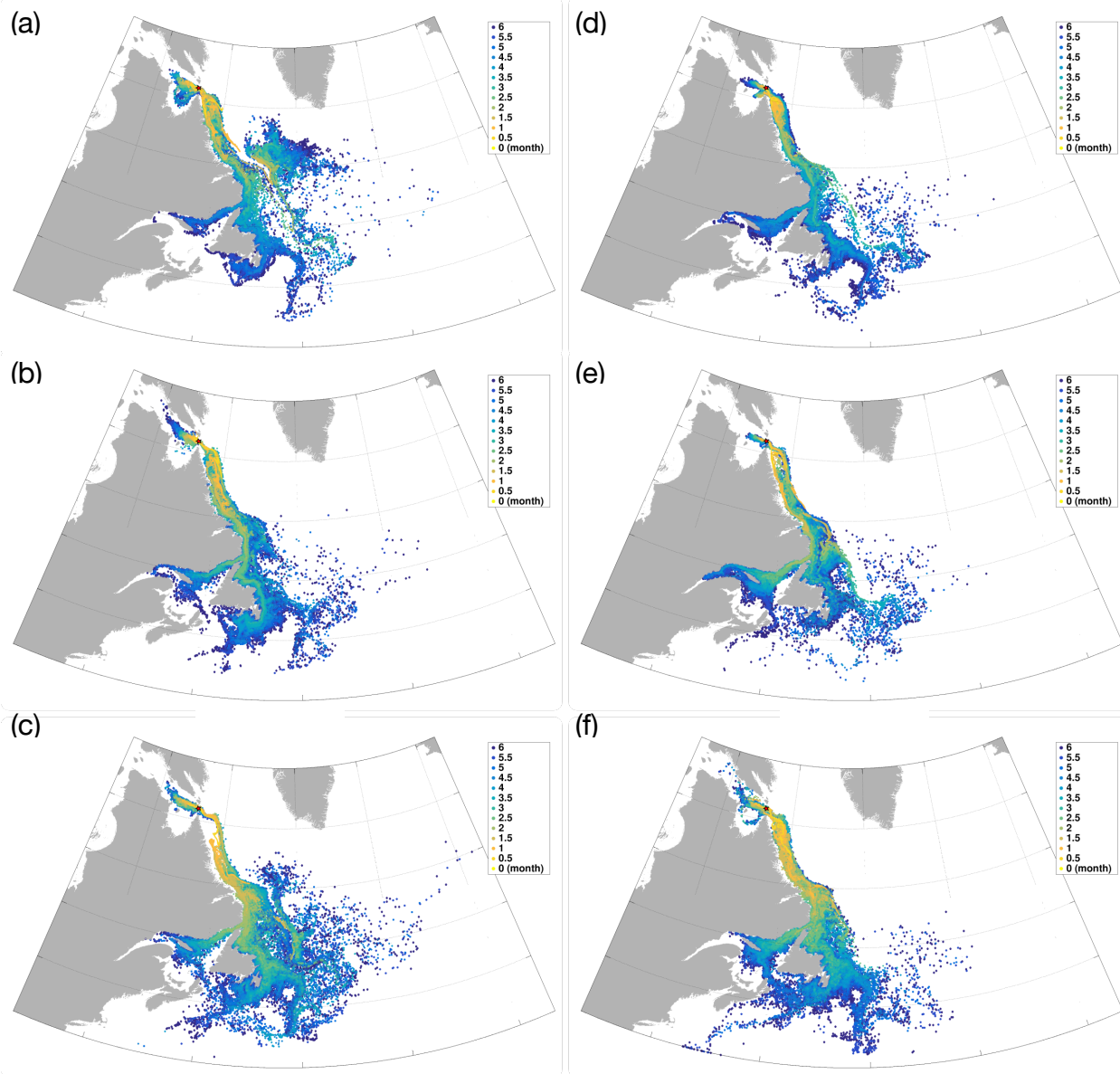


Figure 4.4: Advective pathway of particles from HSE (Hudson Strait East) during first six months after release, colour map shows locations of the particles every 2 weeks (1/2 month). (a), (b), and (c) are released in 2008, June 1st and August 1st, and October 30th, respectively. (c), (d), and (f) are released in 2010, in June 1st and August 1st, and October 30th, respectively.

4.3.2. Western Hudson Strait Releases

The releases in western Hudson Strait (HSSW and HSNW) exhibited two directions of propagation: eastward via Hudson Strait and westward into Hudson Bay and Foxe Basin. Propagating eastward along the southern side of Hudson Strait, particles circumnavigated Ungava Bay and exited Hudson Strait 6 months after release. Once exiting Hudson Strait, they followed the Labrador Current and exhibited similar pathways to those released in Eastern Hudson Strait, with a time lag of 4~6 months. On the inshore side of the Labrador Current, the particles exhibited less offshore mixing until traversing Flemish Pass. Whilst some particles spread into the interior of North Atlantic Ocean, the majority of particles were found in the Gulf of Saint Lawrence and on the Scotian Shelf.

Particles released in western Hudson Strait (WHS) also propagated westward into Foxe Channel immediately after release. These particles were separated into four branches by Southampton Island, Coats Island, and Mansel Island. The four branches consisted of one northward branch into the Foxe Basin and three southward ones into Hudson Bay. Entering Foxe Basin, the particles generally travelled along the northern coast of Southampton Island (fig. 4.3-c and 4.3-d). Some particles turned southward into Hudson Bay via Roes Welcome Sound, and those remaining in Foxe Basin exhibited a smaller rate of spreading due to the lower surface velocities (Saucier *et al.*, 2004). Although particles were found within Foxe Basin almost immediately after the release, only approximately 50% of the waterbody was occupied by the end of the two-year integration. The other three branches propagated southward into the Hudson Bay around 4 months after being released (fig. 4.3-c and 4.3-d). Once entering Hudson Bay, they exhibited broad spreading rather than following a distinctive pathway. The particles occupied most of northern Hudson Bay at the end of the simulation.

The releases from western Hudson Strait exhibited strong annual variability, linked to the NAO index. During a NAO+ year, the particles favoured northward spreading, with greater propagation into Foxe Basin, or to the North Atlantic Ocean. During an NAO- year, the particles exhibited more southward propagation into Hudson Bay (figure 4.5). However, the main pathways of the Western Hudson Strait releases were consistent throughout the experiment period as the NAO only plays a role in promoting the surface mixing of particles. Therefore, we have found that for all the particles released in western Hudson Strait, the highest probability is for them to be found in Foxe Channel, along the southern coast of Hudson Strait, and in Ungava Bay, indicating high concentration of pollutant.

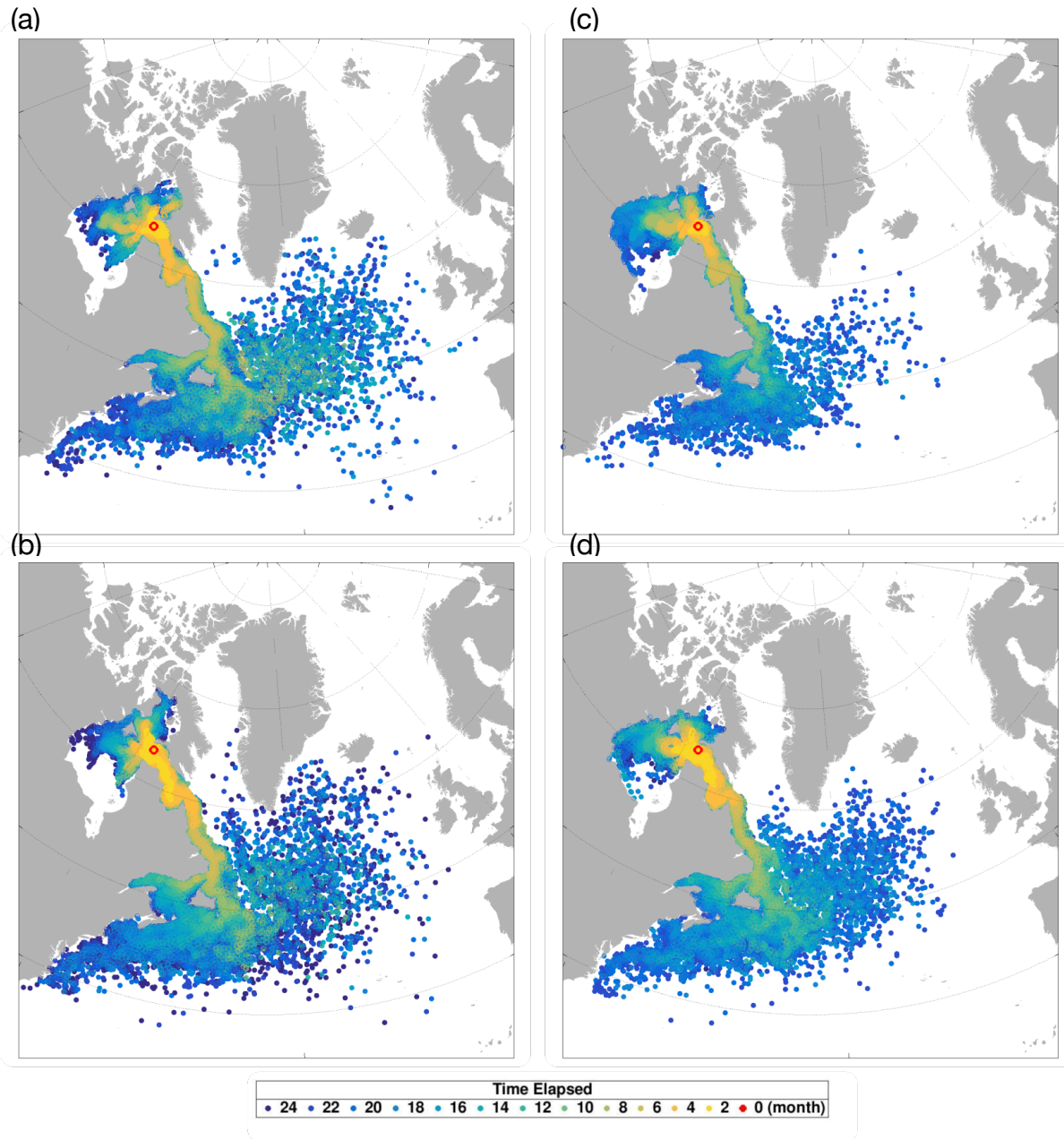


Figure 4.5: advective pathways of particles released from HSNW (Hudson Strait Northwest), colour map indicated position of particles with elapsed time of 2 months. Colourmap indicates locations of particles every two months, and red stars illustrate the initial release location (at month 0). (a) and (b) are released in 2008, June 1st and October 30th, respectively; (c) and (d) are released in 2009, June 1st and October 30th, respectively.

4.3.3. Foxe Basin, Foxe Channel, and Hudson Bay Releases

The particles released in the interior of the HBC were mostly found still within the Complex after two years of integration. However, they were not consistently constrained to the waterbodies that they were seeded in. The particles released in Foxe Basin exhibited a generally southward propagation to Hudson Bay and Hudson Strait. When released in Foxe Channel (FC) and northern Hudson Bay (SI), the particles followed the westward inflow into Foxe Basin and Hudson Bay, as well as the eastward outflow into Hudson Strait. The releases in the interior of Hudson Bay, on the other hand, were contained by the cyclonic circulation within the waterbody.

Particles released in Foxe Basin, rather than forming a distinctive pathway, spread over a large area along the western coast during the first six months after release. This was caused by two factors: (1) the inflow from northern Hudson Strait that promoted westward flow; and (2) the polar inflow via Fury and Hecla Strait was comparably small and inconsistent throughout the year, so that it could not provide a consistent southerly current (Straneo and Saucier, 2008). When reaching the northern side of the Southampton Island approximately one year after release, the particles took two pathways: one branch turned westward, traversed Roes Welcome Sound, then propagated south along the western coast of the Hudson Bay; the other branch turned eastward in Foxe Channel. After turning east, those particles travelled into Foxe Channel forming an eastward branch exiting Hudson Strait and a westward branch propagating along the southern coast of Southampton Island, joining the particles that traversed Roes Welcome Sound. Particles also travelled with the boundary current along the western coast of Hudson Bay.

The particles released in Foxe Channel exhibited three pathways, flowing into all three water bodies. After release, some particles propagated westward and then were divided by the Southampton Island before travelling into Foxe Basin and Hudson Bay. For the particles that travelled northward, some joined the cyclonic circulation in Foxe Basin, with others only circumnavigating Southampton Island and entering Hudson Bay via Roes Welcome Sound approximately 6 months after release. Joining the southward branch, these particles propagated southward along the western coast of Hudson Bay. Additionally, after broadly spreading in northern Hudson Bay and southern Foxe Basin, particles propagated eastward via Hudson Strait.

They entered Hudson Strait eight months after release, with only a small portion joining the Labrador Current by the end of two years of integration.

The particles released within Hudson Bay are mostly limited to Hudson Bay, with only limited export to Hudson Strait occurring in some years. The particles firstly travel southward along the coast of Hudson Bay, following the boundary current for the first four months. Then some particles spread northward, whilst others followed the cyclonic circulation into James Bay. It is usually towards the end of the simulation (after 20 months of integration) that particles entered Hudson Strait.

The releases in the northern HBC (Foxye Basin, Foxye Channel, and northern HB) exhibited inter-annual variability due to the formation of ice in Foxye Basin during late autumn (figure 4.6). Additionally, the variability of the polar outflows via Fury and Hecla Strait could influence the spread of particles in Foxye Basin, as stronger polar outflow promoted the southward flow along the western coast of Foxye Basin. Furthermore, they also experienced annual variability associated with the NAO index: NAO+ promoted eastward transport into the Hudson Strait, whilst NAO- resulted in more particles found along the western coast of Hudson Bay.

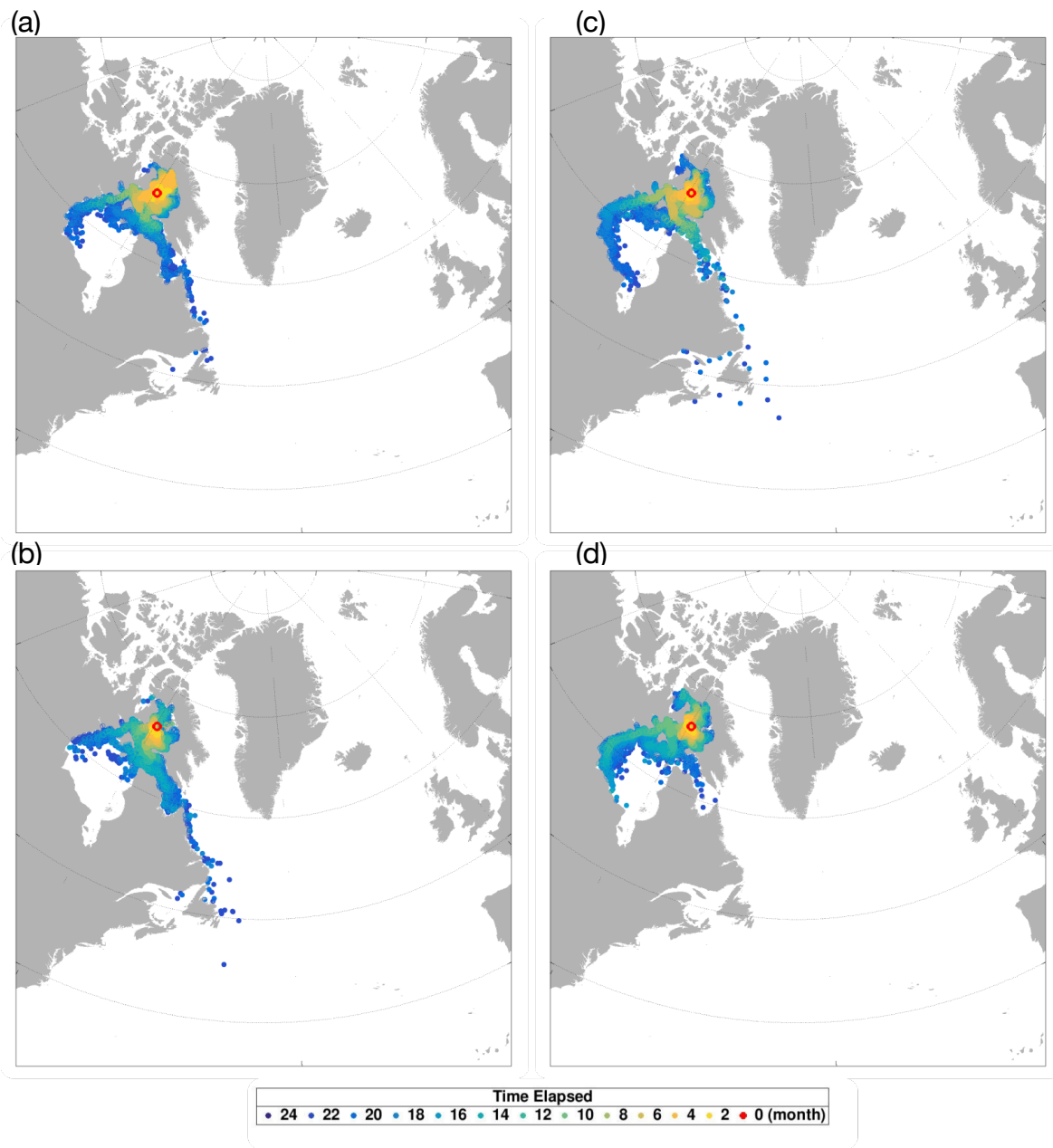


Figure 4.6: advective pathways of particles released from FB (Foxe Basin), colour map indicated position of particles with elapsed time every 2 months, and the red star illustrate the release location. (a) and (b) are released in 2008, June 1st and October 30th, respectively; (c) and (d) are released in 2009, June 1st and October 30th, respectively.

4.4. Discussion

In this section, we will examine the simulations in the HBC in terms of their horizontal spreading area, direct distance of travel, full trajectory throughout the integration, subduction due to advection, variability and uncertainty. Based on the calculations of these parameters, we will determine for which site, the particles exhibited the largest spread with the highest level of variability, and its atmospheric and oceanic contribution.

4.4.1. Horizontal Spreading Area

The horizontal spreading area of particles is a crucial factor in evaluating the severity of the spill. The horizontal spreading area is computed by dividing the model domain into 1/12 degree grid cells, and then determining the number of grid cells occupied by particles. These grid cells were then converted into square kilometres with respect to the horizontal mesh, thus the area occupied by the particles can be calculated. We calculated the average spreading area of all releases from each release site; their standard deviation to represent the level of variability. Furthermore, the envelope area was calculated to represent the total area affected by at least one release; and the ratio of the average area to the envelope area, representing the level of uncertainty throughout the simulation period from each release site (fig. 4.7).

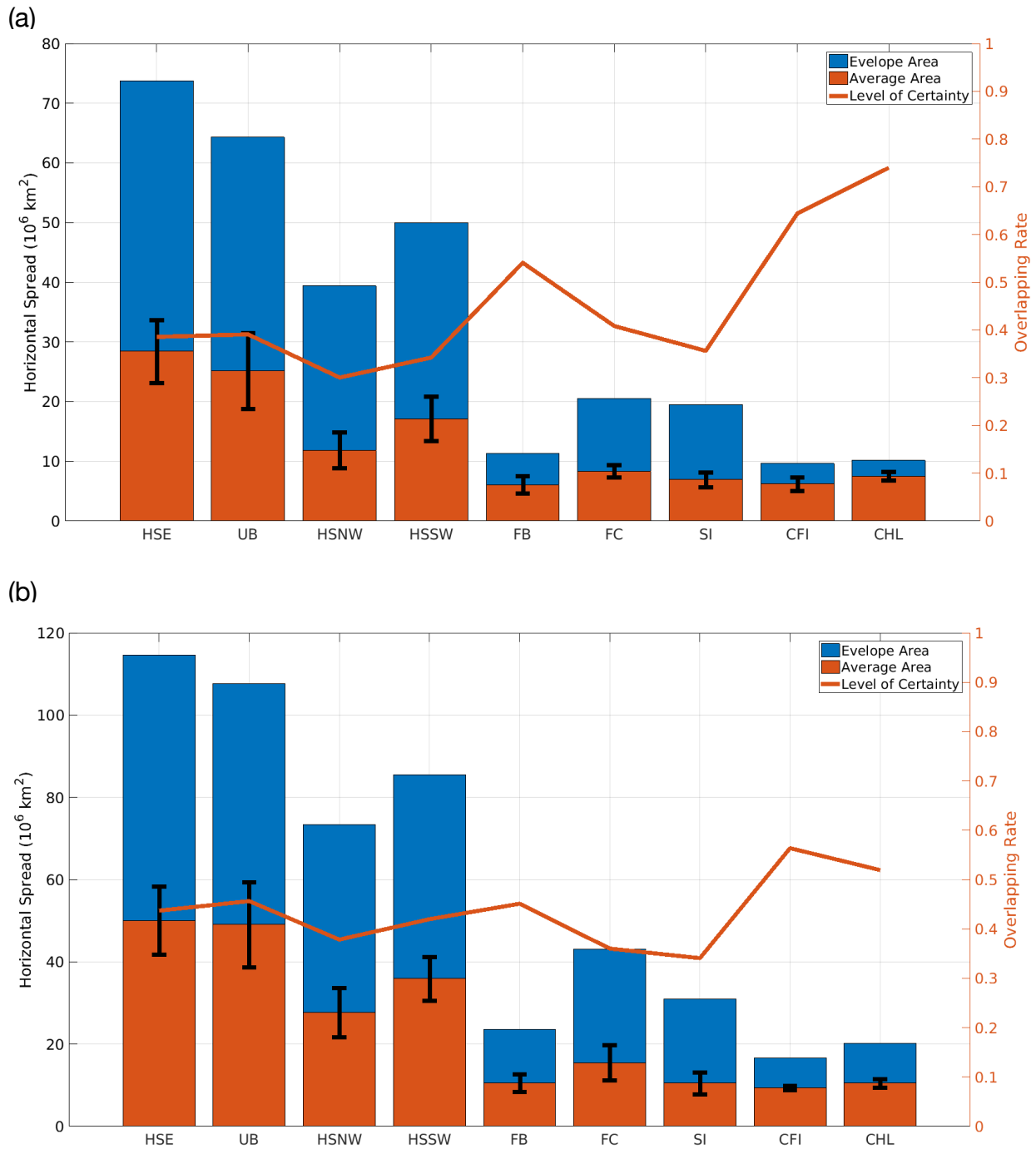


Figure 4.7, average horizontal spreading area, envelope area, variability and uncertainties one year (a) and two years after the release (b). HSE: Hudson Strait East, UB: Ungava Bay, HSNW: Hudson Strait Northwest, HSSW: Hudson Strait Southwest, FB: Foxe Basin, FC: Foxe Channel, SI: Southampton Island, CFI: Chesterfield Inlet, and CHL: Churchill

The average spreading areas and envelope areas correlate well with the propagation of the particles: the Eastern Hudson Strait releases (HSE and UB) have the largest spreading area and envelope area as most particles spread into the North Atlantic Ocean. Comparing to HSE, the UB releases have smaller envelope area as a higher concentration of particles are found to remain within Ungava Bay before joining the Labrador Current, rather than the HSE releases, which exhibited less concentration and more mixing into the North Atlantic Ocean. The releases in Eastern Hudson Strait also exhibited high standard deviation, representing large variability of the spreading area. The small overlapping rates indicated a large level of uncertainty, as the propagation of particles in the North Atlantic Ocean exhibited a high level of variability with overall large spreading area.

Western Hudson Strait releases are the second largest group when considering their spreading area. They contributed to the eastward portion of particles propagating into Hudson Strait and then the Labrador Current. When comparing the two WHS sites, the particles released from the southern side (HSSW) exhibited a larger area of spread due to its proximity to the outflow along southern Hudson Strait. The smaller horizontal spread from the releases on the northern side (HSNW) is due to the proximity of the release site to the inflow. The two releases in the WHS exhibited smaller variability and uncertainty comparing to those at the EHS due to the smaller portion of particles exiting the HBC.

Among the sites within the interior of the Complex, those released in Foxe Channel and northern Hudson Bay exhibited larger spreading and envelope areas. The FC and SI releases have a small level of certainty due to the different pathways that the particles followed under different NAO regimes with a strong east-/westward preference. However, it did not result in large variability in spreading area due to the slower rate of transport.

The releases from Foxe Basin and in interior of Hudson Bay have the smallest spreading with the highest level of certainty as most particles remained within the HBC throughout the simulation. They also presented the smallest variability, due to the fact that although seasonal and interannual variability exists in the circulation of Hudson Bay and Foxe Basin, only the direction of propagation was influenced, rather than the resultant area.

4.4.2. Distances

We calculated the direct distances that particles travelled after one and two years of integration from their initial location to determine how far they travelled. As the footprint of pollutant presents a crucial environmental threat, we are also interested in the full trajectory of particles throughout the simulation (figure 4.8). The strength of recirculation is calculated by calculating the ratio between the direct distance and full trajectory (figure 4.9).

The distances that particles travelled reflected their rate of propagation so that the results correlated well with their circulation pathways. The Eastern Hudson Strait releases exhibited the largest distances. The second group consisted of the two sites in WHS, with those released near the southern coast exhibiting larger distances than those on the northern coast due to the former's proximity to the outflow into the Labrador Current. The particles released in the interior of the HBC have the smallest distance travelled due to the slower rate of surface velocity in Foxe Basin and Hudson Bay and a smaller area of propagation. However, when comparing the distances and horizontal spreading of particles released in Foxe Basin and Hudson Bay, we found that although those released from Hudson Bay had a smaller spreading area, they travelled larger distances than those released in Foxe Basin and Foxe Channel. This is caused by two reasons: (1) the surface velocity in Hudson Bay is faster than that in Foxe Basin; (2) for those particles released in Foxe Basin and Foxe Channel, there are more particles that exited the HBC and joined the Labrador Current than those from Hudson Bay releases. The quantity and large spread of these particles resulted in the larger spreading area from Foxe Basin and Foxe Channel. However, they are not enough to offset the average propagation rate.

When comparing the distances travelled in the first year to the full two years of integration, we found that the full trajectory travelled in the first year is approximately half of that of the two year simulation, indicating that the rate of propagation is similar during the two years after the release. However, it did not result in equivalent increases in distance from the initial location, implying that during the second year, the particles were more subject to recirculation. Therefore, we calculated the ratio between the direct distance and the full trajectory to determine the strength of recirculation for the first year and two full years of simulation. All the releases in the HBC show a stronger signal of recirculation during the second year of release. This correlated well with the circulation pathways and time scales for each release sites.

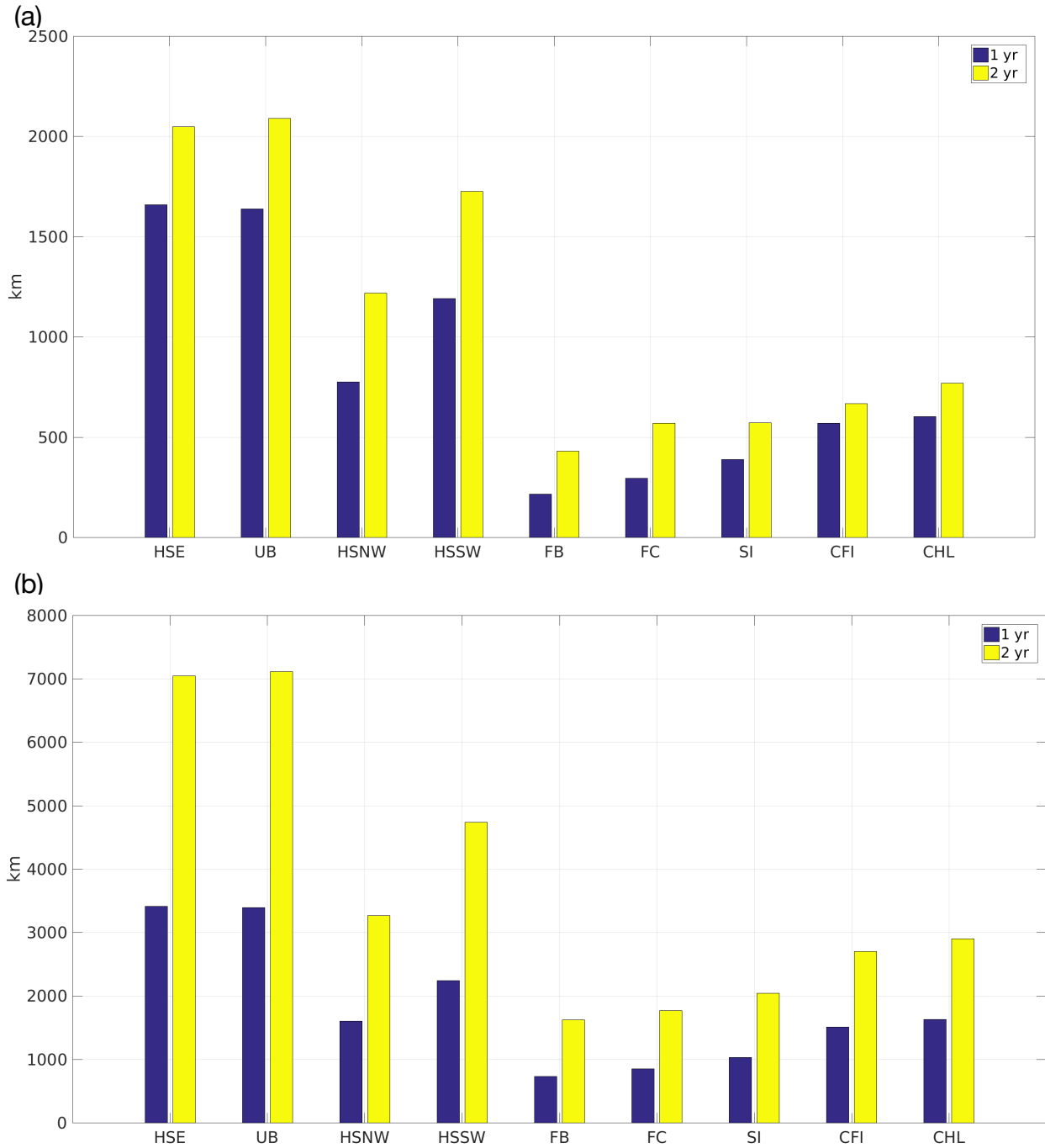


Figure 4.8: average direct distance and full trajectory of particles for all releases from each release site. HSE: Hudson Strait East, UB: Ungava Bay, HSNW Hudson Strait Northwest, HSSW: Hudson Strait Southwest, FB: Foxe Basin, FC: Foxe Channel, SI: Southampton Island, CFI: Chesterfield Inlet, and CHL: Churchill.

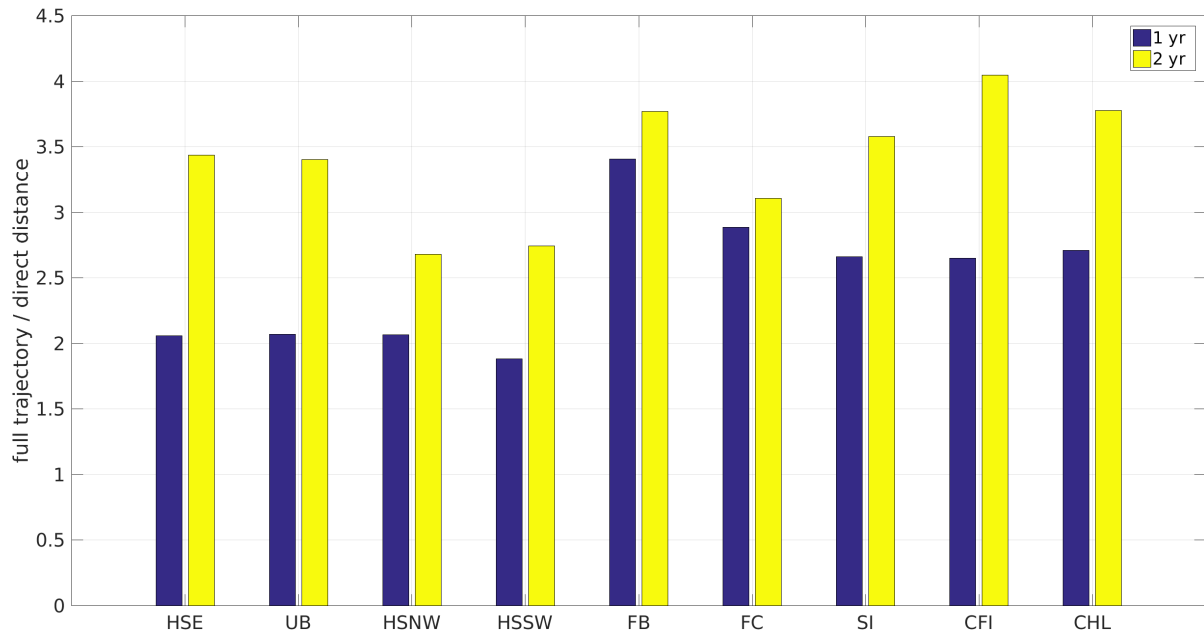


Figure 4.9: strength of recirculation (ratio between the full trajectory to direct distance) for each release sites within Hudson Bay Complex. HSE: Hudson Strait East, UB: Ungava Bay, HSNW Hudson Strait Northwest, HSSW: Hudson Strait Southwest, FB: Foxe Basin, FC: Foxe Channel, SI: Southampton Island, CFI: Chesterfield Inlet, and CHL: Churchill.

4.4.3. Deep Spread

For this study, we considered ship fuel accidentally spilt on the surface to be the focus, so that all particles were set to be released at the sea surface. However, they were vertically mixed by ocean dynamics, posing a significant environmental threat as oil trapped deeper in the water column is extremely difficult to recover. Therefore, we calculated the percentage of particles found with a depth greater than 90 m after one and two years of the release due to subduction caused by advection (figure 4.10).

The percentage of deep spread was closely correlated to the number of particles that propagated eastward. Those released from the Eastern Hudson Strait had the highest percentage of deep spread as the majority of these particles proceeded into the Labrador Current immediately after the release, and then exhibited a large spread over the North Atlantic Ocean (figure 4.11-a and 4.11-b). The two sites in western Hudson Strait exhibited significant differences in the percentage of deep spread due to more particles released from the HSSW exiting Hudson Strait (figure 4.11-c and 4.11-d). FC and SI releases exhibited a larger deep spread when compared to the other release sites in the interior of HBC as some of the particles from both of these release sites propagated eastward (figure 4.11-e to 4.11-k).

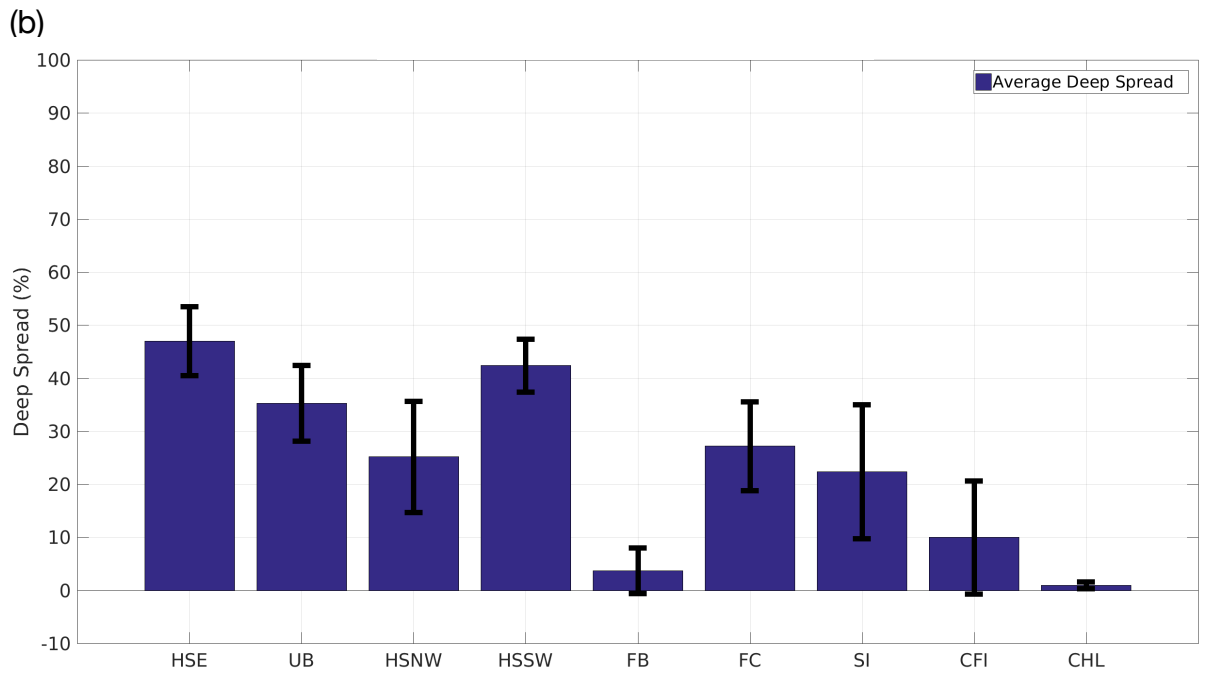
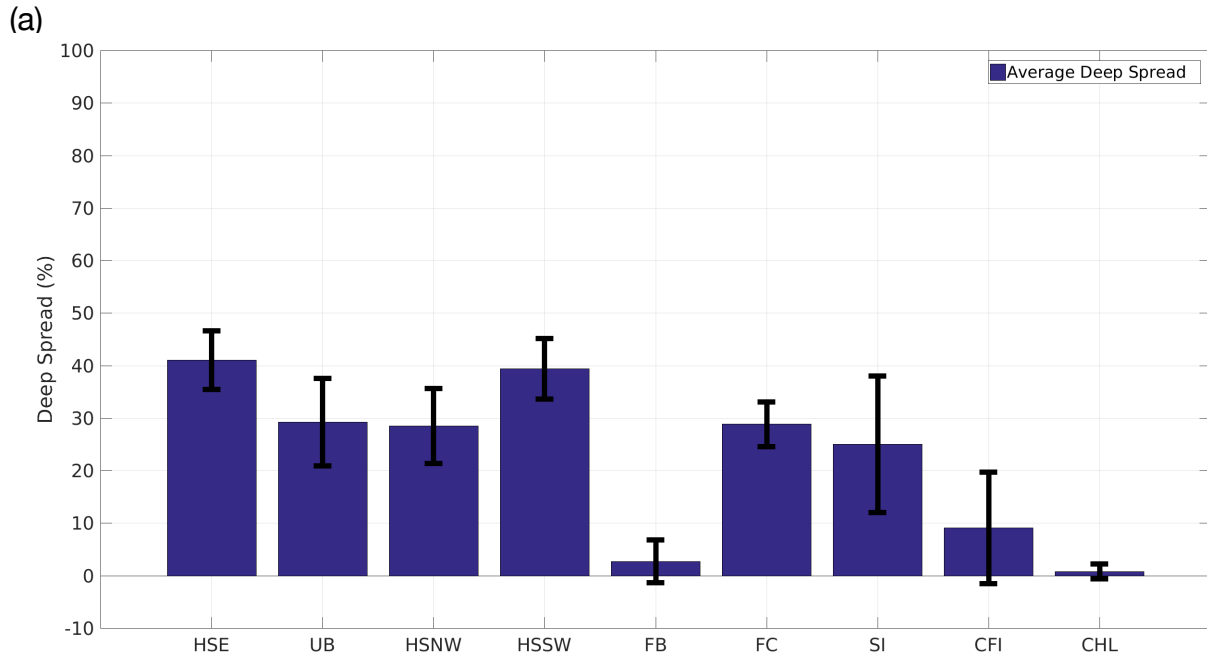
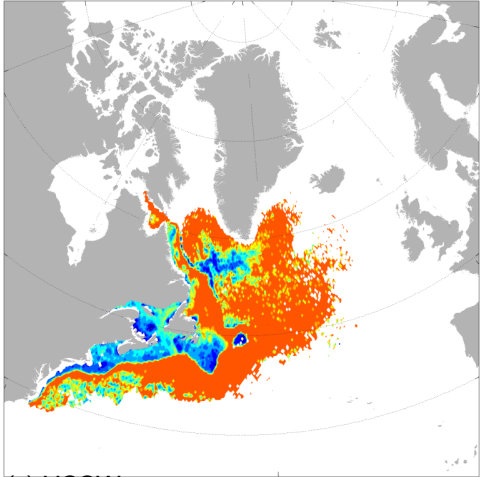
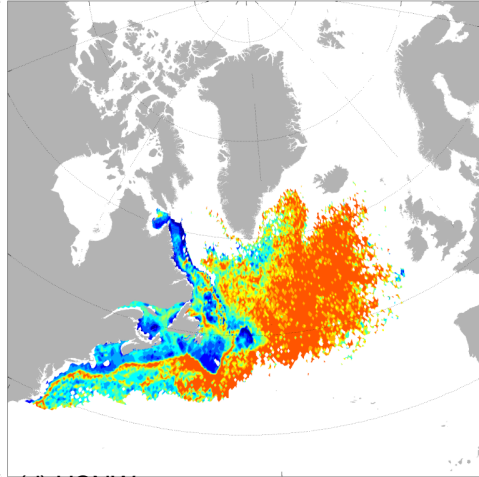


Figure 4.10: average percentage of particles with depth exceeding 90 m one year (a) and two years (b) after the release. Black bars indicate standard deviation. HSE: Hudson Strait East, UB: Ungava Bay, HSNW Hudson Strait Northwest, HSSW: Hudson Strait Southwest, FB: Foxe Basin, FC: Foxe Channel, SI: Southampton Island, CFI: Chesterfield Inlet, and CHL: Churchill.

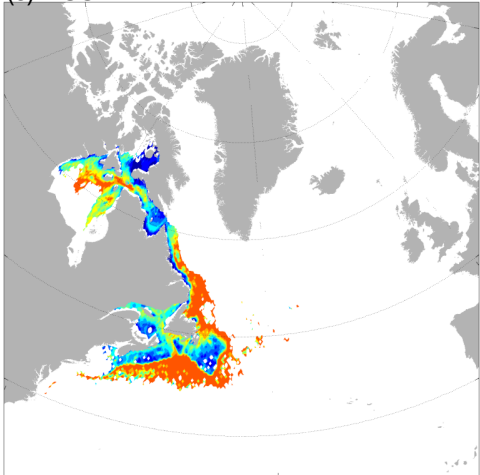
(a) HSE



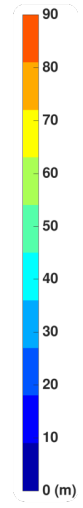
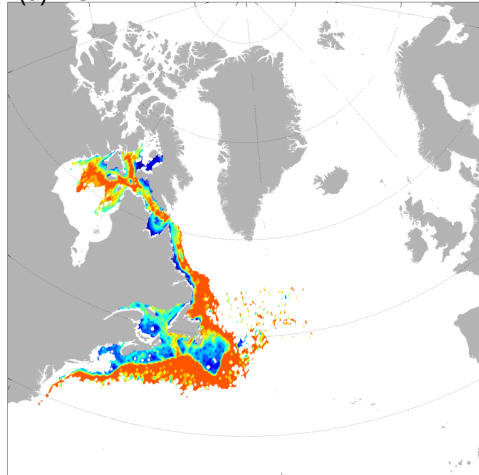
(b) UB



(c) HSSW



(d) HSNW



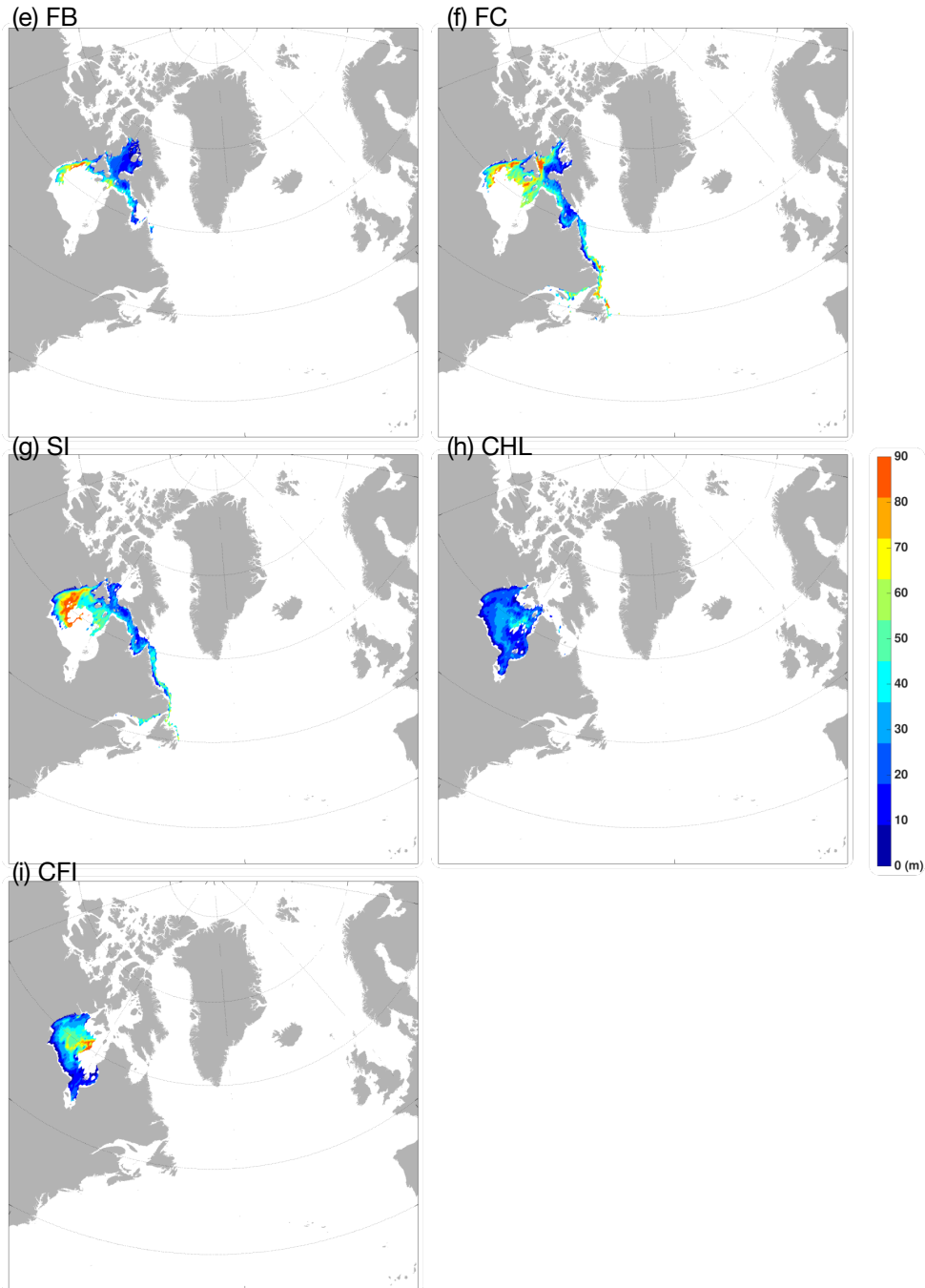


Figure 4.11: particle depth at the end of two year simulation from each of the release sites marked by the red star, all released from June 1st, 2008. Colour map indicated elapsed time in months. (a) Hudson Strait East, (b) Ungava Bay, (c) Hudson Strait Southwest, (d) Hudson Strait Northwest, (e) Foxe Basin, (f) Foxe Channel, (g) Southampton Island, (h) Churchill, and (i) Chesterfield Inlet.

4.4.4. Variability and Sensitivity

When calculating the spreading area, distances, and percentage of deep spread, we found a different level of variability between release sites caused by the annual and inter-annual variability in the circulation pathways. Therefore, we explicitly calculated the annual and seasonal averages for each release site in this section, to determine from which sites, the particles exhibited significant sensitivity to the different release time.

We investigated the interannual and annual variability in spreading area from each release sites (fig. 4.12 and 4.13, respectively). When examining the spreading area one year after the release (fig. 4.12-a), we found a decrease towards the end of the operating season, especially for those particles released in the Eastern Hudson Strait. When released at the end of the operating season, there were significantly less eastward spread into the offshore during the first year of integration. This could be caused by shift of NAO index from negative to weak positive phase towards winter. Two years after the release (fig. 4.12-b), the inter-annual variability decreased as more particles propagated into the North Atlantic Ocean. This recirculation of particles released at the end of the operating season occurred after they passed Newfoundland and turned westward. The particles spread into the North Atlantic Ocean were found with a 4~6 month time lag when compared to those released at the beginning of the operating season, resulting in fewer particles spread into the Labrador Sea and Nordic Seas.

The annual variability (fig. 4.13) is more significant, especially for the particles released in Hudson Strait. In eastern Hudson Strait (HSE and UB), we found maximum spreading area in 2008 and 2011, whilst minimum in 2007 and 2009. Released in western Hudson Strait (HSNW and HSSW), the largest spreading area was from 2011 releases, whilst the smallest in 2015. Particles released in Foxe Basin, Foxe Channel, and Hudson Bay showed insignificant annual variabilities when comparing to those from Hudson Strait. The majority of particles released in eastern Hudson Strait propagated into the North Atlantic Ocean; their circulation was linked to the NAO. The annual NAO data was downloaded from the Climate Prediction Centre (CPC), National Oceanic and Atmospheric Administration (available from: <https://www.cpc.ncep.noaa.gov/products/precip/CWlink/pna/nao.shtml>). For the eastern Hudson Strait

releases, the strong positive NAO during two years of integration after released in 2008 and 2011 promoted large spreading, whilst the strong NAO- phase in 2010 resulted in the minimum spreading area. Released in western Hudson Strait, only a few of particles propagated into the North Atlantic Ocean. Therefore, we observed some similarities in the annual variability, indicating that NAO only played a limited role.

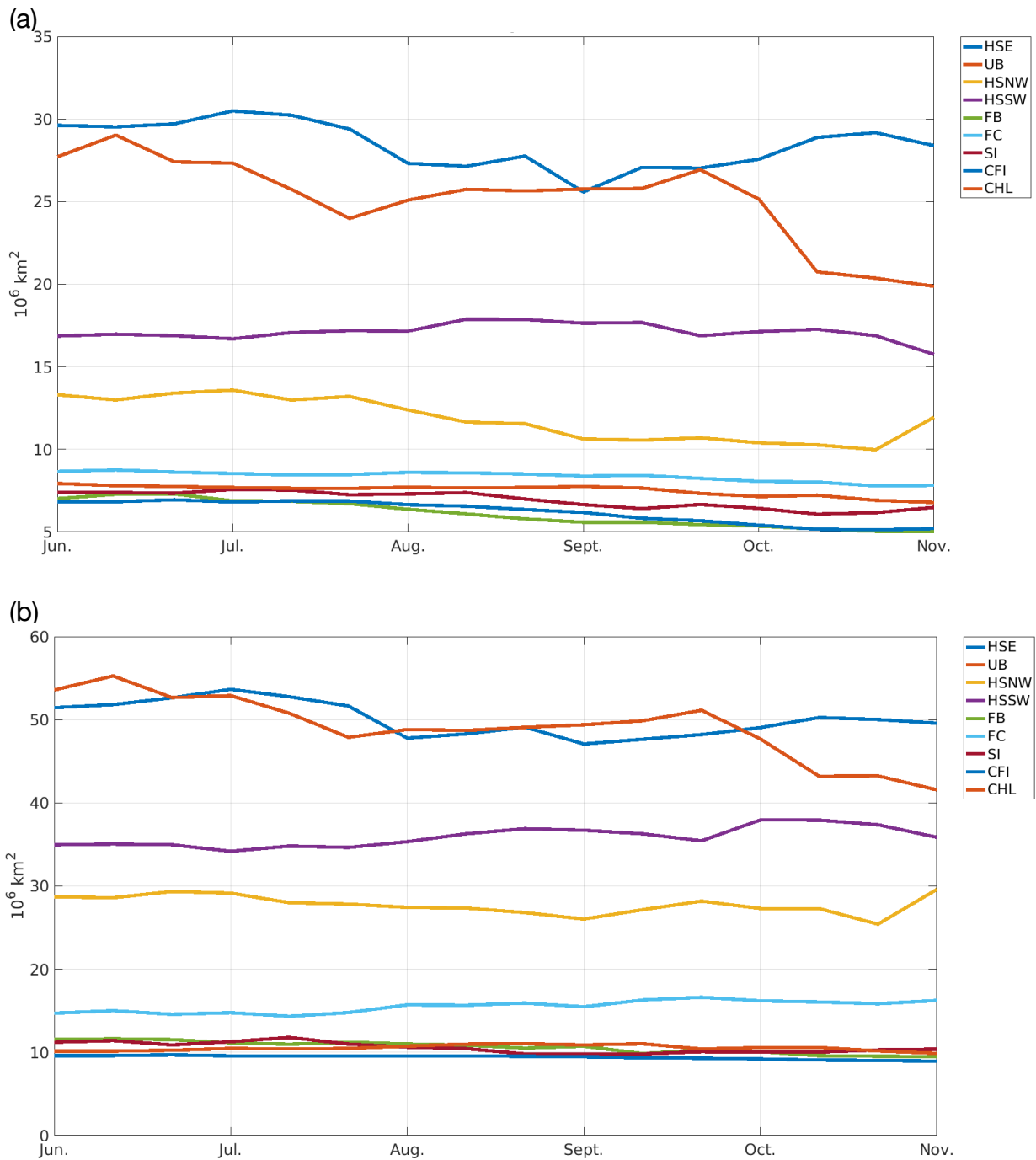


Figure 4.12, Inter-annual average horizontal spreading area from each release date during one year (a) and two years (b) simulation for each release sites. HSE: Hudson Strait East, UB: Ungava Bay, HSNW Hudson Strait Northwest, HSSW: Hudson Strait Southwest, FB: Foxe Basin, FC: Foxe Channel, SI: Southampton Island, CFI: Chesterfield Inlet, and CHL: Churchill.

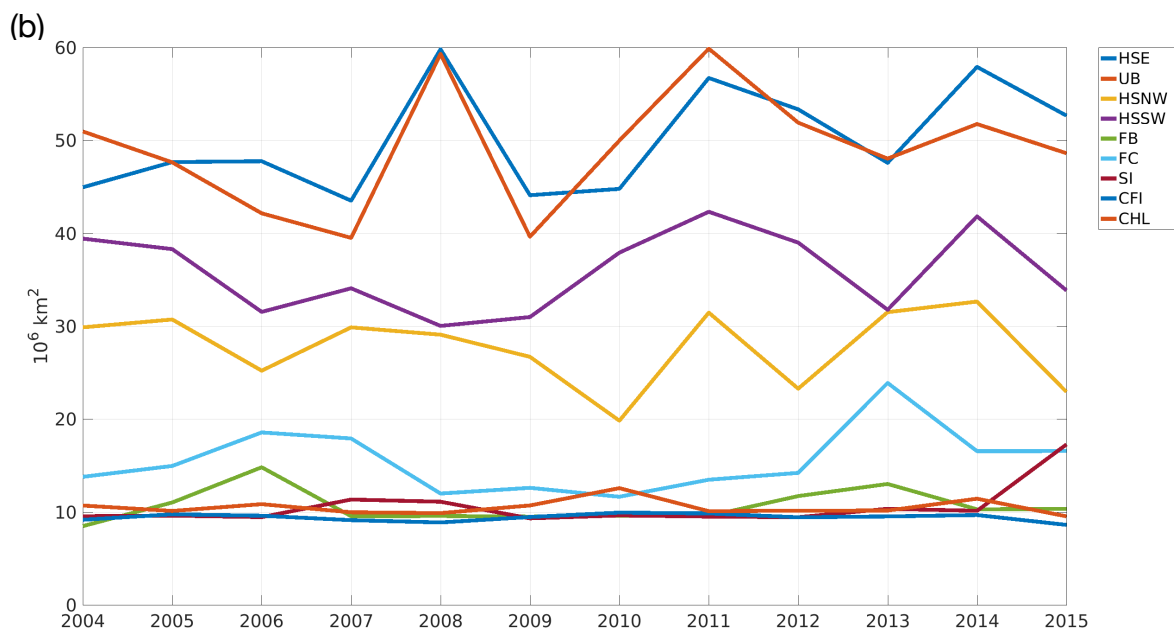
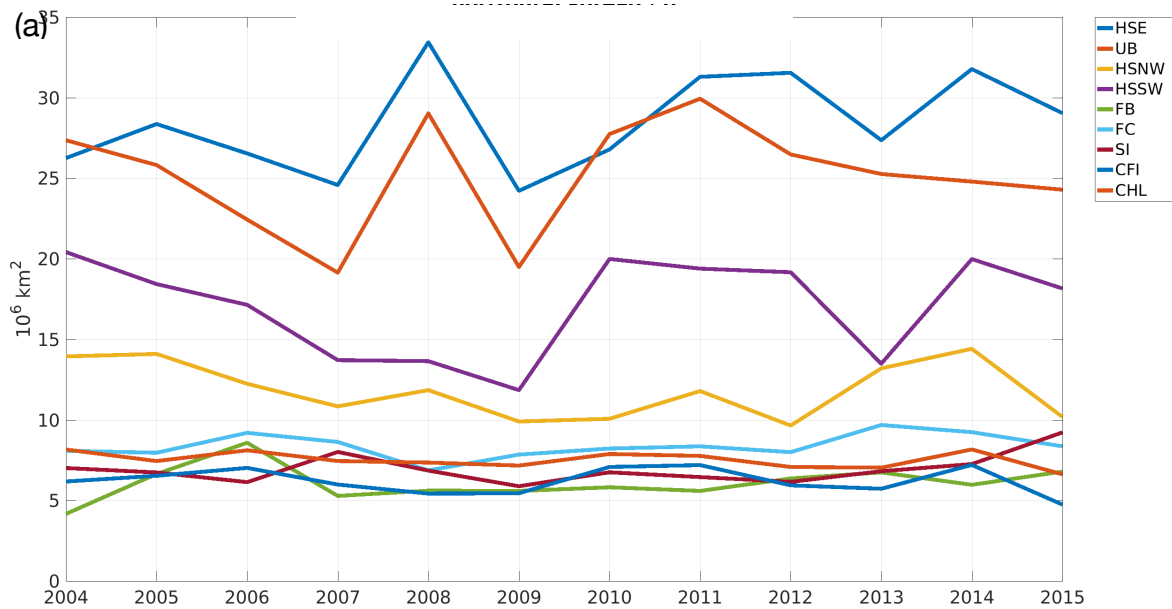


Figure 4.13, Yearly averages of horizontal spreading area during one year (a) and two years (b) simulation for each release sites. HSE: Hudson Strait East, UB: Ungava Bay, HSNW Hudson Strait Northwest, HSSW: Hudson Strait Southwest, FB: Foxe Basin, FC: Foxe Channel, SI: Southampton Island, CFI: Chesterfield Inlet, and CHL: Churchill.

Due to the complexity of water exchange in the eastern HBC, the spread of particles is extremely sensitive to the location of release. For instance, in eastern Hudson Strait, the distance between HSE and UB is less than 175 km, however, the particles exhibited different circulation pathways. The particles released in the HSE spread further north and east, resulting in a larger percentage of deep spread. Another example is those released in western Hudson Strait. The two release sites (HSSW and HSNW) are approximately 130 km apart. The simulation results exhibited large differences as the HSSW releases mainly followed the eastward outflow along the southern coast whilst the HSNW releases followed the westward inflow along the northern coast.

Furthermore, in order to represent different types of pollutant, we investigated the spreading area and distances of particles released over a larger initial area of 10 km by 10 km. We have found that the spread and propagation of particles released in the HBC were not sensitive to a different initial area with differences smaller than 5% (not shown).

A limitation of this research at present is the passive particles used to represent pollutant. Although we attempted to represent the product of weathering processes occurring days after the accidental spill, there are processes, such as sedimentation and emulsification, that can take place months after the spill (Afenyo *et al.*, 2016). Another limitation of this work is the lack of encapsulation, by which oil is trapped with sea ice, and travels with sea ice. Whether oil drifts with oceanic advection or sea ice movement depends on the sea ice concentration: if sea ice concentration exceeds 60%, the transport pathways of oil would travel with the drift of sea ice instead of oceanic advection (Venkatesh *et al.*, 1990). These processes will be considered in future studies.

4.5. Conclusion

In this study, we examine the transport pathways and spreading of pollutant spilt due to oceanic advection in the Hudson Bay Complex along the Arctic Bridge and the southern route of the Northwest Passage traversing Foxe Basin. Released in the Hudson Bay Complex, the particles followed three main pathways: eastward outflow via the southern coast of Hudson Strait into the Labrador Current, and following inflow by the Baffin Island Current along the northern coast of Hudson Strait, the weak anti-cyclonic circulation in the Foxe Basin, and the cyclonic circulation in the Hudson Bay.

Among all 9 release sites, we have found that the releases in the Western Hudson Strait exhibited the largest spreading area, furthest distances, and the largest portion of particles propagated deep into the water column. Almost immediately after the release, the particles joined the Labrador Current and exhibited a large spread into the interior of the North Atlantic Ocean four months after the release. The Eastern Hudson Strait releases also exhibited the largest uncertainty as their propagation is extremely sensitive to the North Atlantic Oscillation. Over a relatively short time period (1~2 years), particles released from eastern Hudson Strait could be found over most of the North Atlantic Ocean, even in the Nordic Seas. Over 50% of the particles were found at depth over 90 metres, presenting the most severe consequences and being extremely challenging for recovery operations.

This study focused on the role of oceanic advection in the spread of pollutant spilt in the Hudson Complex. Although limitations exist in the lack of reaction between the pollutant and the ocean, this work provides an oceanographic overview illustrating the general circulation pathways and trajectories that pollutant would take. Furthermore, this study highlighted the release sites with the most severe outcome, illuminating a focus for detailed case studies of oil spills.

Acknowledgement

The high-resolution NEMO simulation run by the Oceanic Modelling group from the University of Alberta, whose output can be made available by contacting Prof. Dr. Paul Myers via pmyers@ualberta.ca. ARIANE integration was performed via Compute Canada (computeCanada.ca). For model evaluation, we obtained field measurements at Davis Strait via the long-term monitoring programme, which began in September 2004, processed by Curry *et al.* (2011). Satellite observation for sea ice concentration was provided by the integrated Climate Data Record of Passive Microwave Sea Ice Concentration, available via <https://nsidc.org/data/G02202/versions/3>.

Bibliography

- Afenyo, M., Veitch, B., & Khan, F. (2016). A State-of-the-Art Review of Fate and Transport of Oil Spills in Open and Ice-Covered Water. *Ocean Engineering*, *119*, 233-248. Doi:/10.1016/J.Oceaneng.2015.10.014
- Andrews, J., Babb, D., & Barber, D. G. (2018). Climate Change and Sea Ice: Shipping in Hudson Bay, Hudson Strait, and Foxe Basin (1980–2016). *Elem Sci Anth*, *6*(1), 19. Doi:10.1525/Elementa.281
- Blanke, B., & Raynaud, S. (1997). Kinematics of the Pacific Equatorial Undercurrent: an Eulerian and Lagrangian Approach From GCM Results. *Journal of Physical Oceanography*, *27*(6), 1038-1053.
- Courtois, P., Hu, X., Pennelly, C., Spence, P., & Myers, P. G. (2017). Mixed Layer Depth Calculation in Deep Convection Regions in Ocean Numerical Models Doi:Https://Doi.Org/10.1016/J.Ocemod.2017.10.007
- Curry, B., Lee, C. M., & Petrie, B. (2011). Volume, Freshwater, and Heat Fluxes Through Davis Strait, 2004–05. *Journal of Physical Oceanography*, *41*(3), 429-436. doi:10.1175/2010JPO4536.1
- Dawson, J., Pizzolato, L., Howell, S. E. L., Copland, L., & Johnston, M. E. (2018). Temporal and Spatial Patterns of Ship Traffic in the Canadian Arctic From 1990 to 2015. *Arctic*, *71*(1), 15-26. Doi:10.14430/Arctic4698
- Drozdowski, A., Nudds, S., Hannah, C. G., Niu, H., Peterson, I., & Perrie, W. (2011). *Review of Oil Spill Trajectory Modelling in the Presence of Ice*. Canada
- DRAKKAR, Barnier, 2007 Eddypermitting ocean circulation hindcasts of past decades. *CLIVAR Exchanges* *12* (3), 8–10.
- Feucher, C., Garcia-Quintana, Y., Yashayaev, I., Hu, X., & Myers, P. G. (2019). Labrador Sea Water Formation Rate and its Impact on the Local Meridional Overturning

- Circulation. *Journal of Geophysical Research: Oceans*, 124(8), 5654-5670. Doi:10.1029/2019JC015065
- Fratantoni, P. S., & McCartney, M. S. (2010). Freshwater Export From the Labrador Current to the North Atlantic Current at the Tail of the Grand Banks of Newfoundland Doi:https://doi.org/10.1016/j.jdsr.2009.11.006
- Garcia-Quintana, Y., Courtois, P., Hu, X., Pennelly, C., Kieke, D., & Myers, P. G. (2019). Sensitivity of Labrador Sea Water Formation to Changes in Model Resolution, Atmospheric Forcing, and Freshwater Input. *Journal of Geophysical Research: Oceans*, 124(3), 2126-2152. Doi:10.1029/2018JC014459
- Gillard, L. C., Hu, X., Myers, P. G., & Bamber, J. L. (2016). Meltwater Pathways From Marine Terminating Glaciers of the Greenland Ice Sheet. *Geophysical Research Letters*, 43(20), 10,873-10,882. Doi:10.1002/2016GL070969
- Grivault, N., Hu, X., & Myers, P. G. (2018). Impact of the Surface Stress on the Volume and Freshwater Transport Through the Canadian Arctic Archipelago From a High-Resolution Numerical Simulation. *Journal of Geophysical Research: Oceans*, 123(12), 9038-9060. Doi:10.1029/2018JC013984
- Hu, X., Sun, J., Chan, T. O., & Myers, P. G. (2018). Thermodynamic and Dynamic Ice Thickness Contributions in the Canadian Arctic Archipelago in NEMO-LIM2 Numerical Simulations. *The Cryosphere*, 12(4), 1233-1247. Doi:10.5194/tc-12-1233-2018
- Hu, X., Myers, P. G., & Lu, Y. (2019). Pacific Water Pathway in the Arctic Ocean and Beaufort Gyre in Two Simulations With Different Horizontal Resolutions. *Journal of Geophysical Research: Oceans*, 124(8), 6414-6432. Doi:10.1029/2019JC015111
- Hughes, K. G., Klymak, J. M., Hu, X., & Myers, P. G. (2017). Water Mass Modification and Mixing Rates in a 1/12° Simulation of the Canadian Arctic Archipelago. *Journal of Geophysical Research: Oceans*, 122(2), 803-820. Doi:10.1002/2016JC012235
- Hurrell, J. W., Kushnir, Y., Ottersen, G., & Visbeck, M. (2003). The North Atlantic Oscillation: Climatic Significance and Environmental Impact Doi:10.1029/GM134

- Jones, E. P., & Anderson, L. G. (1994). Northern Hudson Bay and Foxe Basin: Water Masses, Circulation and Productivity. *Atmosphere-Ocean*, 32(2), 361-374. Doi:10.1080/07055900.1994.9649502
- Kelly, S., Popova, E., Aksenov, Y., Marsh, R., & Yool, A. (2018). Lagrangian Modeling of Arctic Ocean Circulation Pathways: Impact of Advection on Spread of Pollutants. *Journal of Geophysical Research: Oceans*, 123(4), 2882-2902. Doi:10.1002/2017JC013460
- Mertz, G., Narayanan, S., & Helbig, J. (1993). The Freshwater Transport of the Labrador Current. *Atmosphere-Ocean*, 31(2), 281-295. Doi:10.1080/07055900.1993.9649472
- Østreg, W., Eger, K. M., Fløistad, B., Jørgensen-Dahl, A., Lothe, L., Mejlinder-Larsen, M., . . . Wergeland, T. (2013). *Shipping In Arctic Waters: A Comparison Of The Northeast, Northwest And Trans Polar Passages* Doi:10.1007/978-3-642-16790-4
- Østreg, W. (2013). *Shipping in Arctic Waters : a Comparison of the Northeast, Northwest and Trans Polar Passages*. Berlin ;New York: Springer. Retrieved From [Http://Link.Springer.Com/10.1007/978-3-642-16790-4](http://Link.Springer.Com/10.1007/978-3-642-16790-4)
- Parkinson, C. L. (2014). Spatially Mapped Reductions in the Length of the Arctic Sea Ice Season. *Geophysical Research Letters*, 41(12), 4316-4322. Doi:10.1002/2014GL060434
- Pennelly, C., Hu, X., & Myers, P. G. (2019). Cross-Isobath Freshwater Exchange Within the North Atlantic Subpolar Gyre. *Journal of Geophysical Research: Oceans*, 124(10), 6831-6853. Doi:10.1029/2019JC015144
- Prinsenber, S. J. (1986). In Martini I. P. (Ed.), *Chapter 12 on the Physical Oceanography of Foxe Basin* Elsevier. Doi:/10.1016/S0422-9894(08)70905-X
- Prowse, T. D., Furgal, C., Chouinard, R., Melling, H., Milburn, D., & Smith, S. L. (2009). Implications of Climate Change for Economic Development in Northern Canada: Energy, Resource, and Transportation Sectors. *AMBIO: a Journal of the Human Environment*, 38(5), 272-281. Retrieved From [Https://Doi.Org/10.1579/0044-7447-38.5.272](https://Doi.Org/10.1579/0044-7447-38.5.272)

- Ridenour, N. A., Hu, X., Jafarikhasragh, S., Landy, J. C., Lukovich, J. V., Stadnyk, T. A., . . . Barber, D. G. (2019a). *Sensitivity of Freshwater Dynamics to Ocean Model Resolution and River Discharge Forcing in the Hudson Bay Complex* Doi:/10.1016/J.Jmarsys.2019.04.002
- Ridenour, N. A., Hu, X., Sydor, K., Myers, P. G., & Barber, D. G. (2019b). Revisiting the Circulation of Hudson Bay: Evidence for a Seasonal Pattern. *Geophysical Research Letters*, 46(7), 3891-3899. Doi:10.1029/2019GL082344
- Saucier, F., Senneville, S., Prinsenber, S., Roy, F., Smith, G., Gachon, P., . . . Laprise, R. (2004). Modelling the Sea Ice-Ocean Seasonal Cycle in Hudson Bay, Foxe Basin and Hudson Strait, Canada. *Climate Dynamics*, 23(3), 303-326. Doi:10.1007/S00382-004-0445-6
- Serreze, M. C., & Stroeve, J. (2015). Arctic Sea Ice Trends, Variability and Implications for Seasonal Ice Forecasting. *Philosophical Transactions of the Royal Society A: Mathematical, Physical and Engineering Sciences*, 373(2045), 20140159. Doi:10.1098/Rsta.2014.0159
- Smith, G. C., Roy, F., Mann, P., Dupont, F., Brasnett, B., Lemieux, J., . . . Bélair, S. (2014). A New Atmospheric Dataset for Forcing Ice–Ocean Models: Evaluation of Reforecasts Using the Canadian Global Deterministic Prediction System. *Quarterly Journal of the Royal Meteorological Society*, 140(680), 881-894. Doi:10.1002/Qj.2194
- Sørstrøm, S. E., Brandvik, P. J., Buist, I., Daling, P., Dickins, D., Faksness, L., . . . Singsaas, I. (2010). *Joint Industry Program On Oil Spill Contingency For Arctic And Ice-Covered Waters : Summary Report..* Trondheim
- Straneo, F., & Saucier, F. (2008a). The Outflow From Hudson Strait and its Contribution to the Labrador Current Doi:Https://Doi.Org/10.1016/J.Dsr.2008.03.012
- Straneo, F., & Saucier, F. J. (2008b). The Arctic–Subarctic Exchange Through Hudson Strait. In R. R. Dickson, J. Meincke & P. Rhines (Eds.), *Arctic–Subarctic Ocean Fluxes: Defining the Role of the Northern Seas in Climate* (Pp. 249-261). Dordrecht: Springer Netherlands.

- Tivy, A., Alt, B., Howell, S., Wilson, K., & Yackel, J. (2007). Long-Range Prediction of the Shipping Season in Hudson Bay: a Statistical Approach. *Weather and Forecasting*, 22(5), 1063-1075. Doi:10.1175/WAF1038.1
- Tivy, A., Howell, S. E. L., Alt, B., McCourt, S., Chagnon, R., Crocker, G., . . . Yackel, J. J. (2011). Trends and Variability in Summer Sea Ice Cover in the Canadian Arctic Based on the Canadian Ice Service Digital Archive, 1960–2008 and 1968–2008. *Journal of Geophysical Research: Oceans*, 116 Doi:10.1029/2009JC005855
- Transport Canada and Canadian Coast Guard. Assessment of Proposals Related to Oil Spill Risk for the South Coast of Newfoundland
- Venkatesh, S., El-Tahan, H., Comfort, G., & Abdelnour, R. (1990). Modelling the Behaviour of Oil Spills in Ice-Infested Waters. *Atmosphere-Ocean*, 28(3), 303-329. Doi:10.1080/07055900.1990.9649380
- Wagner, P., Rühls, S., Schwarzkopf, F. U., Koszalka, I. M., & Biastoch, A. (2019). Can Lagrangian Tracking Simulate Tracer Spreading In A High-Resolution Ocean General Circulation Model? *Journal of Physical Oceanography*, 49(5), 1141-1157. Doi:10.1175/JPO-D-18-0152.1
- Yashayaev, I., & Greenan, B. (2010). Environmental Conditions in the Labrador Sea in 2009.

Chapter 5

The Role of Oceanic Advection and Circulation Pathways in the Spread of Pollutant in the Canadian Northwest Passages

This chapter is independently written and is prepared to become a publication with authorship of Ran Tao and Paul G Myers.

Abstract

Over the past decades, Arctic sea ice has been decreasing dramatically, resulting in more open water for a longer period. This promotes ship traffic transiting the Arctic Ocean, and opens opportunity for the commercial opening of the Northwest Passages (NWP) along the Canadian Arctic. Canadian Arctic consists of complex waterways, harsh environment, and insufficient supportive infrastructures, therefore, increasing ship traffic would promote higher risk of accidents. Therefore, we are motivated to determine the longterm fate and transport pathways of pollutant spilt along the NWP in the Canadian Arctic. In this study, we used a high-resolution numerical model, NEMO (Nucleus for European Modelling of the Ocean) in the regional configuration, ANHA12 (Arctic and Northern Hemisphere Atlantic), with a horizontal resolution of 1/12 degree. We applied an offline Lagrangian particle tracking tool, ARIANE, to simulate

the spread of pollutant to oceanic advection. We highlighted the role of different oceanic circulation regimes to the circulation pathways of pollutant, and examined the simulations in spreading area, distances travelled, and deep spread. By comparing these key factors of releases in different time and site, this study highlighted the ‘worst-case scenario’ of pollutant spilt along the NWP in the Canadian Arctic.

5.1. Introduction

Since the beginning of civilisation, seas of the High North has been longed for its promising resources by mankind for her rough conditions inspired the sense of adventure. Since the end of the 15th century, European explorers have attempted to traverse the Arctic Ocean to discover a promising shortcut to the trading ports of the Pacific Ocean. During the First Kamchatka Expedition in 1728, the Danish explorer Vitus Bering discovered the semi-mythical Strait of Anián, known as Bering Strait in modern days (Williams, 2009). With little knowledge and preparation to the harsh Arctic environment, many quests to the High North ended in darkness and terror. At the beginning of the 20th century, the Norwegian explorer Roald Amundsen successfully traversed the Northwest Passages (NWP), marking the beginning of the modern exploration era to the Arctic Ocean (Mills, 2003).

The NWP consists of seven waterways connecting the Pacific Ocean and the North Atlantic Ocean along the coast of North America (figure 5.1-a). From the North Atlantic Ocean, ships enter the NWP from two routes: (1) via Davis Strait into Baffin Bay, then traverse the waterways of the Canadian Arctic Archipelago (CAA), or (2) via Hudson Strait sailing north into Foxe Basin, then entering the CAA via Fury and Hecla Strait. Via various routes through the channels and straits of the CAA, ships sail to the west entering the Beaufort Sea and exit the Arctic Ocean via Bering Strait. The majority of the NWP stretches through the Canadian Arctic. Domestically, the Canadian Arctic is strongly dependent on maritime transport due to the complexity and remoteness of her geography (Brigham *et al.*, 2009). For the international community, the NWP provides a shorter sea route between the ports in the Pacific and Atlantic

Oceans (Østreng *et al.*, 2013). The deeper waterways of the NWP allow ships to carry more cargo than that is possible when traversing the Suez or Panama Canals (McGarrity and Gloystein, 2013). Making use of the NWP can significantly reduce time and fuel consumption. Both are major interests from the international bulk shipping industry (Stueck, 2013).

From a shipping perspective, the retreat of sea ice in the last decades results in more open water from a longer period (Haas and Howell (2015); Stroeve *et al.* (2007); Serreze and Stroeve (2015)). Furthermore, there has been more ship traffic, attributed to the increasing investments in ice-strengthening vessels, population growth and increasing demands in the Arctic community and expanding exploration to the Arctic resources. Therefore, the total distance that ships travelled in the Canadian Arctic has increased by approximately 300% since the 1990s, with the largest contribution from general cargo vessels and government ice-breakers (Dawson *et al.*, 2018). Significant increases were found with record low sea ice years in the Canadian Arctic, such as 2007 and 2013. The latter marks a turning point when *MS Nordic Orion* was the first sea freighter to successfully transit the NWP with the assistance of the Canadian Coast Guard icebreaker, *Louis S. St-Laurent* (McGarrity and Gloystein, 2013). Her successive traverse heralds a new era for commercial shipping in the NWP and the Canadian Arctic.

Along the coast of North America, the NWP stretches across the Beaufort Sea, the waterways of the CAA, Baffin Bay and Labrador Sea, whose large-scale oceanic circulations are driven by the inflow of Pacific Water (PW) from the west, and the outflow of polar water to the east (figure 5.1-b). Entering the Arctic Ocean via Bering Strait firstly at the Chukchi Sea, Pacific Water follows two pathways: a small amount propagates eastward along the Alaskan coast while the majority follows the Transpolar Drift (TPD) (Hu *et al.*, 2019). Once the latter reaches the northern coast of Greenland, it forms two branches with one directly exiting the Arctic Ocean via Fram Strait with the other forming a return flow. The return flow propagates westward along the northern coast of Greenland, and exits Arctic Ocean via Nares Strait into the Baffin Bay, although some flow continues further before turning east into the northern CAA (Hu *et al.*, 2019).

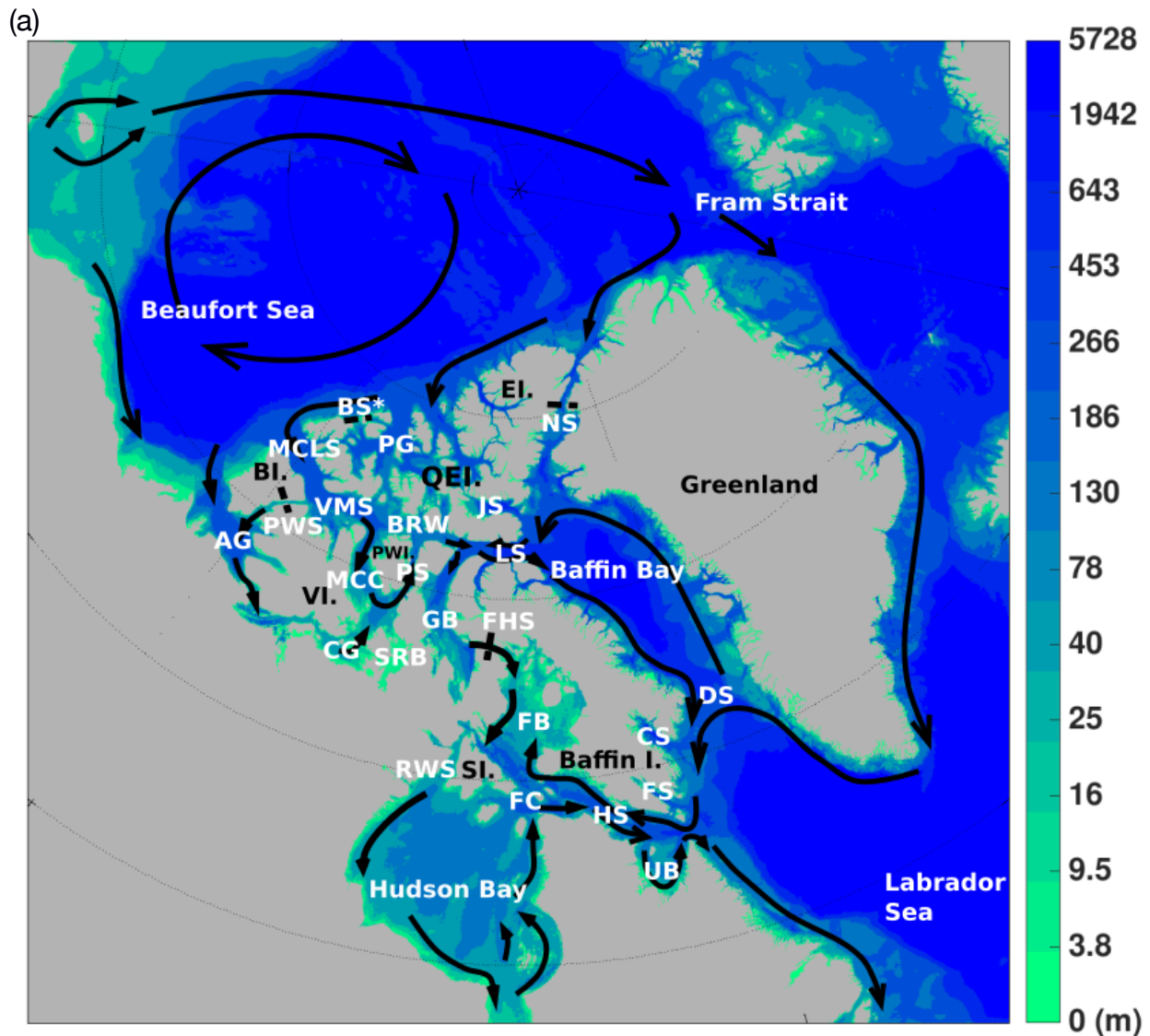


Figure 5.1-a: Geography and oceanic circulation of the Canadian Arctic, black arrows illustrate the general circulation schemes and colour bar indicates bathymetry in metres. MCLS: M'Clure Strait, PWIS: Prince of Wales Strait, VMS: Visount Melville Sound; BRW: Barrow Strait, LS: Lancaster Sound, BS*: Ballantyne Strait, PG: Prince Gustav Adolf Strait, NS: Nares Strait, JS: Jones Sound, AG: Amundsen Gulf, CG: Coronation Gulf, MCC: M'Clintock Channel, SRB: St Roch Basin, GB: Gulf of Boothia, FHS: Fury and Hecla Strait, RWS: Roes Welcome Sound, FC: Foxe Channel, HS: Hudson Strait, UB: Ungava Bay, DS: Davis Strait; CS: Cumberland Sound, and FS: Frobisher Sound; EI.: Ellesmere Island, BI.: Bank Island, VI: Victoria Island, PWI: Prince of Wales Island, and SI.: Southampton Island

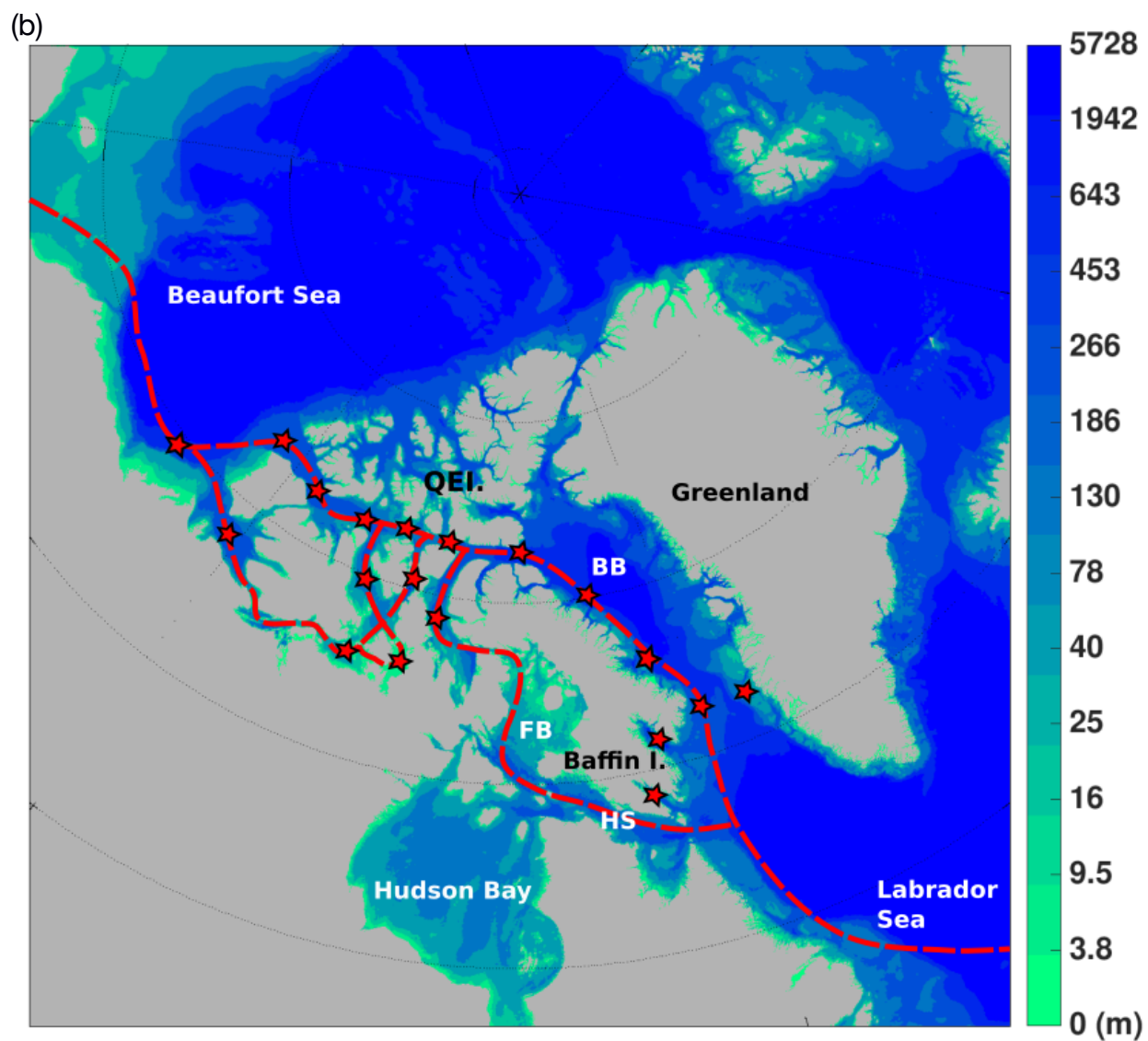


Figure 5.1-b: The approximate location of the release sites are illustrated by red stars, with the NWP in red dashed lines (QEI: Queen Elisabeth Islands).

The CAA is characterised by shallow basins and narrow channels connecting the Arctic Ocean to Baffin Bay. It consists of the Queen Elizabeth Islands (QEI) in the north and the islands in southern CAA, separated by Parry Channel in between. Parry Channel provides a direct pathway between Beaufort Sea and Baffin Bay via M'Clure Strait, Melville Sound, Barrow Strait, and Lancaster Sound. The large-scale circulation in the CAA is dominated by the eastward outflow of polar water. However, there are several smaller-scale southward or westward flows within its waterways. Upon reaching Melville Sound, a large portion of eastward polar outflow turns southward into M'Clintock Channel, which is caused by the enhancement of ageostrophic acceleration due to the change of coastline and a sharp decrease in the bathymetry (Wang *et al.*, 2012). Circumnavigating Prince of Wales Island, the southward drift turns northward into Peel Sound, and returns to Parry Channel at Barrow Strait. Traversing Barrow Strait, whilst a small portion of the eastward outflow turns south into Gulf of Boothia, then enters the Foxe Basin via Fury and Hecla Strait, the majority continues eastward into Lancaster Sound. Lancaster Sound is located at the eastern end of Parry Channel. It exhibits a strong eastward outflow on the southern coast and a westward inflow from Baffin Island Current on the northern coast. The westward inflow only recirculates in Lancaster Sound and Barrow Strait, then exits the CAA with the eastward outflow back into Baffin Bay (Hughes *et al.*, 2017).

Baffin Bay directly receives polar water from the CAA and Nares Strait. Water from both sources travel southward along the western coast of Baffin Bay (Dukhovskoy *et al.*, 2016). Furthermore, the northward West Greenland Current brings polar water that traverses Fram Strait after mixing in the North Atlantic Ocean into Baffin Bay (Yang *et al.*, 2016). Once reaching Davis Strait, the West Greenland Current forms two branches with one turns westward joining Labrador Current and the other enters Baffin Bay along its eastern coast. Baffin Bay exhibits a strong cyclonic circulation, which is bounded by the southward Baffin Island Current along the western coast and northward West Greenland Current along the eastern coast (Dukhovskoy *et al.*, 2016; Münchow *et al.*, 2015). Exiting Baffin Bay via Davis Strait, the Baffin Island Current forms two branches upon reaching the eastern end of Hudson Strait. While the majority of the flow continues southward and joins the Labrador Current, a small portion turns westward into Hudson Strait. It forms two branches, with one penetrates Hudson Strait and the other only

circumnavigates Ungava Bay, and then joins the outflow exiting Hudson Strait (Lazier and Wright, 1993).

The overall eastward outflow of polar water through the Canadian Arctic consistently brings sea ice from the Arctic Ocean via the western gates of the CAA (Howell *et al.*, 2013). With decreasing formation rate of first-year ice and resultant increasing open water, multi-year ice becomes more responsive to oceanic current and geostrophic wind (Kwok *et al.*, 2013). Therefore, the sea ice extent in the CAA does not exhibit a significant decline compared to other regions in the Canadian Arctic (Tivy *et al.*, 2011). Within the CAA, the majority of sea ice is located in the QEI, M'Clure Strait, Viscount Melville Sound, M'Clintock Channel, and Peel Sound (Howell *et al.*, 2008). The accumulation of multi-year ice in these narrow straits creates some most challenging navigational hazards, known as ice chokepoints (Fissel *et al.*, 2011).

Therefore, as sea ice in Arctic Ocean continues to decline and ship traffic in the Canadian Arctic continues to increase, the risk of accidents along the NWP will increase (Lackenbauer and Lajeunesse, 2014). If an accidental spill of ship fuel occurred, the pollutant would firstly undergo weathering processes, which included evaporation, emulsification, photo-oxidation, biodegradation, and dissolution. In the Arctic Ocean, most of these processes are completed within weeks after the spill (Afenyo *et al.*, 2016). Due to the remoteness, complex geography, harsh environment, and the lack of supportive infrastructures in the Canadian Arctic, it is believed that the recovery operations would not be possible within such time-frame (Kelly *et al.*, 2018; Lackenbauer and Lajeunesse, 2014; Prowse *et al.*, 2009; Østreng *et al.*, 2013). After the initial weathering processes, the pollutant spilt in the Arctic Ocean is transported mainly by oceanic advection and sea ice encapsulation (Afenyo *et al.*, 2016). Therefore, it is of particular importance to study the transport pathways and long-term fate of pollutants if spilt along the NWP in the Canadian Arctic to illuminate the most probable location for recovery operations before the pollutant further spreads into the open ocean. In the Arctic Ocean, the common containment and recovery methods are in-situ burning and dispersant (Afenyo *et al.*, 2016). However, the former cannot remove all oil and will result in environmental impact from its burning residue (Transport Canada and Canadian Coast Guard, 2010), whilst the latter could

result in large volumes of oil drifting at depth (Drozdowski *et al.*, 2011), which is extremely difficult to recover (Kelly *et al.*, 2018).

Therefore, we are motivated to examine the circulation pathways and long-term fate of pollutant due to oceanic advection if spilt along the NWP in the Canadian Arctic. This study is completed using high-resolution numerical model, Nucleaus for European Modelling of the Ocean (NEMO), in the Arctic and Northern Hemisphere Atlantic (ANHA) configuration at $1/12^\circ$ (ANHA12). We used the Lagrangian particle tracking tool, ARIANE, to integrate the circulation pathways of pollutant with oceanic advection. From this study, we evaluated the horizontal spreading area, distances and full trajectory, percentage of deep spread, level of variability and uncertainty of each simulation from 25 release sites along the NWP. Illuminating at which sites and when the accidental spill would have the most severe consequence, thus to aid in the future regulation with respect to the increasing ship traffic. Furthermore, by evaluating the most probable regions where the pollutant accumulates, this study can highlight the regions that are most sensitive to the spill of pollutant, thus aid in the development of Marine Protected Areas.

This paper is organised as follows. In section 2, we review the model configuration of NEMO and ANHA12, the integration schemes of ARIANE, and the experiment design for this study. In section 3, the circulation pathways of pollutant are analysed with respect to the time elapsed, variability, and the most probable regions for accumulation is highlighted. In section 4, the simulation results are analysed and discussed numerically in terms of the horizontal spreading area, distances, percentage of deep spread exceeding 90 metres, and sensitivity to different release sites. Lastly in section 5, we discuss the limitations and future directions of this study, and outline the worst-case scenario of the pollutant spills in the NWP.

5.2. Methodology

In this study, we used a high-resolution general circulation ocean model, Nucleus for European Modelling of the Ocean version 3.4 (NEMO), coupled with the sea ice component, LIM2 (Louvain-la-neuve Ice Model). We used the regional configuration of Arctic and Northern Hemisphere Atlantic at $1/12^\circ$ (ANHA12), which consists of the Arctic Ocean, North Atlantic Ocean, and a part of the South Atlantic Ocean with two open boundaries at Bering Strait and 20°S . ANHA12 provides a horizontal resolution of $1/12^\circ$, with the highest resolution of approximately ~ 1.93 km in the Canadian Arctic. It consists of 50 vertical layers, providing enhanced resolution for the surface layers with less than 2 metres for the layers in the top 10 metres. The open boundary conditions and initial conditions of ANHA12 are obtained from the GLobal Ocean ReanalYSis 2 version 3 (GLORYS2v3) (Mercator Ocean, 2017). Its atmospheric forcing is obtained from the Canadian Meteorological Centre's Global Deterministic Prediction System ReForecasts (CGRF) (Smith *et al.*, 2014). The river runoff data is from Dai *et al.* (2009) monthly at $1^\circ \times 1^\circ$ resolution till 2007 and Greenland Ice Sheet discharge data is from Bamber *et al.*, (2012) at $5 \text{ km} \times 5 \text{ km}$ resolution till 2010. After the end of each dataset, data from the last years (2007 and 2010, respectively) is repeated. Previous studies (*e.g.* Grivault *et al.*, (2018); Hu *et al.* (2018); Hu *et al.* (2019); Hughes *et al.* (2017)) have proven that ANHA12 is capable in describing the dynamics of the ocean and sea ice in the Arctic Ocean and within the narrow waterways of the CAA.

We applied the Lagrangian particle tracking tool, ARIANE, to the three-dimensional velocity fields from the model output to determine the circulation pathways of pollutant due to oceanic advection. ARIANE has been extensively used to examine the fate and transport pathways of a highlighted water mass (*e.g.* Feucher *et al.* (2019); Gillard *et al.* (2016); Kelly *et al.* (2018); Ridenour *et al.* (2019)) (Blanke and Raynaud, 1997). However, the Lagrangian calculation that ARIANE uses cannot resolve processes such as convection, therefore, in this study, we only considered subduction due to advection. Its offline integration limits the representation of small scales processes, such as diffusion, which was parameterised in the ocean

tracers and dynamics fields. Furthermore, it should be noted that this study only describes the average circulation of pollutant, rather than the exact pathways that the pollutant would follow.

We have 24 release sites along the NWP within the Canadian Arctic with a primary initial area of $5 \text{ km} \times 5 \text{ km}$ and alternative initial area of $10 \text{ km} \times 10 \text{ km}$ (figure 5.1-b). Table 5.1 lists the coordinates of the release sites. At each simulation site, we deploy 5,000 virtual particles every 10 days during the extended operating season from June 1st to October 31st for 12 years from 2004 to 2015. The particles are integrated for 2 years. The locations of particles were visualised every two months to highlight their circulation pathways and time-scales. By calculating the average probability of particles at the end of each simulation, we were able to determine the regions where the particles would most likely to accumulate or exhibiting high concentration.

For each simulation, we calculated the horizontal spreading area by dividing the model domain into 1/12 degree grid cells. The grid cells occupied by the particles are counted and converted into square kilometres with respect to the horizontal mesh. Furthermore, the area that was affected by at least one release (*i.e.* envelope area) for each release site was calculated and compared with the average spreading area, in order to determine the uncertainty in the spread of particles. The direct distance from the initial locations to the locations of particles one and two years after the release was calculated to determine how far the particles have travelled. We also calculated the full trajectory of particles throughout the integration. By comparing these two values, the strength of recirculation was highlighted. The deep spread was calculated via the percentage of particles with a depth exceeding 90 metres. Lastly, we calculated the annual and seasonal variability in the horizontal spreading area to determine the sensitivity of the spread of particles to the release date. By evaluating the propagation of particles of each release, we can determine over which site and when the spill of the pollutant would have the most severe outcome.

Table 5.1: the approximate location and their regional group of release sites in the NWP.

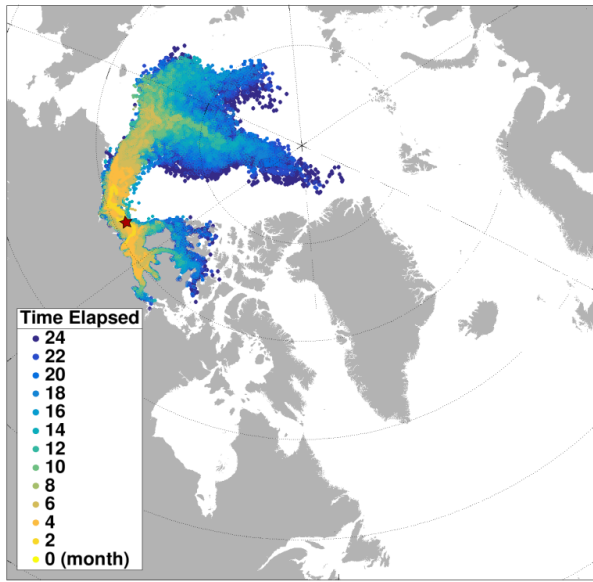
<u>Region</u>	<u>Release Site</u>	<u>Description</u>	<u>Longitude</u>	<u>Latitude</u>
<u>Canadian Beaufort Sea (CBF)</u>	CBF	Canadian Beaufort Sea (offshore)	-131.80	71.15
	CBF_C	Canadian Beaufort Sea (inshore)	-132.17	70.37
<u>Western Parry Channel (WPC)</u>	MCLW	Western M'Clure Strait	-125.22	75.15
	MCLE	Eastern M'Clure Strait	-114.41	73.99
	VMS	Viscount Merville Sound	-104.70	74.08
<u>Eastern Parry Channel (EPC)</u>	VMSE	Eastern Viscount Merville Sound	-100.21	74.22
	BRW	Barrow Strait	-92.24	74.24
	LSW	Western Lancaster Sound	-85.99	74.10
	LSE	Eastern Lancaster Sound	-80.71	74.12
<u>Southwestern CAA (WSCAA)</u>	AG	Amundsen Gulf	-122.11	70.52
	CG	Coronation Gulf	-113.40	68.32
<u>Southeastern CAA (ESCAA)</u>	QMG	Queen Maud Gulf	-101.14	68.77
	MCC	M'Clintock Channel	-102.52	71.82
	PS	Peel Sound	-95.72	72.51
	LSS	Larsen Sound	-98.65	70.41
	SRB	St Rock Basin	-94.89	69.16
	GB	Gulf of Boothia	-90.79	71.02
<u>Baffin Bay (BB)</u>	BBN	Northern Baffin Bay	-68.85	72.37
	BBS	Southern Baffin Bay (offshore)	-63.06	69.18
	BBS_c	Southern Baffin Bay (inshore)	-65.12	68.53
	DSW	Western Davis Strait	-61.36	65.24
	DSE	Eastern Davis Strait	-54.17	65.26
	CS	Cumberland Sound	-66.17	65.48
	FS	Frobisher Bay	-67.31	63.14

5.3. Circulation Pathways and Long-term Fate of Particles

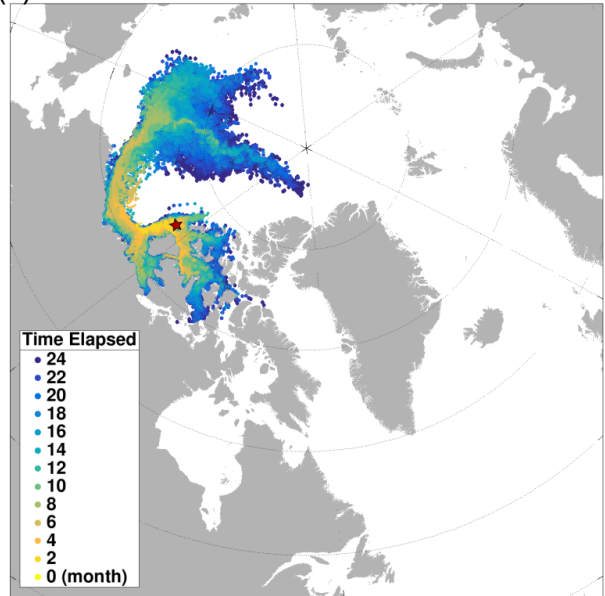
In this section, we first analyse the propagation of particles from each release site with respect to their time scales to highlight the role of different circulation regimes. The average probability of particles for each release site was calculated to illuminate the regions where the particles are most likely to accumulate.

The particles released along the NWP exhibited three main circulation pathways following the dominated circulation of each region. In figure 5.2, we arbitrarily visualised the propagation of particles that exhibited the most typical circulation pathways. (1) Released in the Canadian Beaufort Sea (*e.g.* figure 5.2-a), the majority of particles released propagated westward along the outer bound of the anti-cyclonic Beaufort Gyre (BG), then turned eastward with the TPD. There were a limited amount of particles propagated eastward into the CAA via Amundsen Gulf or M'Clure Strait. (2) most releases in the waterways of the CAA mainly follows the eastward outflow of polar water (*e.g.* figure 5.2-b to 5.2-e) with some releases exhibiting a predominately westward into the Arctic Ocean (*e.g.* figure 5.2-b and 5.2-d). The 15 release sites within the CAA were analysed based on two groups: those located along Parry Channel and within the southern CAA. Released along Parry Channel, the majority of particles followed the eastward polar outflow. Released in the southern CAA, the majority of particles firstly propagated northward into Parry Channel, then joined the eastward outflow. (3) Released in the Baffin Bay (*e.g.* figure 5.2-f, 5.2-h, 5.2-j), particles followed a general southward outflow traversing Davis Strait into the North Atlantic Ocean.

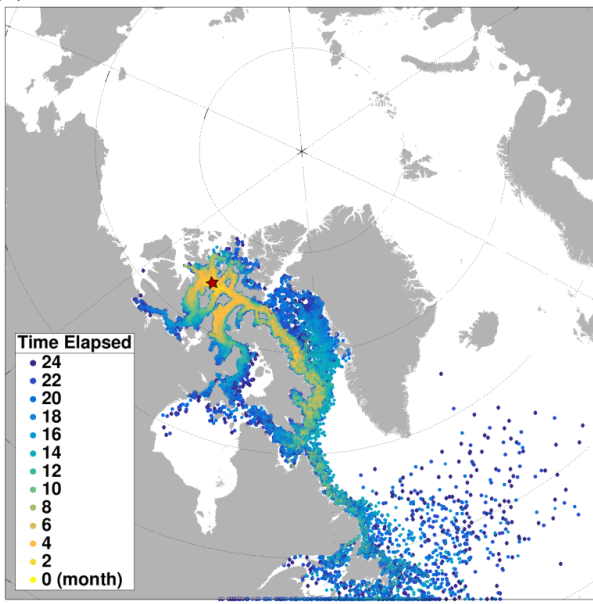
(a)



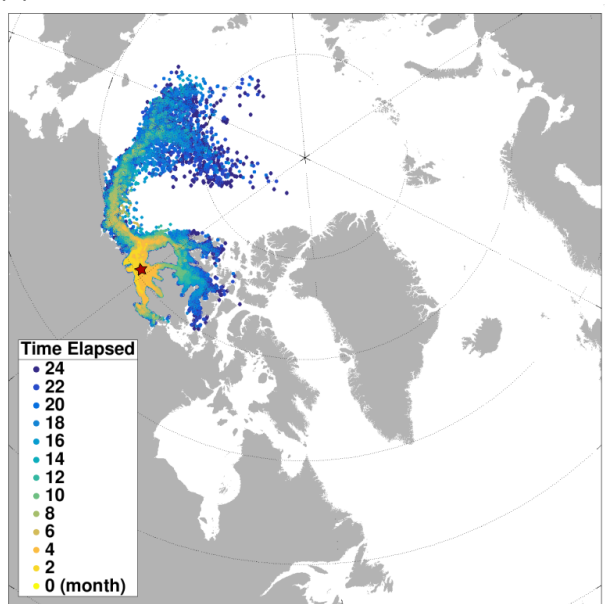
(b)



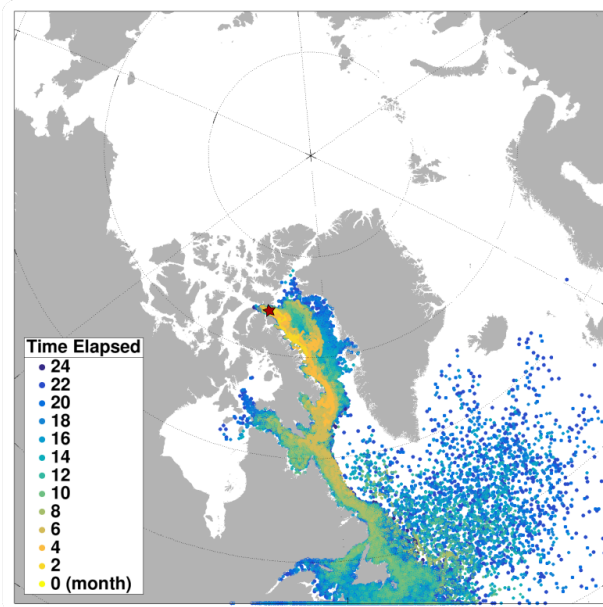
(c)



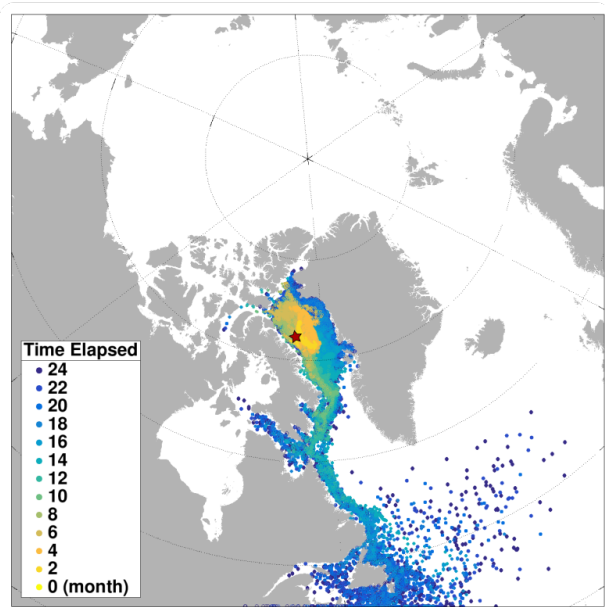
(d)



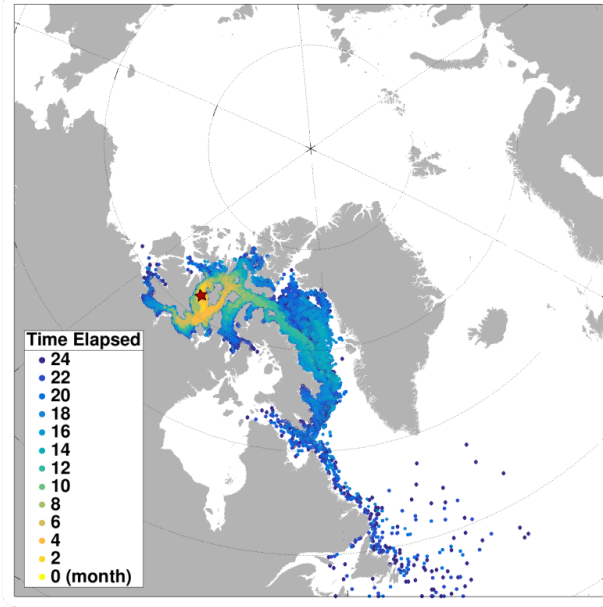
(e)



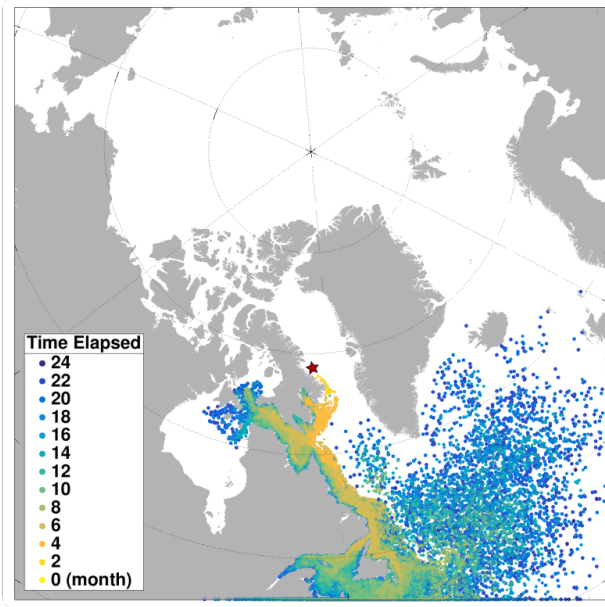
(f)



(g)



(h)



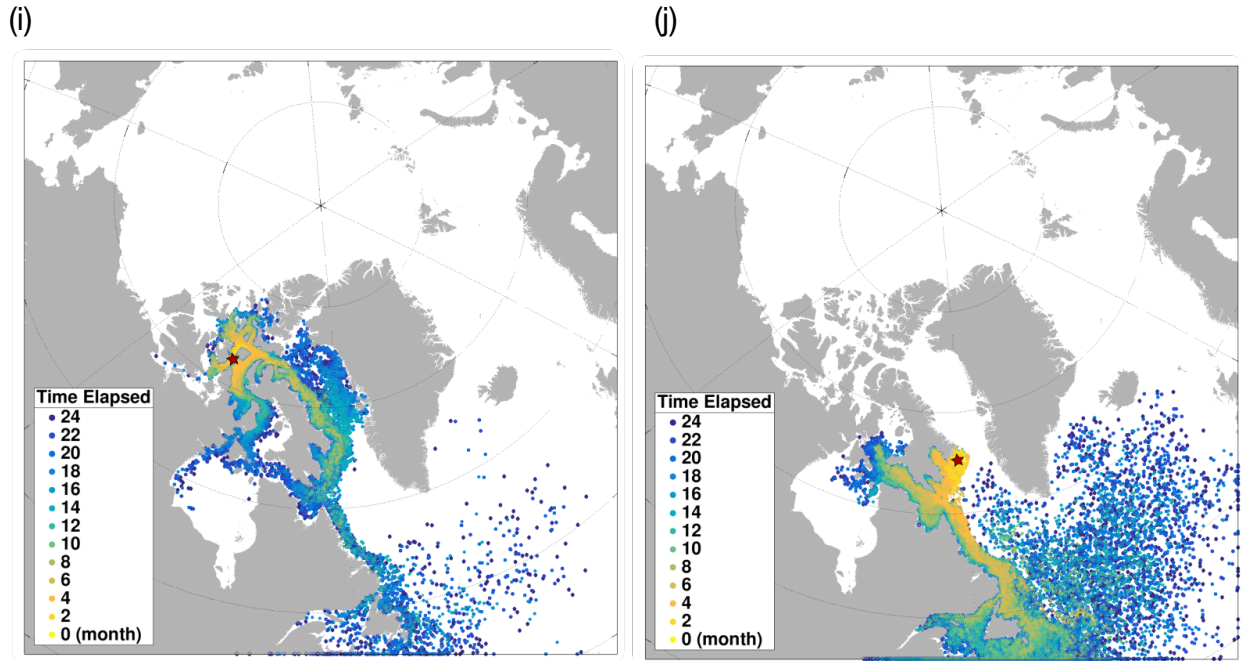


Figure 5.2: Propagation of particles released on the 1st June, 2010. The location of particles were visualised every 2 months. The red star indicated where the particles were seeded initially: (a) Canadian Beaufort Sea, (b) Western M'Clure Strait; (c) Eastern Viscount Melville Sound, (d) Amundsen Gulf, (e) Eastern Lancaster Sound, (f) Baffin Bay North offshore, (g) M'Clintock Channel, (h) Baffin Bay South near shore, (i) Peel Sound, and (j) Davis Strait West.

5.3.1. Canadian Beaufort Sea Releases

There are two release sites in the Canadian Beaufort Sea: CBF and CBF_C, with the latter located 75 km closer to shore than the former. The particles released in the Canadian Beaufort Sea propagated both westward with the BG and eastward into the CAA via Amundsen Gulf or M'Clure Strait (figure 5.3). The majority of particles released in the Canadian Beaufort Sea propagated westward along the outer bound of the anti-cyclonic BG, reached the northern Chukchi Sea in 4~6 months after released. Then these particles exhibited similar circulation pathways to the Pacific inflow: the majority turned east following the TPD, whilst some drift westward and then turned eastward joining the TPD upon reaching East Siberian Sea. There were an only a limited amount of particles that entered CAA. In approximately 4 months after released, the east propagating particles occupied Amundsen Gulf. Some of these particles propagated northward via Prince of Wales Strait, and then turned east in the Parry Channel. At the end of most simulations, these particles were found entering M'Clintock Channel. During some simulation years, there were a small number of particles successfully traversed Parry Channel and entered Baffin Bay (figure 5.3-b and 5.3-d).

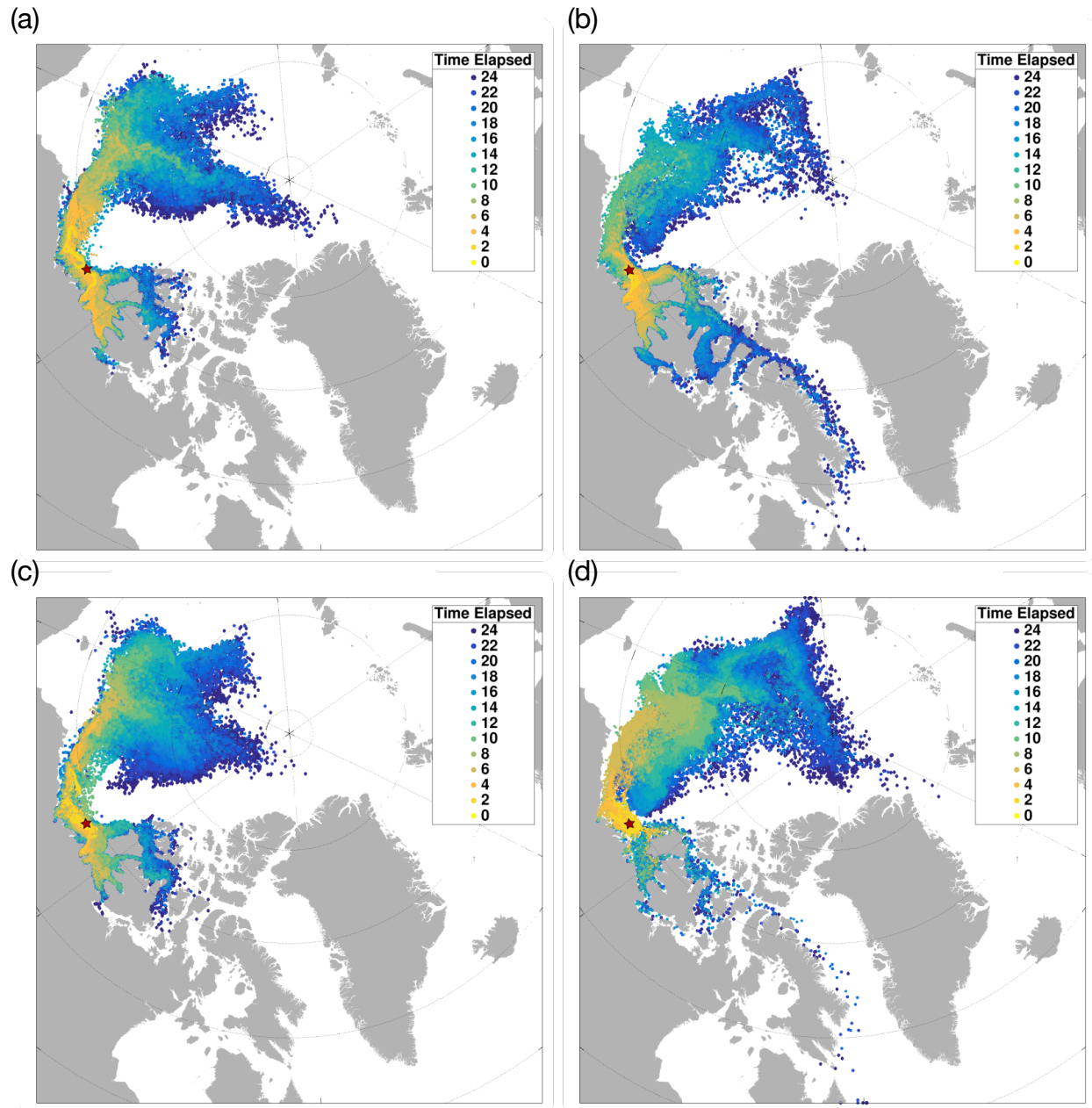


Figure 5.3: Circulation pathways of particles released in the Canadian Beaufort Sea, which is indicated by the red star. The particles were released in (a) June 1st 2010, (b) June 1st 2015, (c) October 10th 2010, and (d) October 10th 2015.

As the majority of particles propagated westward into the Arctic Ocean, their variability in the circulation pathways were found to be strongly linked with variability in the Arctic Oscillation (AO), which describes the strength of fluctuation in the sea level pressure between the Beaufort High and Icelandic Low. A positive AO phase implies a lower pressure over the Arctic, generating cyclonic atmospheric circulation; whereas negative and neutral values correspond to high pressure (Thompson and Wallace, 1998). During positive AO, the origin of the TPD shifts further east, leading to a contraction of the BG, whereas during negative AO, the TPD shift west and results in an enhancement of BG (Kwok *et al.*, 2013). As the strength and size of the BG played an important role in the westward spreading of the particles into the Arctic Ocean, the enhancement of the BG during negative AO phase promoted the larger spreading area. For instance, 2010 (figure 5.3-a and 5.3-c) represent a typical negative AO year (whose record was retrieved from the National Climate Data Center (NCDC): <https://www.ncdc.noaa.gov/teleconnections/ao/>), the enhancement of the BG promoted more westward flow into the Arctic Ocean.

Although the majority of particles propagated westward into the Arctic Ocean, they spread over a large area within a relatively short time-frame with large variability, which resulted in relatively smaller concentrations. By calculating the average probability of all releases in this area, we found that releases in the Canadian Beaufort Sea, particles exhibited higher concentration in the southeastern Beaufort Sea within the proximity of the initial release location and Amundsen Gulf (figure 5.4).

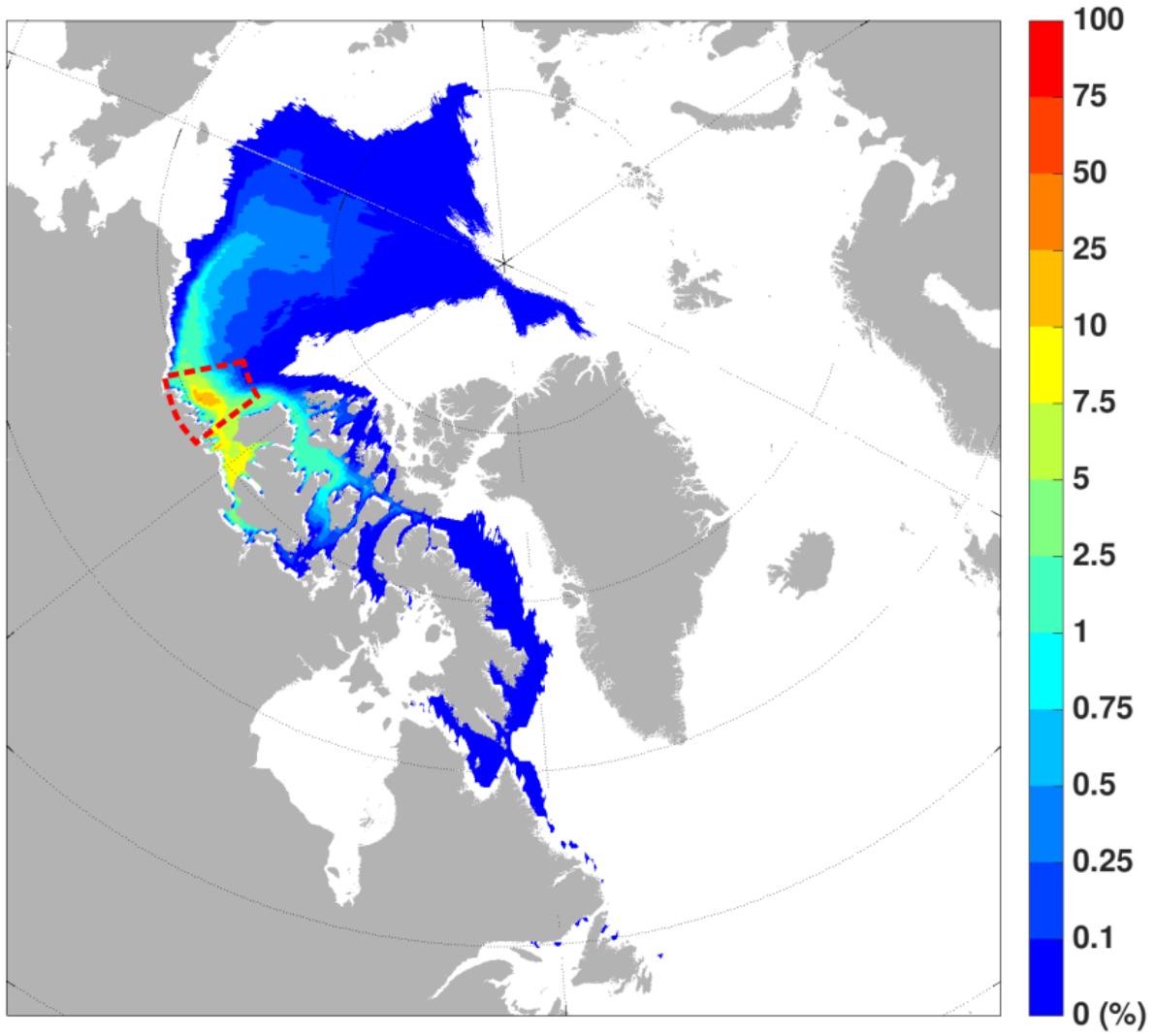


Figure 5.4: Average probability (in percentage) of all simulations from the Canadian Beaufort Sea (region indicated by red dashed line).

5.3.2. CAA Releases

We have 15 release sites within the CAA, with 7 distributed along Parry Channel and 8 in the southern waterways. The majority of particles released in the CAA exhibited an overall eastward outflow and exited the CAA via Lancaster Sound or for a small number, Gulf of Boothia. However, we found a westward flow into the Arctic Ocean from those released in the western straits, whose amount decreased as the particles were seeded further away from the Arctic Ocean. As the majority of particles released in the CAA followed the overall eastward outflow, they exhibited two types of circulation pathways: (1) those released in Parry Channel propagated eastward along Parry Channel; and (2) when released in the southern CAA, the majority would firstly propagate northward into Parry Channel, and then propagate eastward. Therefore, we analysed the circulation pathways of the CAA releases with respect to their initial location.

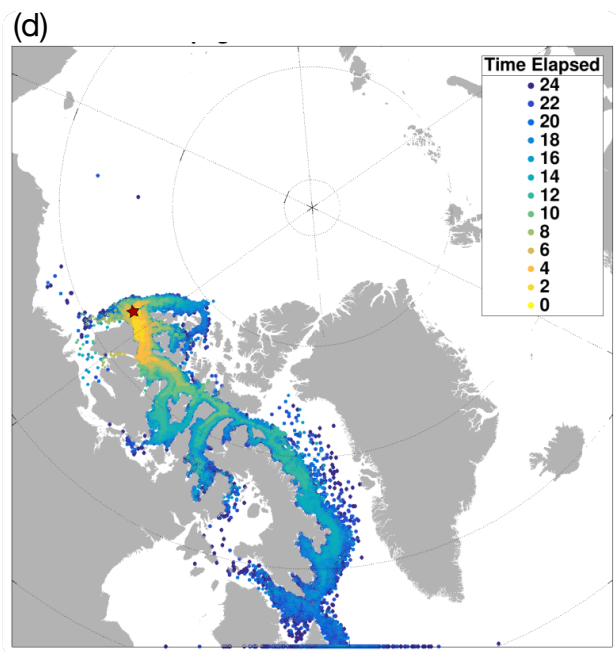
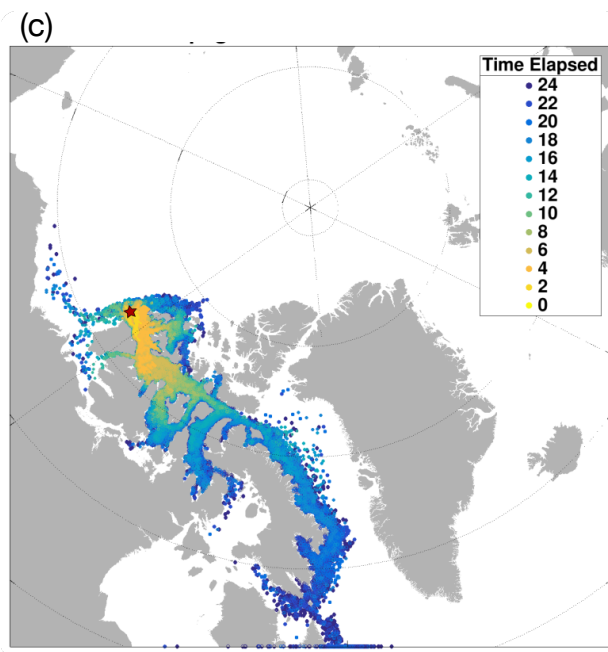
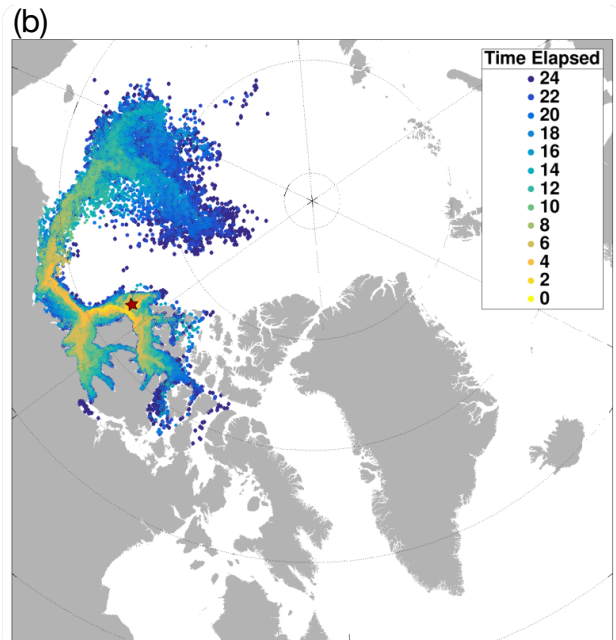
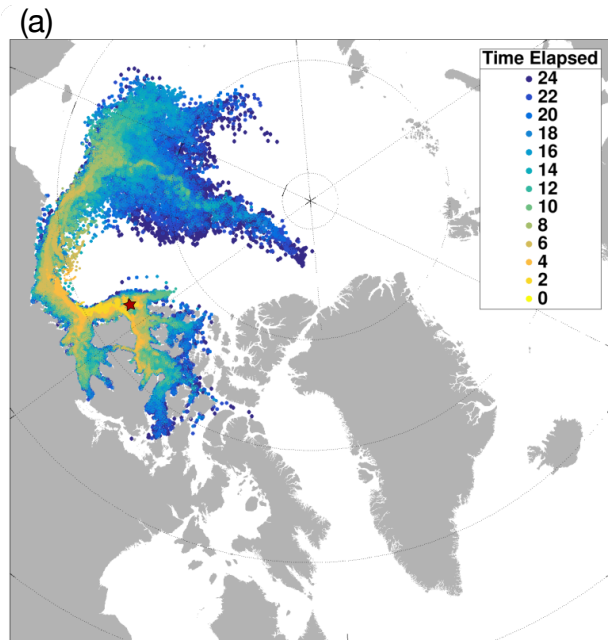
5.3.2.1. Parry Channel Releases

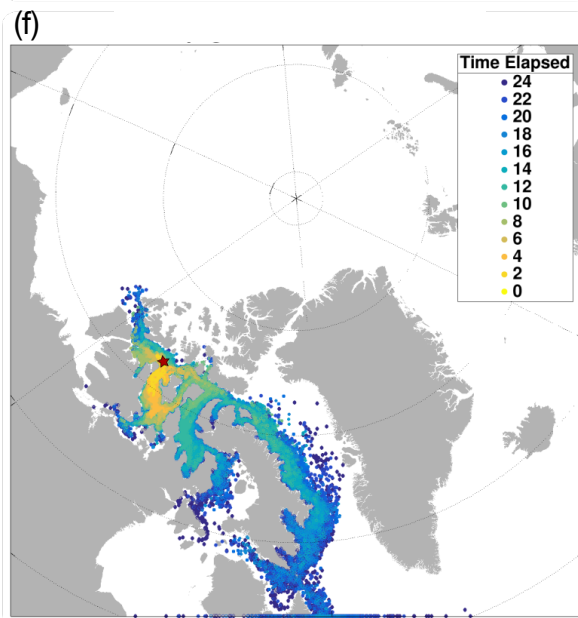
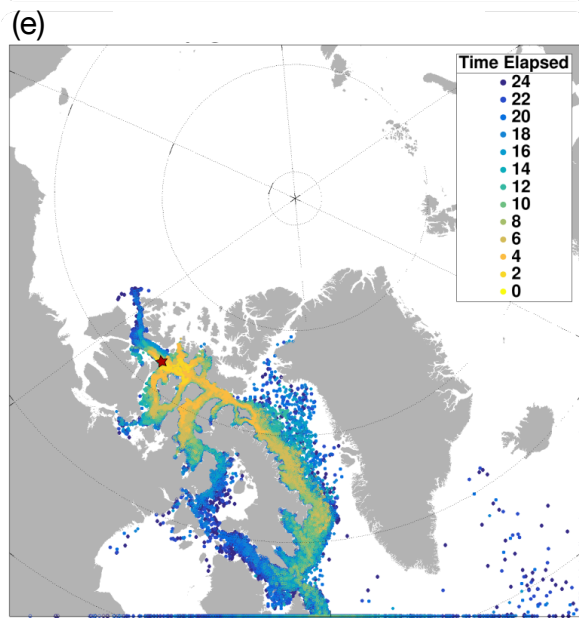
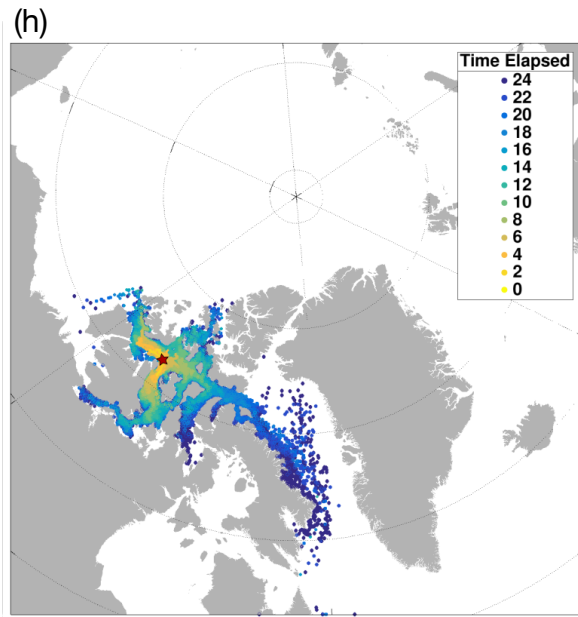
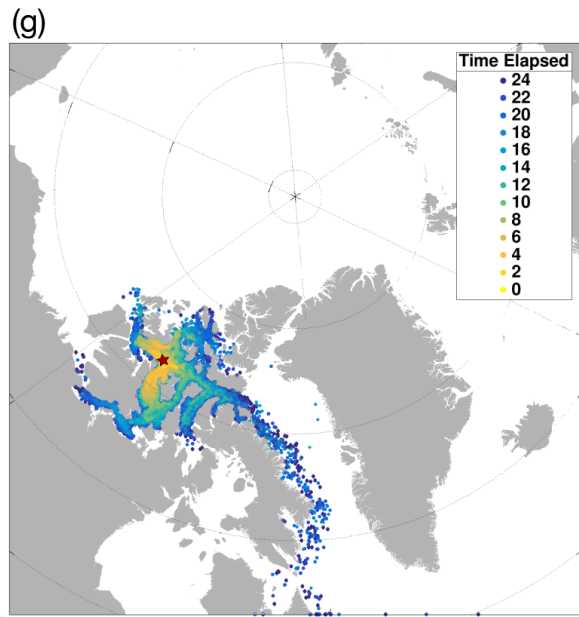
The 7 release sites along Parry Channel consisted of western and eastern M'Clure Strait (MCLW and MCLE), western and eastern Viscount Melville Sound (VMS and VMSE), Barrow Strait (BRW), western and eastern Lancaster Sound (LSW and LSE). Particles released in Parry Channel mainly followed the eastward outflow of polar water. Released at the western Parry Channel (MCLW, MCLE, and VMS), which was west of M'Clintock Channel, particles travelled both westward into Arctic Ocean and eastward with the polar outflow via the CAA. The eastward outflow formed two branches with one drifting southward into M'Clintock Channel and the other traversing Parry Channel directly. Released in eastern Parry Channel (VMSE, BRW, LSW, and LSE), the majority propagated directly eastward exiting the CAA via Lancaster Sound, with a small number of particles drifting southward into Gulf of Boothia.

In western Parry Channel, MCLW releases exhibited the strongest westward flow into Arctic Ocean during AO- years. Immediately after release, particles exited the CAA and were found in the Arctic Ocean (figure 5.5-a to 5.5-d). Further east, the eastward particles seeded from MCLE and VMS (figure 5.5-e to 5.5-h) exhibited a 2 and 4 months time lag respectively. Once

exiting the CAA via M'Clure Strait, the particles travelled in two directions: (1) a small portion turned northward, and then returned to the CAA via the Ballantyne Strait and Prince Fustaf Adolf Strait during the second year of the simulation, (2) the majority turned southward along the western coast of Bank Island, then continued westward with the BG. Then, the particles followed a similar pathway to the westward particles released in the Canadian Beaufort Sea. They joined the TPD one year after the release. The eastward branch of western Parry Channel releases generally followed the outflow of polar water via the waterways of the CAA. Upon reaching M'Clintock Channel in 2~4 months after release, the eastward particles formed two branches: (1) some particles continued travelling eastward to Barrow Strait in 8~10 months after release, (2) the others turned south into M'Clintock Channel. The latter recirculated the Prince of Wales Island and returned to Barrow Strait approximately one year after release. From Barrow Strait, the particles formed two branches while a small portion drifted southward into Gulf and Boothia. Those that propagated into the Gulf of Boothia almost immediately occupied the entire waterbody in around 20 months after release. However, only few particles were found to traverse Fury and Hecla Strait by the end of the two year simulation. On the other hand, the majority continued eastward and exited the CAA via Lancaster Sound approximately 20 months after the release.

The particles released in eastern Parry Channel (*e.g.* LSE: figure 5.5-i to 5.5-l) exhibited a more direct eastward outflow compared to those released in western Parry Channel. Entering Baffin Bay approximately 2 months after release, the particles followed the Baffin Island Current, and traversed Davis Strait in 2 to 4 months. Their circulation pathways is similar to the Baffin Bay release that is described in section 5.3.3.





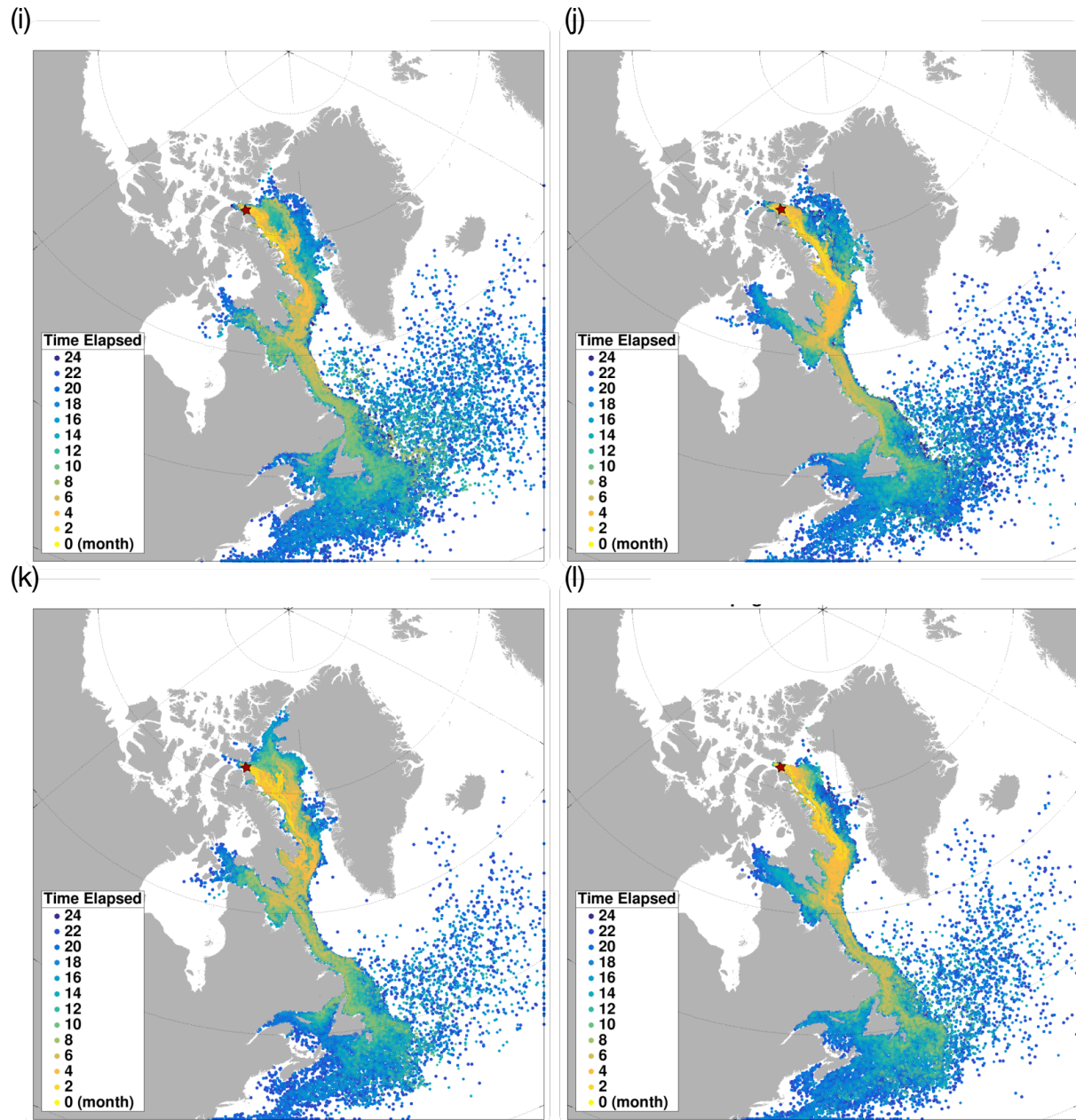


Figure 5.5: Circulation pathways of particles released in Western M'Clure Strait (a, b, c, d), Western Viscount Melville Sound (e, f, g, h), and Eastern Lancaster Sound (i, j, k, l). From each release site, we visualised the propagation of particles released in June 1st 2010, October 10th 2010, June 1st 2015, and October 10th 2015, respectively.

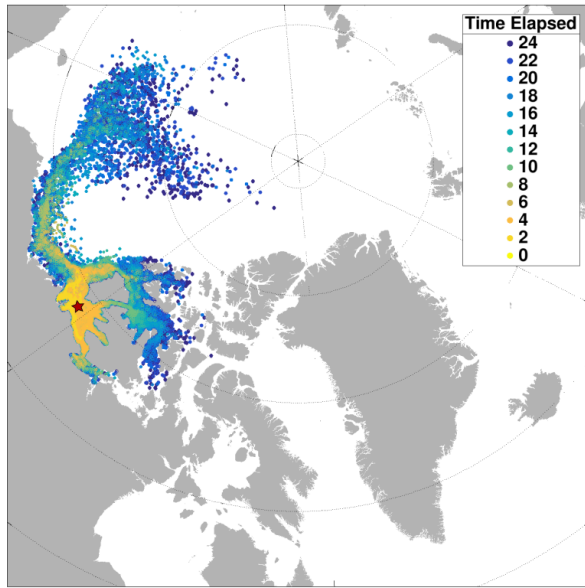
5.3.2.2. Southern CAA Releases

There were 8 release sites in the southern CAA: Amundsen Gulf (AG), Coronation Gulf (CG), Queen Maud Gulf (QMG), M'Clintock Channel (MCC), Peel Sound (PS), Larson Sound (LSS), St. Roch Basin (SRB), and Gulf of Boothia (GB). The particles released in the southern CAA exhibited similar circulation pathways to those released in Parry Channel in terms of the west-/eastward directions with respect to where they were seeded initially: when released in AG (figure 5.6-a to 5.6-d) and CG, particles propagated both westward into the Arctic Ocean and eastward into the CAA. In 2~4 months after release, particles firstly covered a larger area occupying the gulf where they were seeded initially, and then spread in three directions: (1) a small portion propagated eastward along the southern straits and reached Cambridge Bay by the end of the two year simulation; (2) directly northward traversing Prince of Wales Strait along the eastern coast of Banks Island and turned eastward in Parry Channel approximately 10 months after release. Then, the pathways of the east propagating particles exhibited similar pathways to those released in western Parry Channel, which is described in detail in section 5.3.2.1. (3) particles travelled westward entering the Arctic Ocean approximately 4 months since the release date. They exhibited two pathways with one branch propagating northward along the western coast of Banks Island, and then turning east into M'Clure Strait. Particles were found to enter the western end of Parry Channel 8~10 months after release. Although some particles continued northward and propagated into the waterways of the QEI, they were of small amount and were only found in Prince Gustaf Adolf Sea at the end of the simulation. The other branch of particles propagated westward following the outer bound of the anti-cyclonic Beaufort Gyre along the coast, exhibiting similar pathways to those released in the Canadian Beaufort Sea (5.3.1).

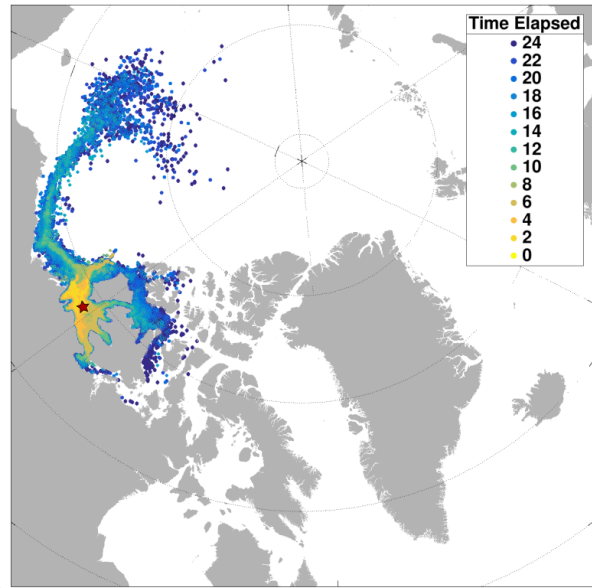
Released in the eastern part of the southern CAA (QMG, MCC, LSS, PS, and SRB), particles travelled in two directions: westward toward the Arctic Ocean and northward into Parry Channel (*e.g.* MCC: figure 5.6-e to 5.6-h). The westward branch exhibited a similar pathway to those seeded from the southwestern sites, with a mean time lag of approximately 2 months. The northward branch propagated into Parry Channel in 6~10 months after release, then followed a similar pathway of those released in eastern Parry Channel (5.3.2.1). An exception is found for

the GB releases (figure 5.6-i to 5.6-l), seeded from an isolated gulf at the eastern end of southern CAA. Instead of the westward flow into the Arctic Ocean, particles released from GB followed the direct outflow in 4~6 months after release via Fury and Hecla Strait, or propagated northward into Lancaster Sound and entered Baffin Bay. Although the particles released in the southwestern CAA exhibited similar circulation pathways, we found large variability in their time scales due to the different circulation schemes at each release site. For instance, the particles released in MCC followed circumnavigated the Prince of Wales Islands before entering Parry Channel via Peel Sound, whilst those released in Peel Sound exhibited a direct northward flow into Parry Channel.

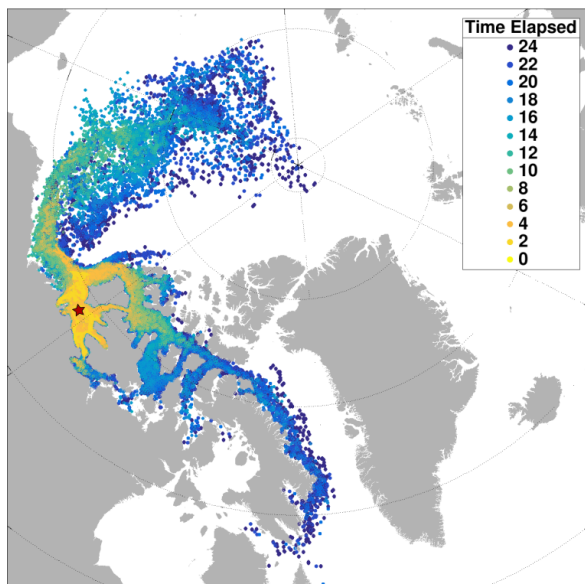
(a)



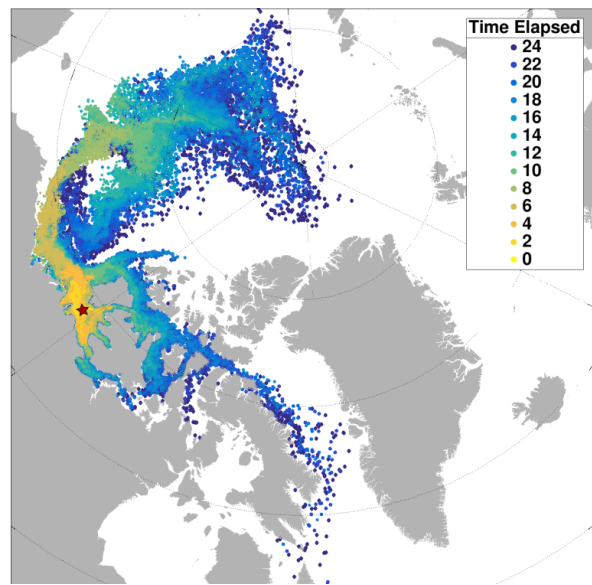
(b)



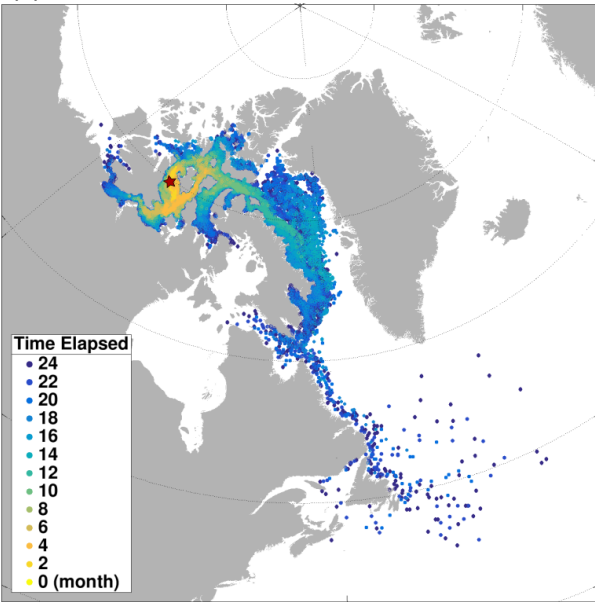
(c)



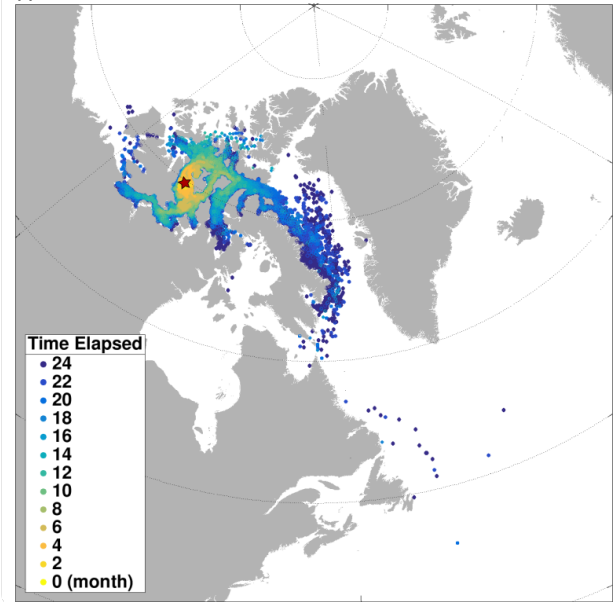
(d)



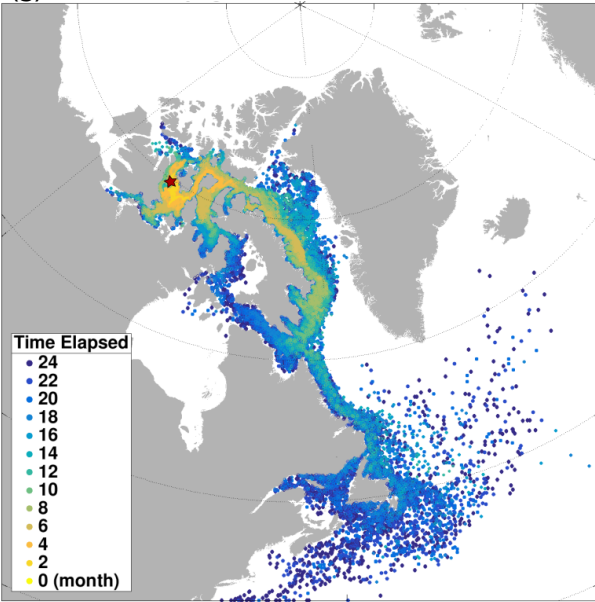
(e)



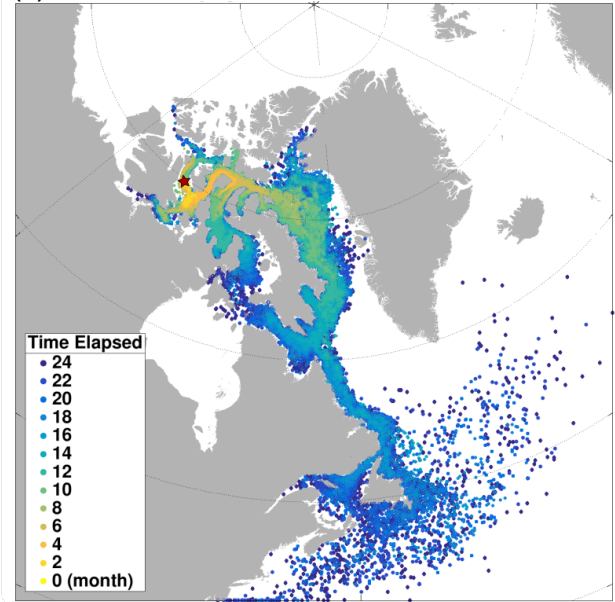
(f)



(g)



(h)



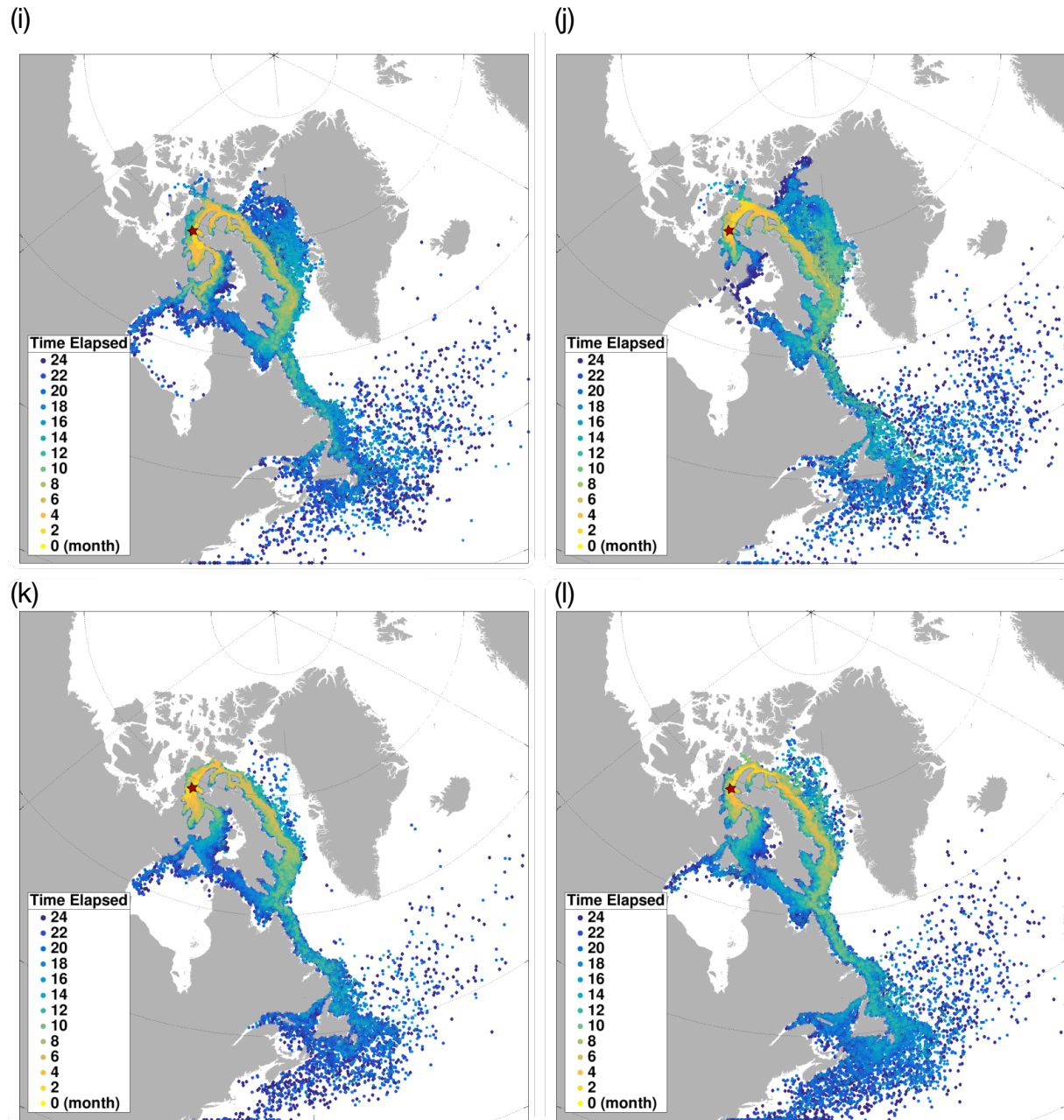


Figure 5.6: Circulation pathways of particles released in Amundsen Gulf (a, b, c, d), M'Clintock Channel (e, f, g, h), and Gulf of Boothia (i, j, k, l). From each release site, we visualised the propagation of particles released in June 1st 2010, October 10th 2010, June 1st 2015, and October 10th 2015, respectively.

5.3.2.3. Circulation Pathways of the CAA Releases

Overall, the majority of particles released in the western CAA (MCLW, AG, and CG) propagated westward into Arctic Ocean whilst the other releases generally followed the eastward polar outflow. The spreading area of the western CAA releases was strongly linked to the strength of the BG, with an enhanced BG during negative AO phase promoted a larger spreading area in the Arctic Ocean. However, the mechanism behind the variability in the particles released in the eastern CAA were more complicated.

The strength of the eastward outflow via the CAA is influenced by the variability of the BG: the strength of BG is enhanced during negative AO, the polar outflow via the CAA is decreased compared to that during a positive AO phase (Jahn *et al.*, 2009). After the particles entered Baffin Bay, their circulation pathways were linked to the variability of the North Atlantic Oscillation (NAO), which describes the strength of fluctuation in the sea level pressure between the Icelandic Low and Azores High (Hurrell *et al.*, 2003). The data record for NAO was obtained from the NCDC: <https://www.ncdc.noaa.gov/teleconnections/nao/>. During positive NAO, the enhanced pressure gradient over the North Atlantic Ocean promotes larger spreading area northward into the northern Baffin Bay and North Atlantic Ocean.

We found that the particles released in the CAA were most likely to accumulate in the proximity of where they were seeded initially. In figure 5.7, we plotted the average probability of all releases within the CAA to determine that which region was most sensitive to the spread of particles.

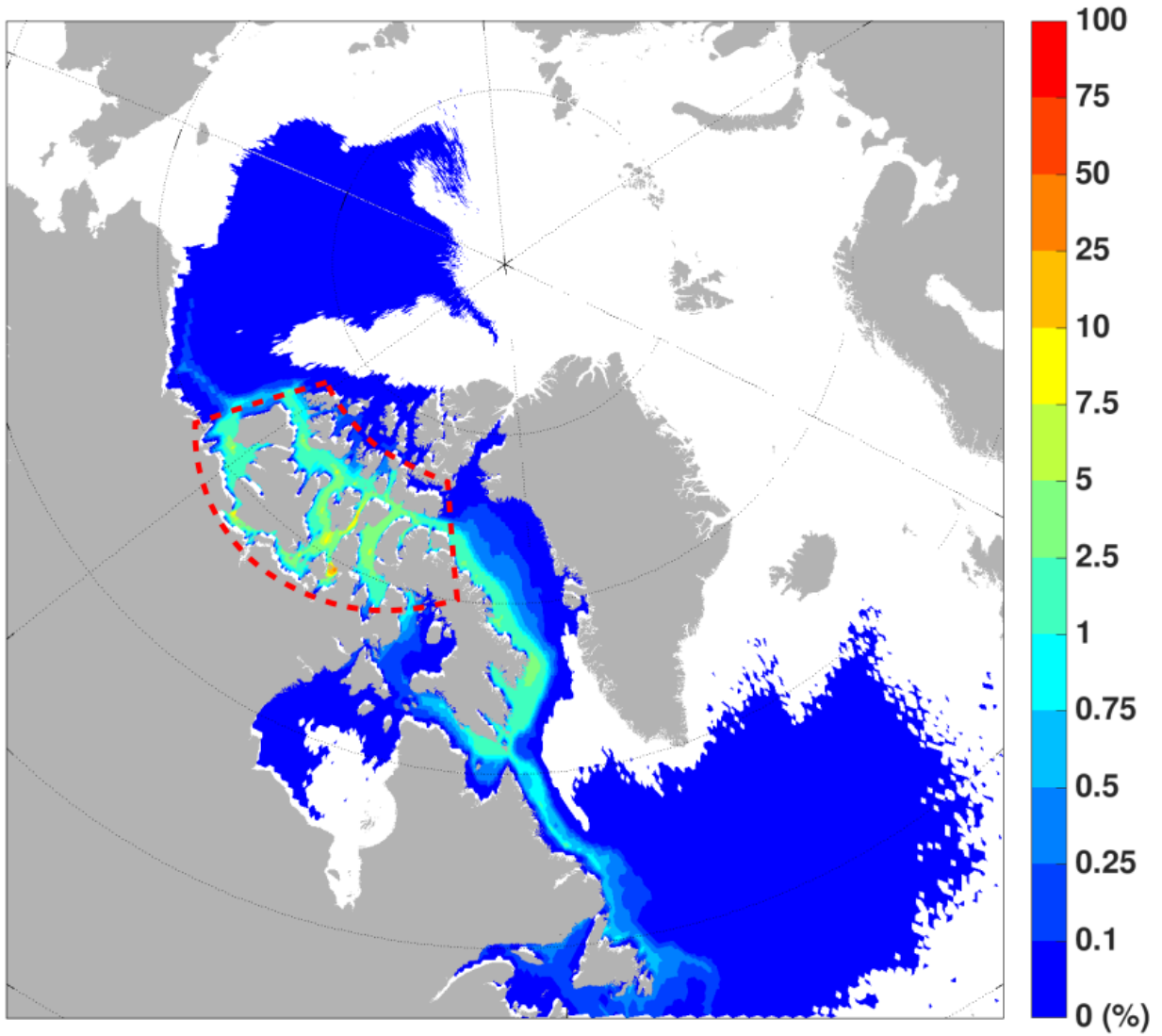


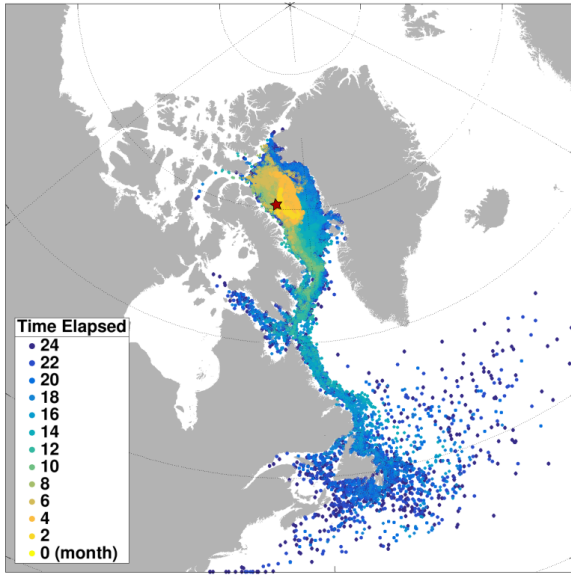
Figure 5.7: Average probability (in percentage) of all simulations from all CAA release sites (region indicated by red dashed line).

5.3.3. Baffin Bay Releases

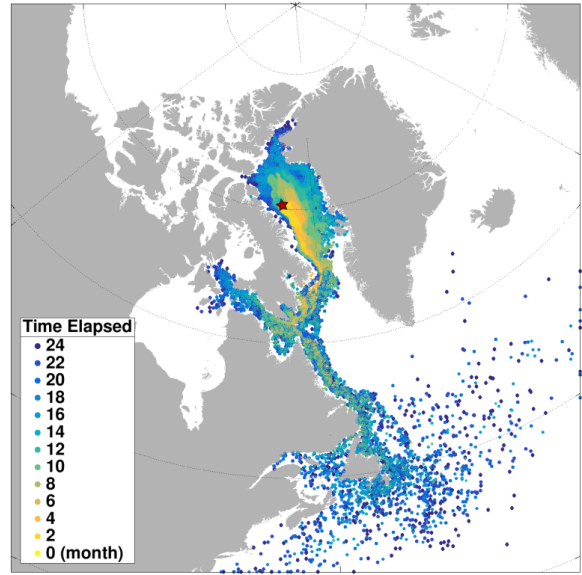
There were 7 release sites in Baffin Bay: Northern Baffin Bay (BBN), Southern Baffin Bay offshore (BBS), Southern Baffin Bay near shore (BBS_C), Western and Eastern Davis Strait (DSW and DSE), Frobisher Sound (FS), and Cumberland Sound (CS). Particles released in Baffin Bay showed two type of circulation pathways (figure 5.8): (1) the particles firstly propagated northward with the West Greenland Current, circumnavigated Baffin Bay, and then joined the second route; or directly (2) exited Baffin Bay with Baffin Island Current via Davis Strait. With direct southward outflow in the Baffin Island Current along the western coast of Baffin Bay, the particles traversed Davis Strait in 2~4 months after release. However, if released further from shore, we observed a second type of circulation when some particles joining the northward West Greenland Current along the eastern coast of Baffin Bay. In the northern Baffin Bay, the some of these particles spread into Nares Strait and Lancaster Sound. However, they only circumnavigated at the mouths, and did not penetrate further during the two year integration. The majority of the particles propagated northward circumnavigated Baffin Bay, with some particles traversing Davis Strait approximately 22 months after released. More were found to remained in the interior of Baffin Bay at the end of the simulation.

Traversing Davis Strait with Baffin Island Current, particles formed two branches approximately 2 months after the release, with one turning westward into Hudson Strait, and the other continuing southward joining the Labrador Current. Whilst some of the west propagating particles only circulated at the mouth of Hudson Strait and joined the Labrador Current 6~8 months later, some particles continued westward along the northern coast of Hudson Strait and entered Foxe Basin and Hudson Bay by the end of simulation. The majority of the particles continued southward with the Labrador Current.

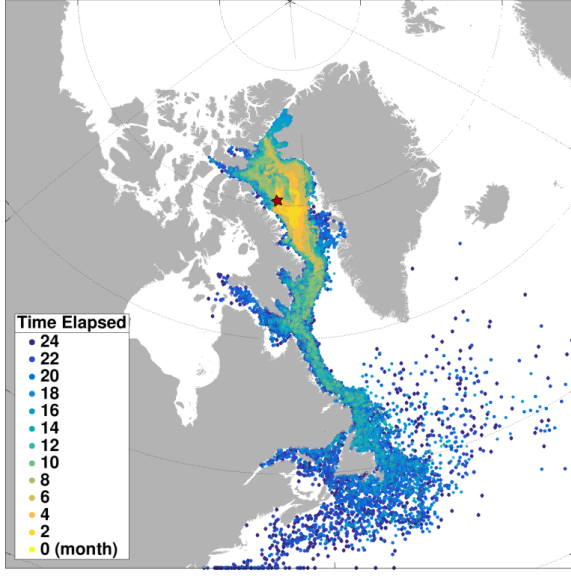
(a)



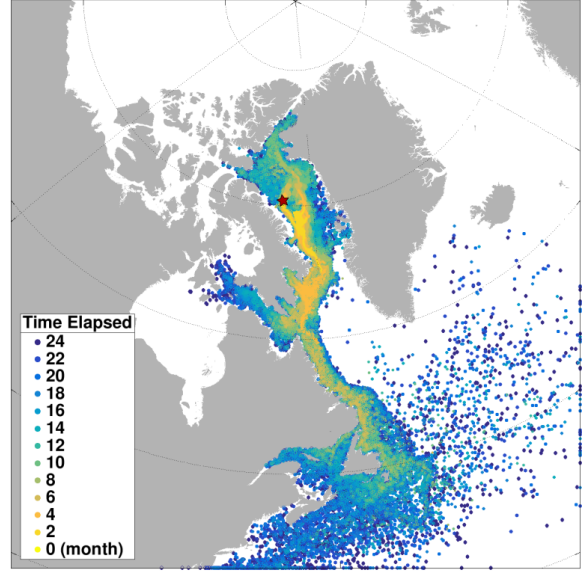
(b)



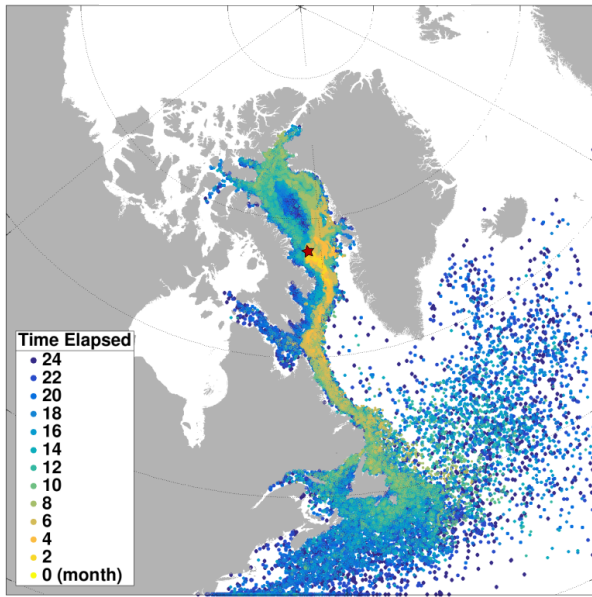
(c)



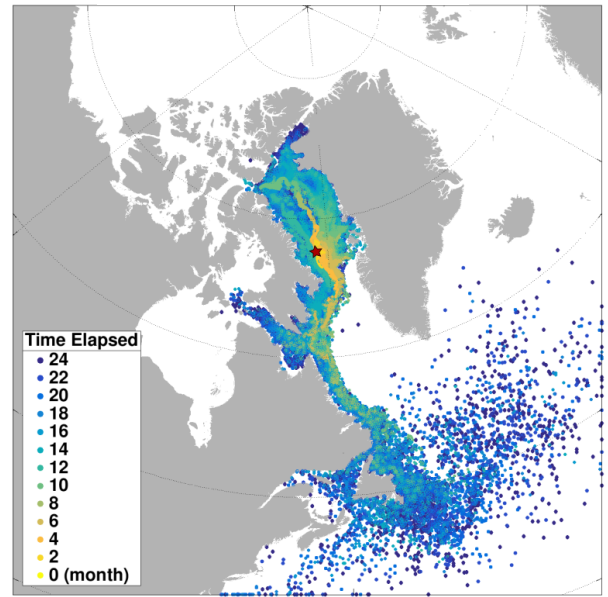
(d)



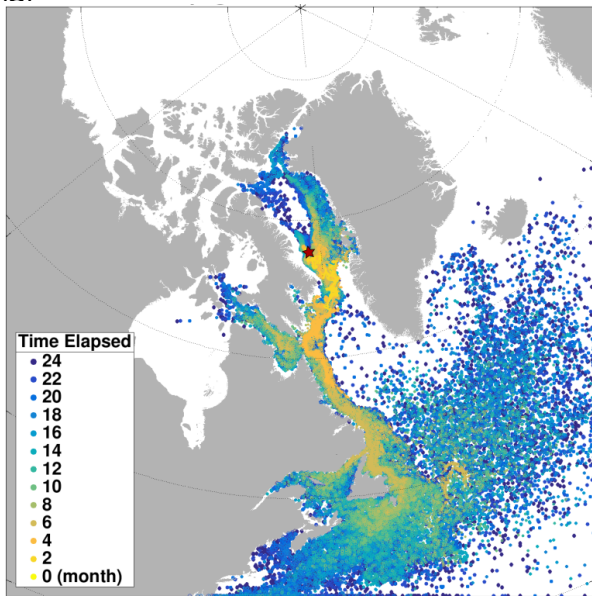
(e)



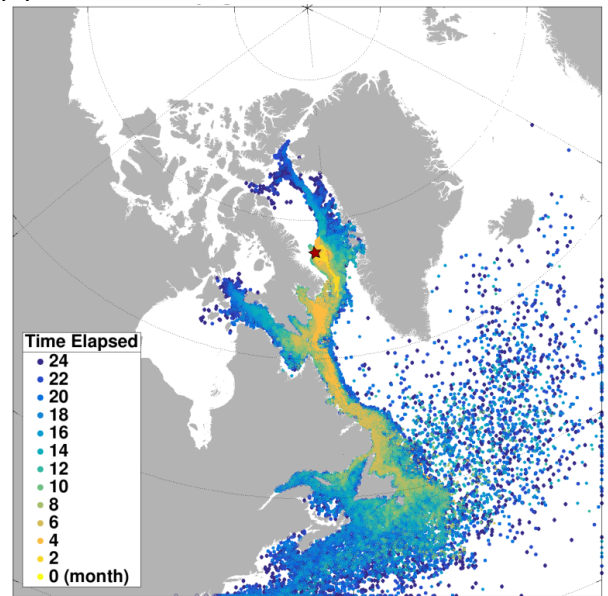
(f)



(g)



(h)



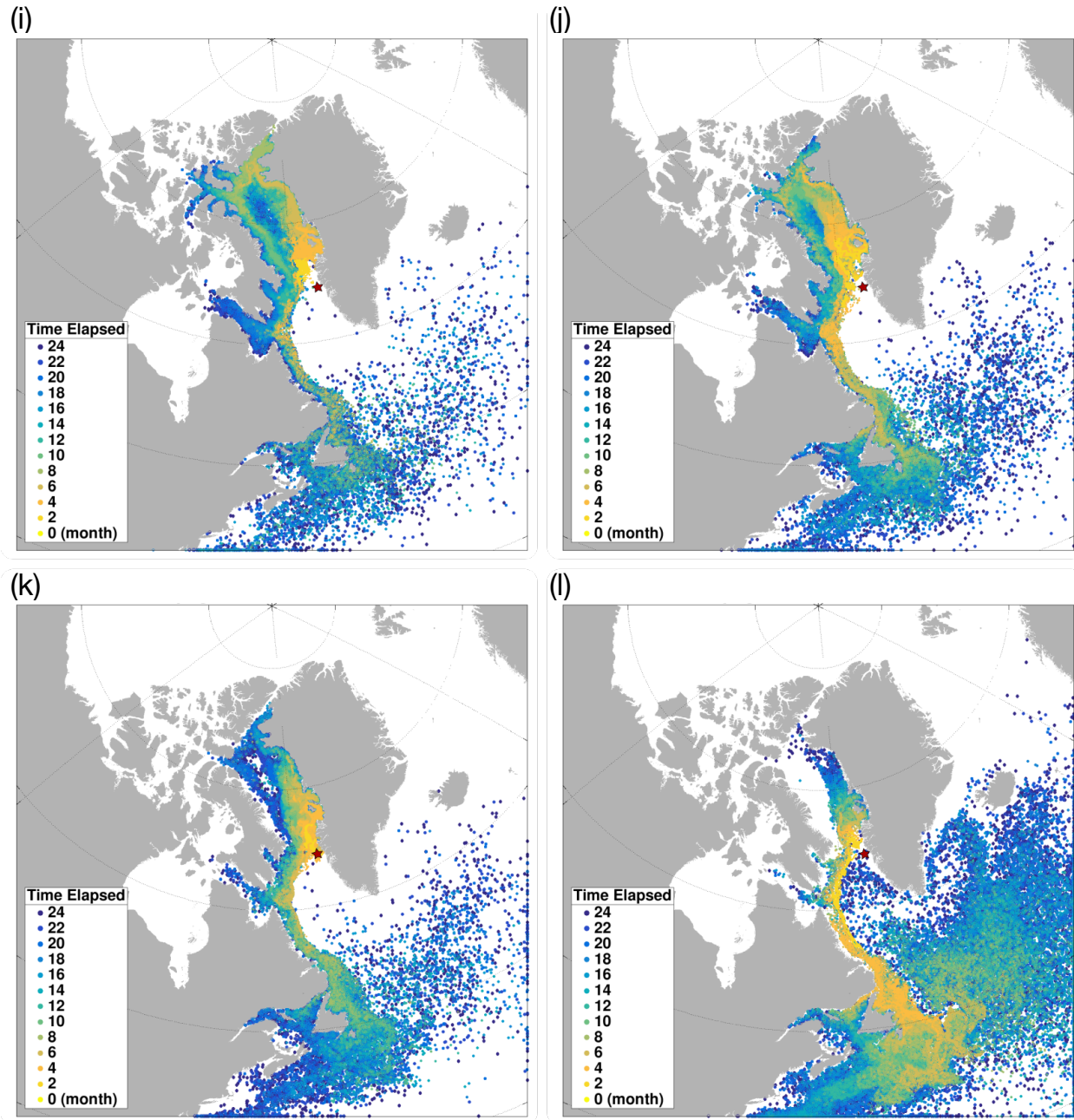


Figure 5.8: Circulation pathways of particles released in Northern Baffin Bay (a, b, c, d), Southern Baffin Bay nearshore (e, f, g, h), and Davis Strait East (i, j, k, l). From each release site, we visualised the propagation of particles released in June 1st 2010, October 10th 2010, June 1st 2015, and October 10th 2015, respectively.

The spread of particles released in Baffin Bay was linked with the variability of the NAO. During negative (positive) NAO, the baroclinic circulation in Baffin Bay enhanced (weakened) with weakened (stronger) inflow of polar water and northward flow of West Greenland Current. For instance, 2010 (figure 5.8) represent a strong negative NAO year. The strong northward West Greenland Current promoted more northward transport in Baffin Bay, resulting in particles propagating into Nares Strait. However, such variability only reflects the spread of particles. When considering all releases in Baffin Bay, we found that particles were most likely to accumulate in the interior of the bay and along the southeastern and southern coast of Baffin Island (figure 5.9).

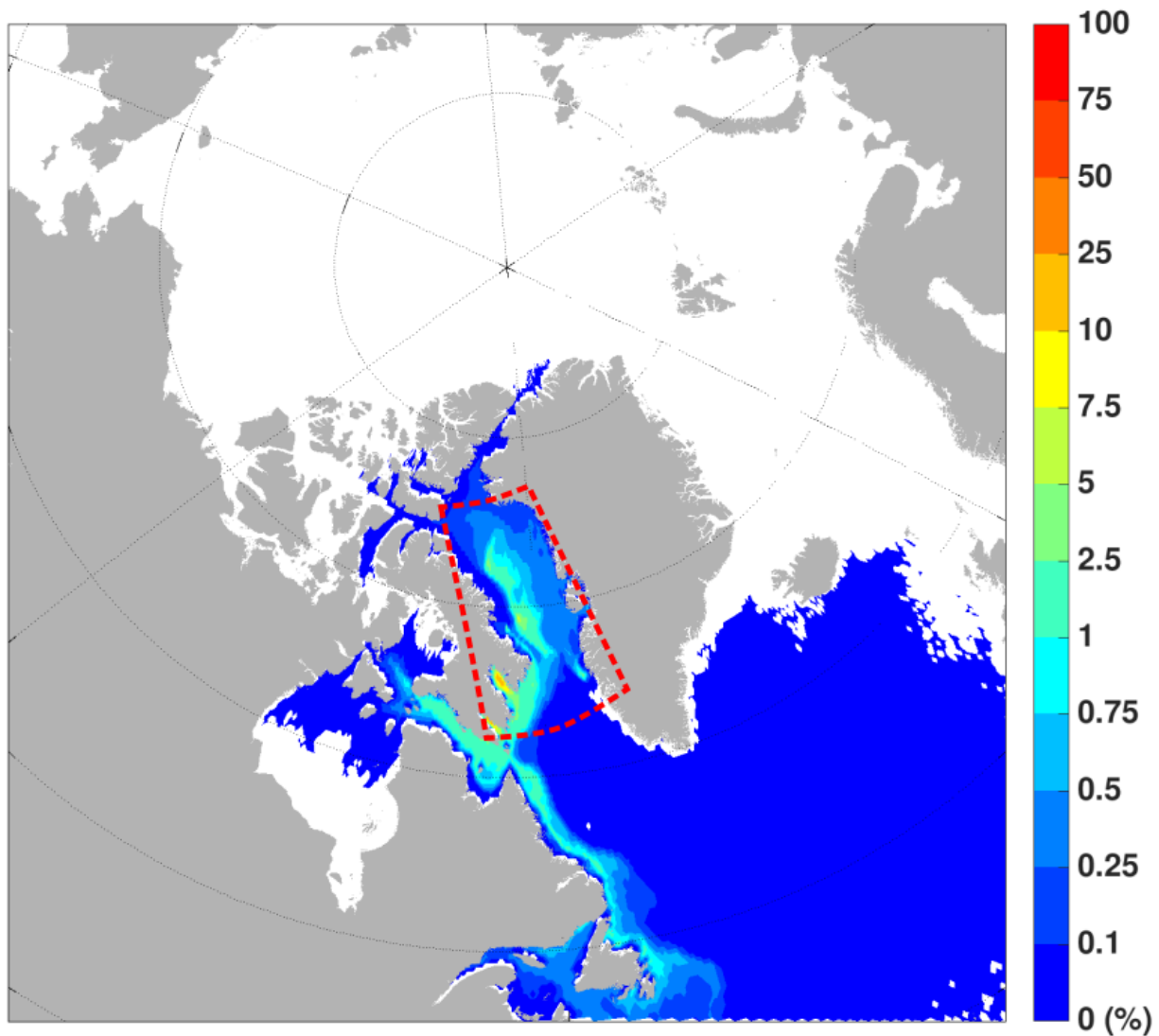


Figure 5.9: Average probability (in percentage) of all simulations from all Baffin Bay release sites (region indicated by red dashed line).

5.4. Discussion

We examined all simulations in the NWP numerically with respect to their horizontal spreading area, direct distances, full trajectory, deep spread due to advection, variability and uncertainty. We divided the release sites into 6 groups with respect to their locations and the circulation pathways exhibited (table 5.1). For each group, the regional average values were calculated in order to overview the spread of particles among all releases in the NWP, and to determine which regions exhibited higher level of threats. Then, we investigated the individual release sites within these regions with respect to the parameters listed above to determine the release site, from which the particles exhibited largest spread. Furthermore, we calculated the longterm and seasonal averages of the spread of particles to determine the sensitivity of the simulation results to different release dates. As well we highlight the role of different atmospheric circulation nodes to the spread of particles.

5.4.1. Horizontal Spreading Area

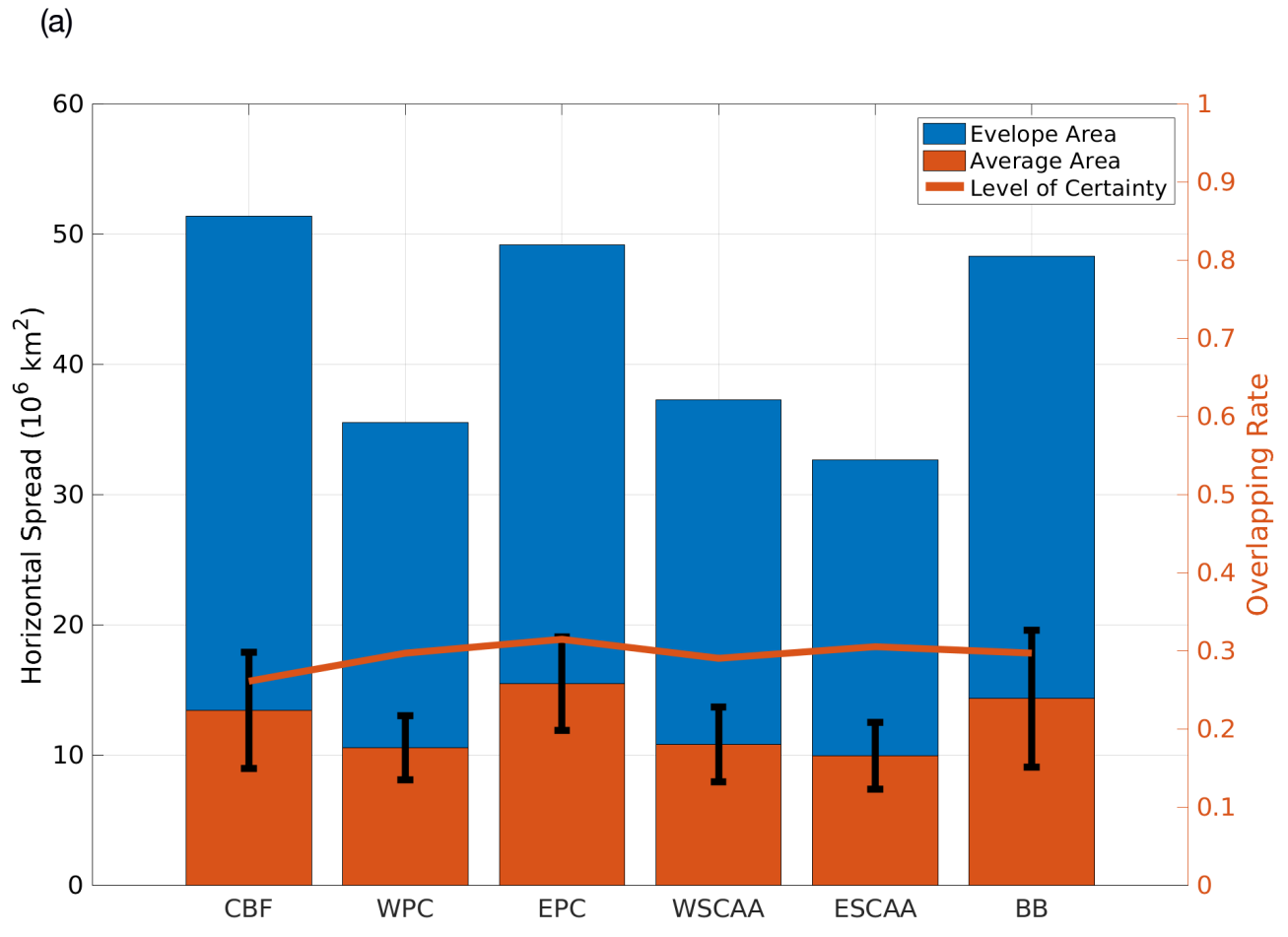
We first evaluated the regional horizontal spreading area in terms of their envelope area, average area, and their standard deviations to indicate the level of variabilities. Furthermore, we calculated the ratio between the average area and envelope area, which indicates the level of uncertainty in the spread of particles from each region.

During the first year, the particles released from EPC (Eastern Parry Channel) and BB (Baffin Bay) exhibited the largest spreading area due to the majority of the particles propagating into Baffin Bay and the North Atlantic Ocean, respectively (figure 5.10-a). Although those particles released in the CFB did not exhibit the largest spreading area, they exhibited the largest envelope area. This was caused by the slower surface velocity and strong variability of the Beaufort Gyre. This is particularly significant when examining the regional average spreading area of the two year simulations. Although the CBF (Canadian Beaufort Sea), EPC, and BB exhibited similar level of spreading area, the envelope area of CBF is approximately 50% larger than the other regions. Furthermore, we found larger variability in the level of certainty from the

two year simulations, of which, those released from EPC, ESCAA (Southeastern CAA), and BB exhibited large level of certainty as the majority of particles released from these regions followed the direct outflow of polar water into the North Atlantic Ocean (figure 5.10-b).

When examining the horizontal spreading area from each release sites in detail, we found that their envelope area and average spreading area correlated well with their circulation pathways. Among the Parry Channel (fig. 5.11) and southern CAA releases (fig. 5.12), the particles released from both the western (MCLW, AG) and eastern (BRW, LSW, and LSE) ends exhibited the largest spreading area as they immediately propagated into the Arctic Ocean and North Atlantic Ocean respectively. The large envelope area from MCLW releases also correlated well with the large variability of the Beaufort Gyre. For the particles released in the southern CAA, we found that the particles released in SRB had small spreading areas, especially compared to the results from LSS, whose initial location was only 100 km away.

The Baffin Bay releases exhibited largest spreading area as the majority of particles propagated into the North Atlantic Ocean. When examining the individual release sites within Baffin Bay, we found that most of these releases exhibited positive correlation with respect to the distances from the initial location to the open water. Two exceptions were found for the particles released in Cumberland Sound and Frobisher Sound, from where, instead of traversing Davis Strait directly, the particles first circulated within these sounds during the first year after release.



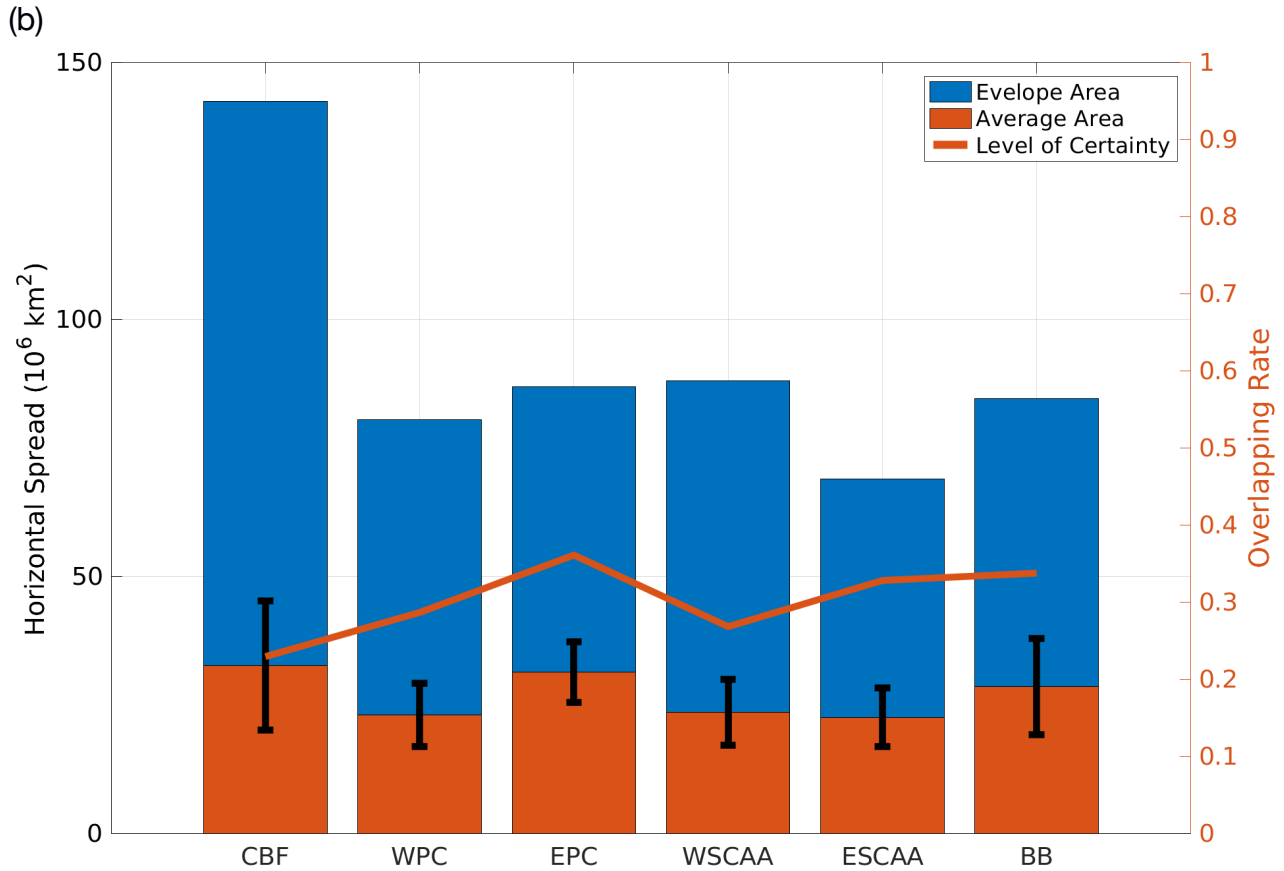


Figure 5.10: Regional average horizontal spreading area of NWP releases during the first year of simulation (a) and two year simulation (b). CBF: Canadian Beaufort Sea releases, WPC: Western Parry Channel releases; EPC: eastern Parry Channel releases, WSCAA: southwestern CAA releases, ESCAA: southeastern CAA releases, and BB: Baffin Bay releases. Note that black bar represents the standard deviation of the average area.

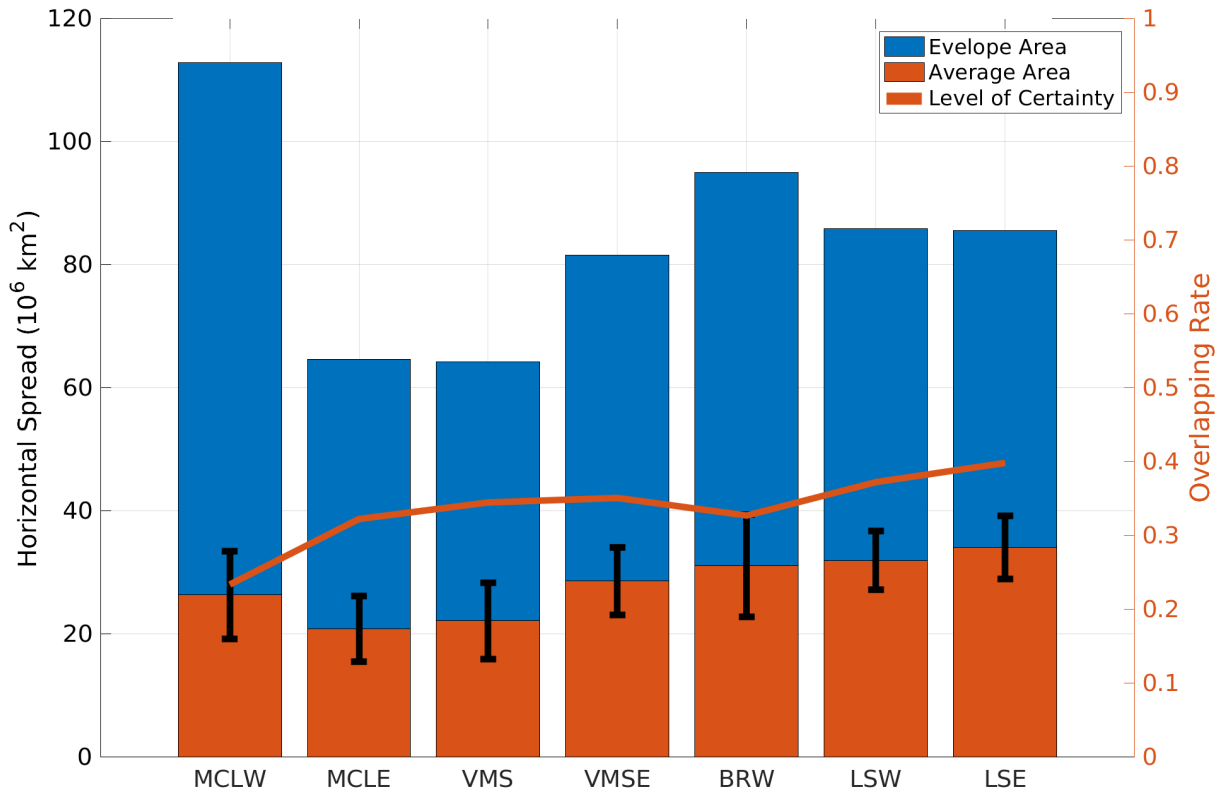


Figure 5.11: Average spreading area of all releases from Parry Channel two years after released. MCLW: western M’Clure Strait, MCLE: eastern M’Clure Strait, VMS: western Viscount Melville Sound, VMSE: eastern Viscount Melville Sound, BRW: Barrow Strait, LSW: western Lancaster Sound, and LSE: eastern Lancaster Sound. Note that the black bars represent the standard deviation of the averages.

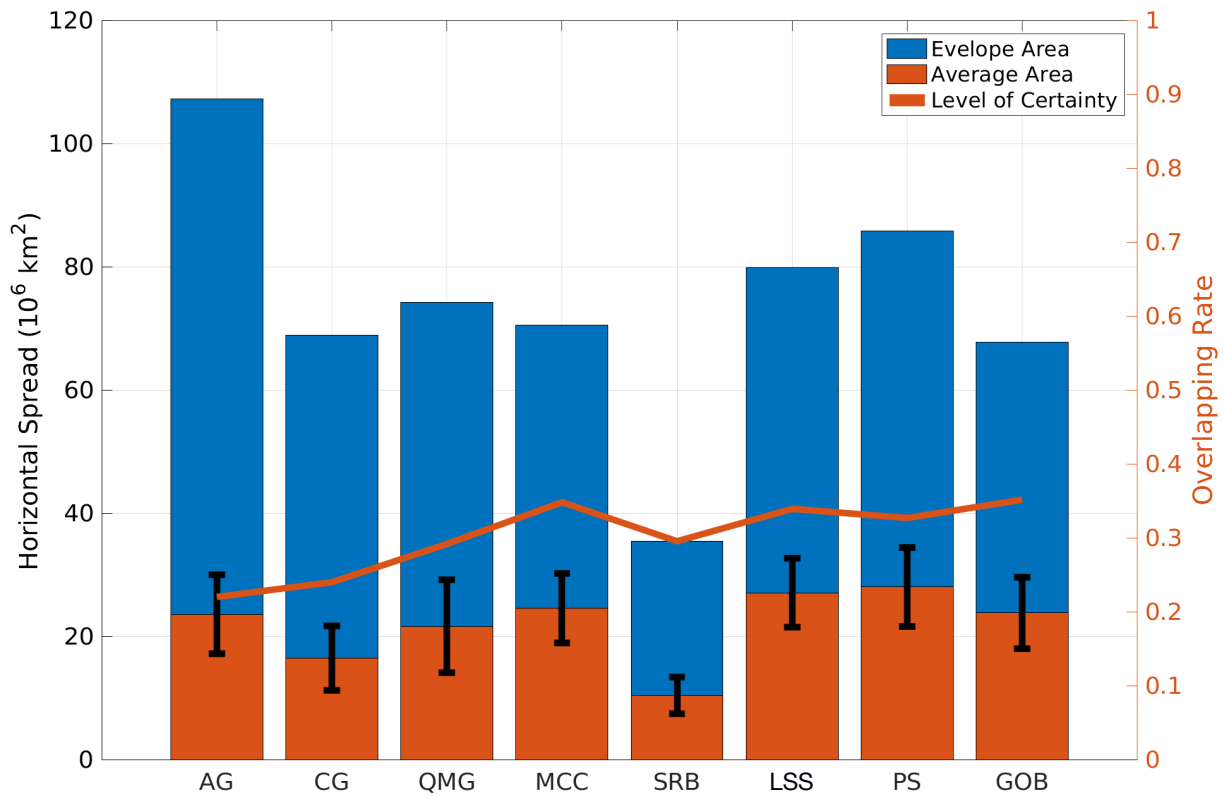


Figure 5.12: Average spreading area of all releases from southern CAA two years after released. AG: Amundsen Gulf, CG: Coronation Gulf, QMG: Queen Maud Gulf, MCC: M’Clintock Channel, SRB: St Roch Basin, LSS: Larson Sound, PS: Peel Sound, and GB: Gulf of Boothia. Note that the black bars represent the standard deviation of the averages.

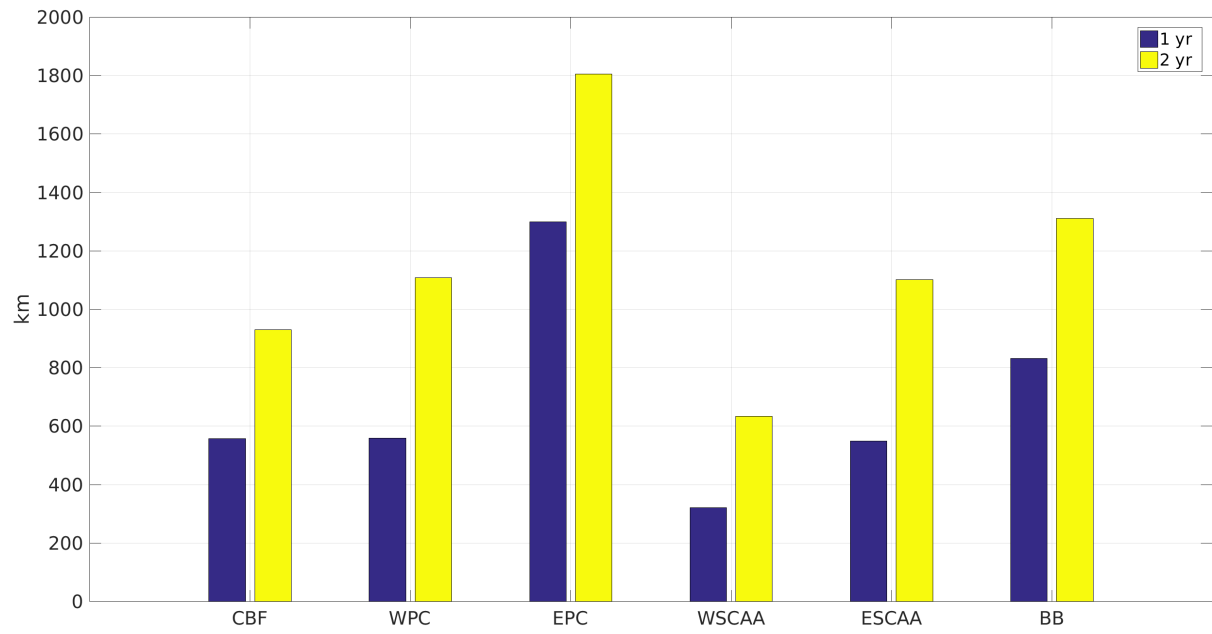
5.4.2. Distances

The long-term fate of particles was then evaluated by examining the distances between the particles' location one and two years after release compared to their initial locations. Furthermore, we calculated the full trajectory the particles travelled throughout the simulation to highlight their footprint. By comparing the ratio between direct distance and full trajectory, we were able to further analyse the circulation pathways in terms of the strength of recirculation.

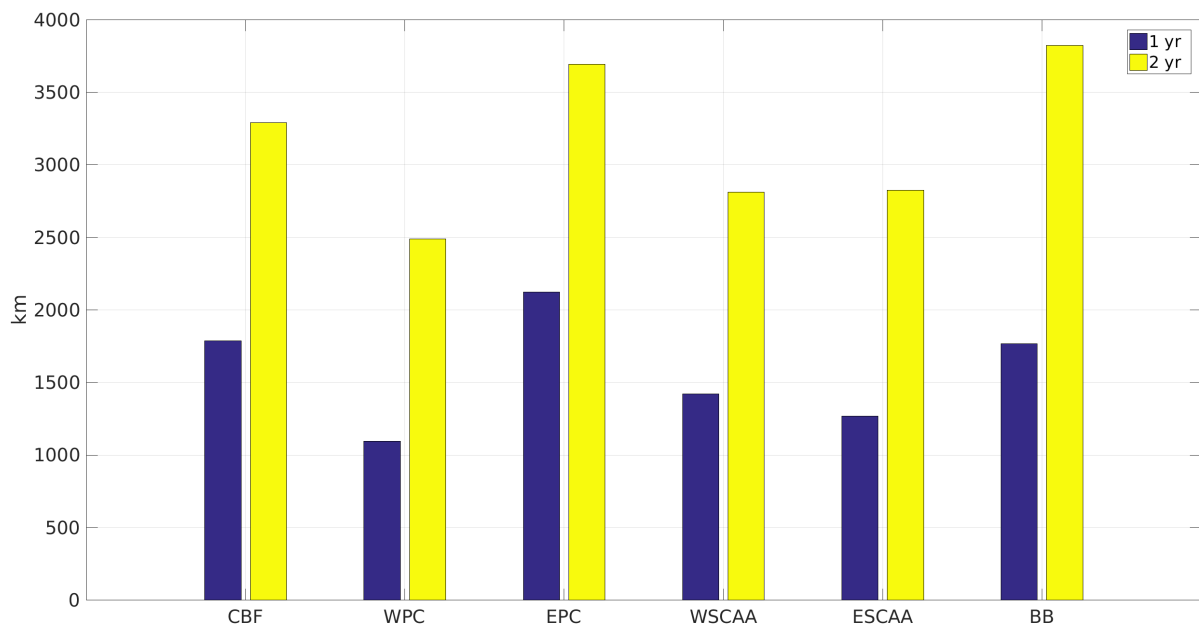
We found that EPC group exhibited the largest direct distances, as the majority of particles released in eastern Parry Channel almost immediately exited the CAA via Lancaster Sound, then propagated southward with the Baffin Island Current (figure 5.13-a). Comparing to the EPC releases, the particles seeded in Baffin Bay did not exhibit equivalently large direct distances as some particles joined the West Greenland Current and remained in Baffin Bay throughout the two years of simulation. This is particularly significant when examining the regional mean of the full trajectory travelled (figure 5.13-b). Furthermore, the particles seeded in the Canadian Beaufort Sea also exhibited large trajectory, however, this did not result in large direct distances.

Therefore, we calculated the ratio between the direct distances to the full trajectory to determine the rate of recirculation (figure 5.13-c). Besides the CBF group which had a strong signal of recirculation, the strongest signal of recirculation is from the WSCAA (Southwestern CAA) group (AG and CG). Released in the western end of southern CAA, these particles propagated in two directions: westward into the Arctic Ocean, joining the Beaufort Gyre, or northeastward traversing the straits of CAA. Spreading into the straits of the CAA, the eastward propagating particles exhibited a large rate of recirculation, yet less direct distances. It should be noted that among the southern CAA releases, the particles released in SRB exhibited the highest rate of recirculation during the first year of simulation. This is because the majority of particles released here were found within the St Roch Basin during the first year after release as they were constrained by the swash of Back River discharge during the summer months.

(a)



(b)



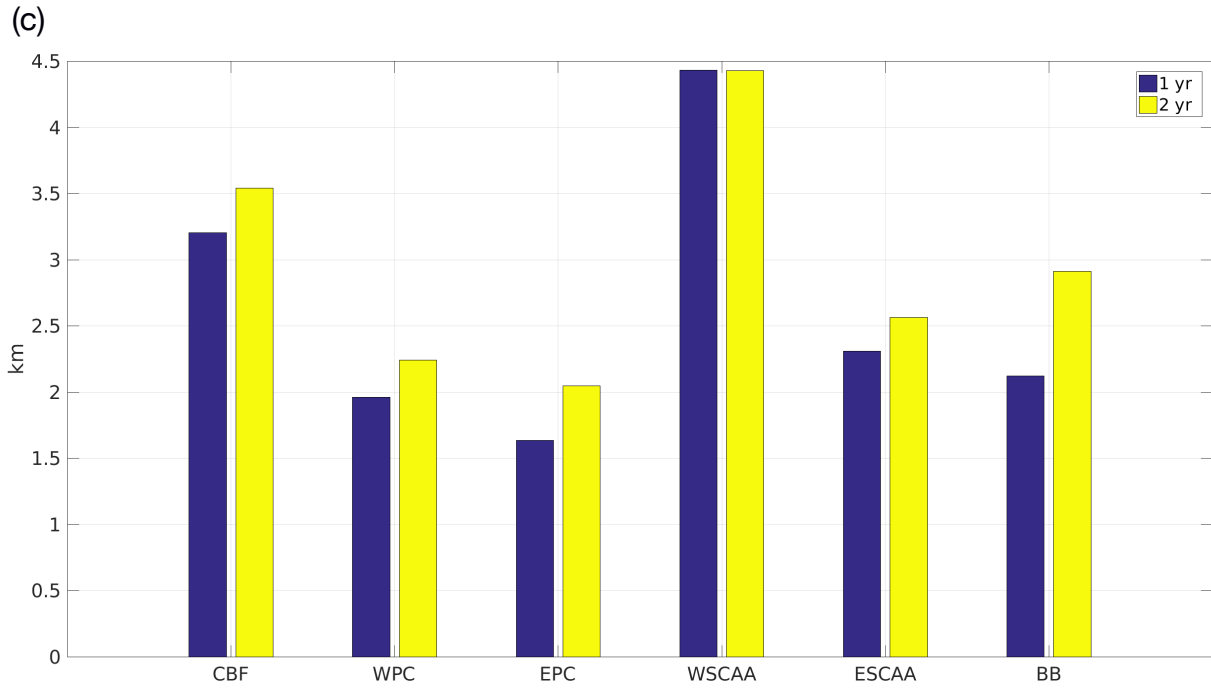


Figure 5.13: Regional average direct distance (a), full trajectory (b), and rate of recirculation (c) for all releases. CBF: Canadian Beaufort Sea releases, WPC: Western Parry Channel releases; EPC: eastern Parry Channel releases, WSCAA: southwestern CAA releases, ESCAA: southeastern CAA releases, and BB: Baffin Bay releases.

5.4.3. Deep Spreading

In this study, we consider the source of pollutant to be ship fuel that was accidentally spilt near the ocean surface. However, particles do not remain at the surface during the integrations. Being mixed with ocean currents, particles propagated deep into the water column, posing a significant environmental threat. In this section, we calculated the average percentage of particles with depth exceeding 90 metres, which would be extremely difficult to recover.

We compared the average percentage of particles over 90 metres for each region (fig. 5.14). We found that BB releases exhibited the largest percentage of deep spread both one and two years after release (*e.g.* figure 5.15-a and 5.15-b). Released in Baffin Bay, some particles propagated deep into the water column due to the strong vertical mixing within top 500 meters. During the first year of integration (figure 5.15-c), the EPC exhibited the largest percentage of deep spread as the majority of the particles were found in Baffin Bay. As they spread into North Atlantic Ocean during the second year, the percentage of deep spread decreased (figure 5.15-d). Released in western Parry Channel (WPC) (figure 5.15-e and 5.15-f) and southern CAA (WSCAA (figure 5.15-g and 5.15-h) and ESCAA (figure 5.15-i and 5.15-j)), we found the particles with depth over 90 metres within the CAA. Released in the CBF, as the majority of particles travelled with the BG and TPD on the surface (figure 5.15-k and 5.15-l).

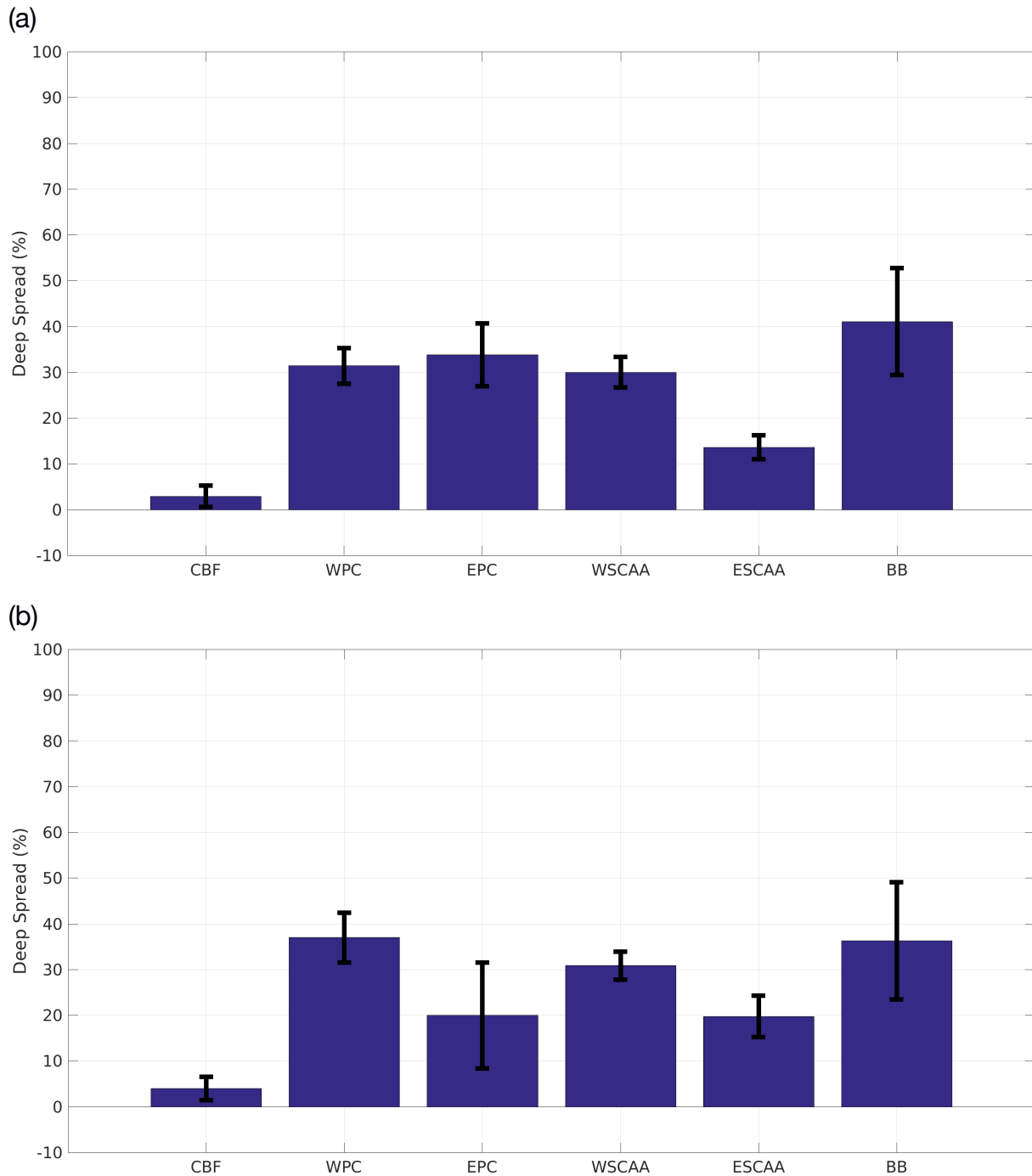
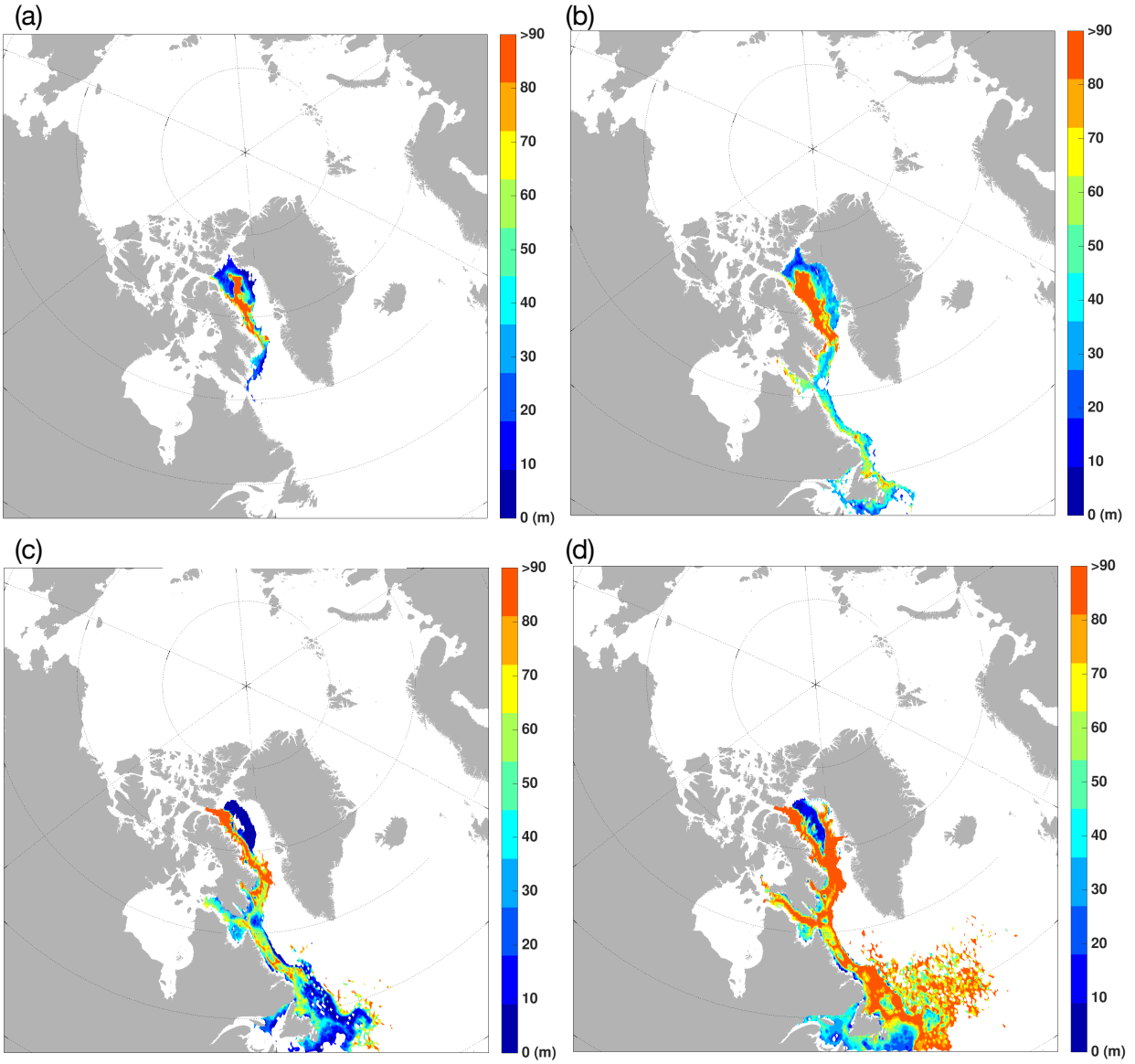
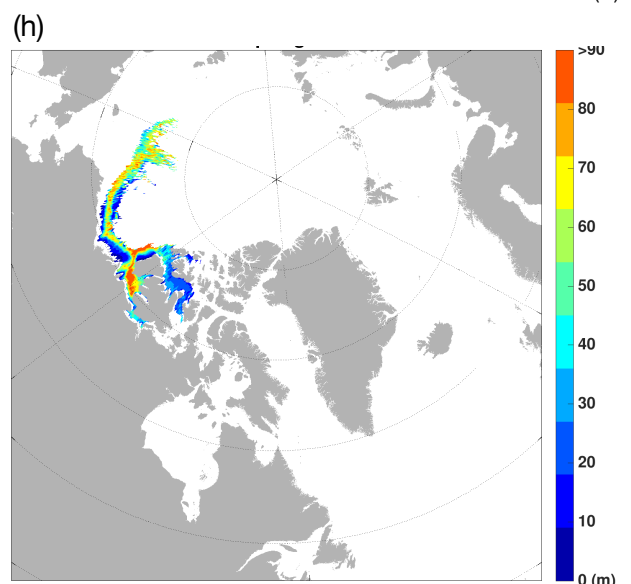
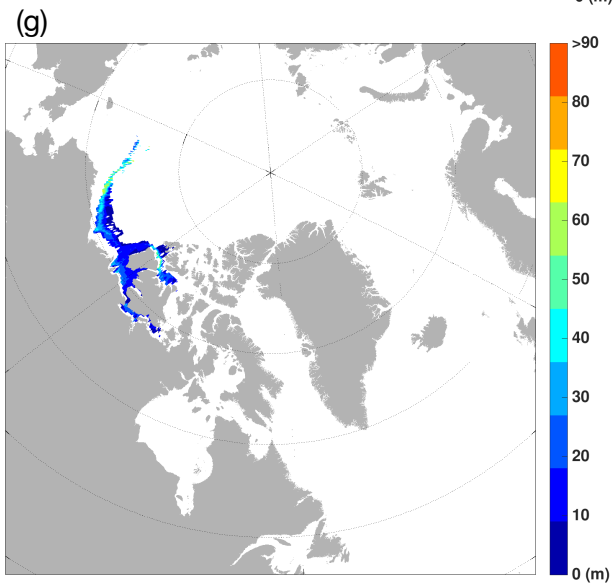
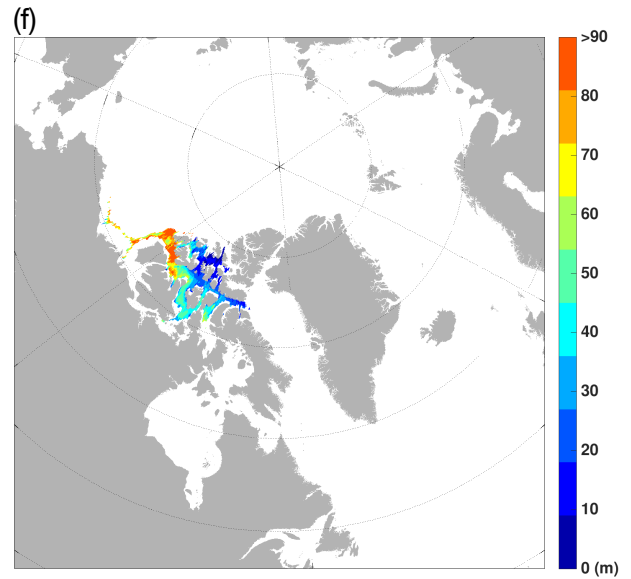
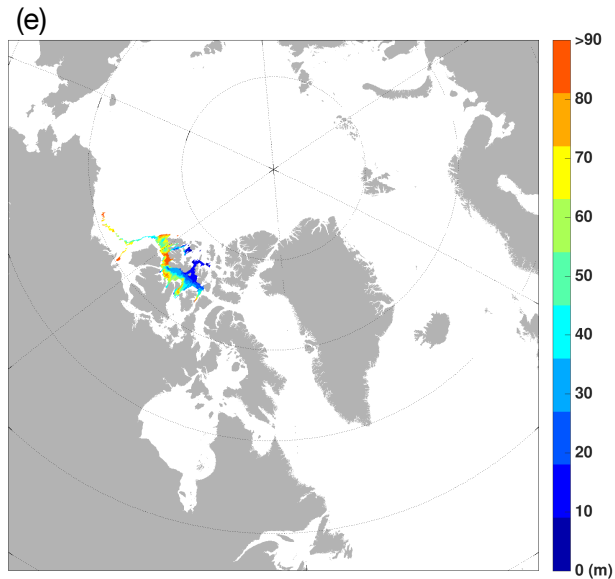


Figure 5.14: Regional average of deep spread (percentage of particles with depth exceed 90 metres) one year (a) and two years (b) after released. CBF: Canadian Beaufort Sea releases, WPC: Western Parry Channel releases; EPC: eastern Parry Channel releases, WSCAA: southwestern CAA releases, ESCAA: southeastern CAA releases, and BB: Baffin Bay releases. Note that the black bars represent the standard deviation of the averages.





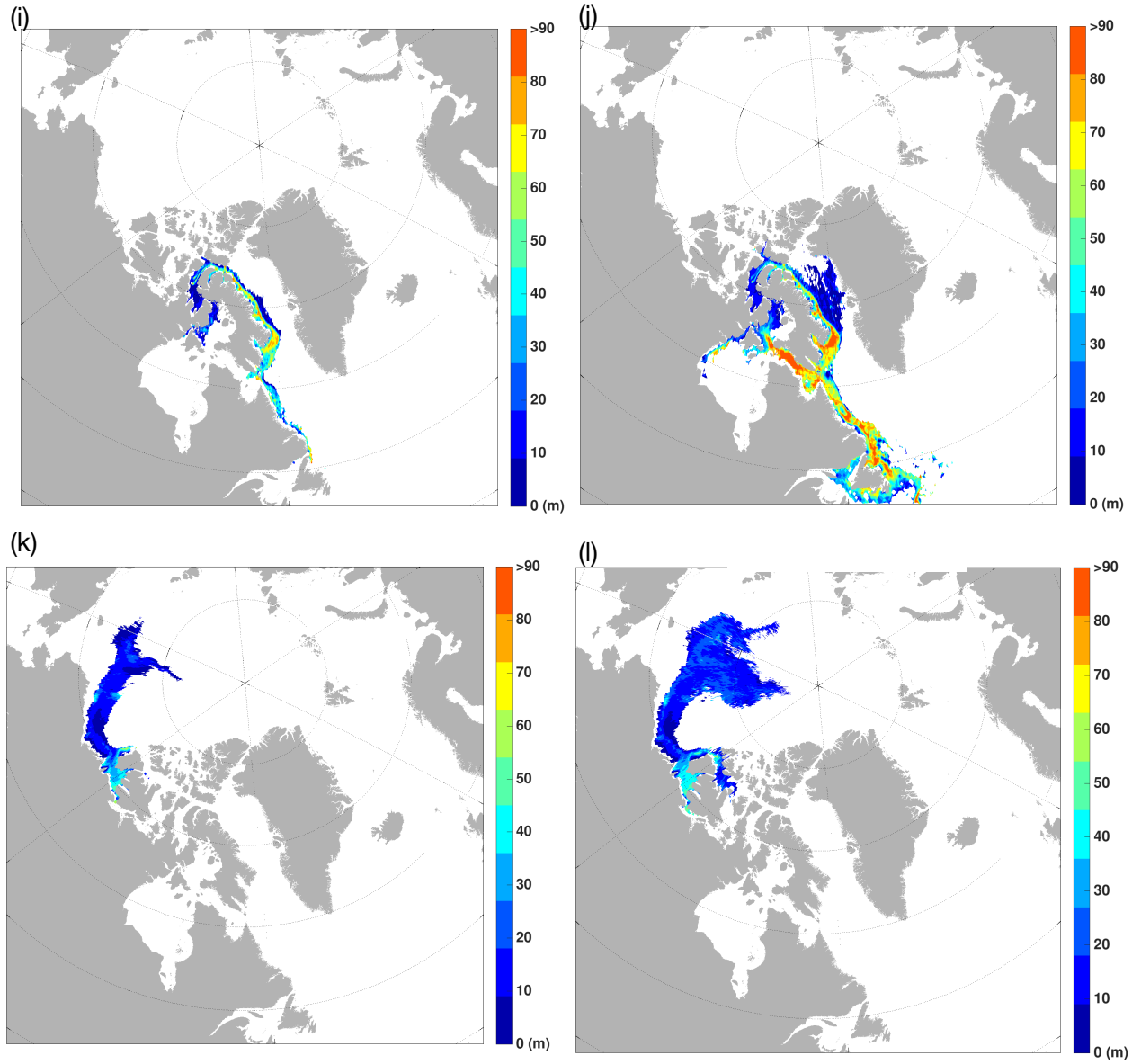


Figure 5.15: depth of particles released on June 1st 2010 from: Northern Baffin Bay (a and b), eastern Lancaster Sound (c and d), eastern M'Clure Strait (e and f), Amundsen Gulf (g and h), Gulf of Boothia (i and j), and Canadian Beaufort Sea (k and l) one year and two years after released respectively.

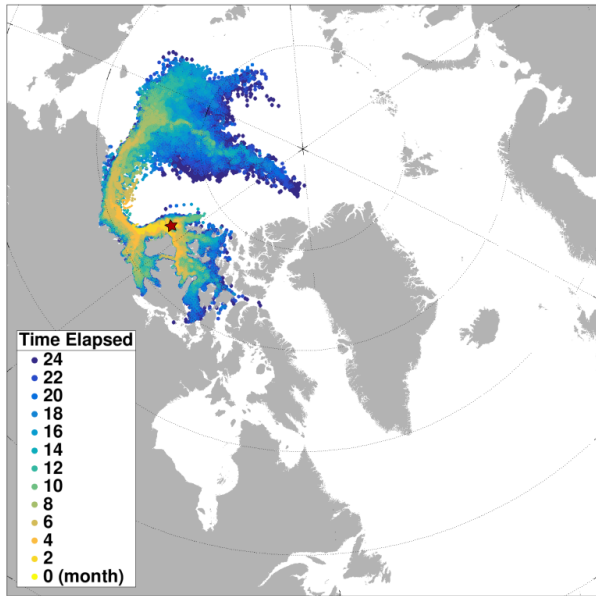
5.4.4. Sensitivity and Limitations

Released along the NWP, the particles exhibited different pathways associated with the different circulation regimes of where they were seeded. Although there was similarity in their general pathways and similarity in the resultant spreading area, we found that the circulation pathways were extremely sensitive to the initial location. In figure 5.16, we explicitly visualised the circulation pathways of particles released on June 1st, 2010.

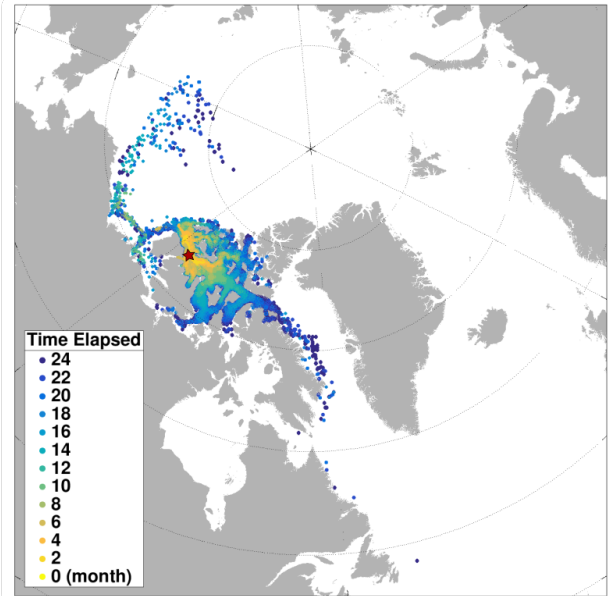
MCLW (figure 5.16-a) and MCLE (figure 5.16-b) are less than 450 km apart, however, they exhibited significant different circulation pathways. Located at the western end of Parry Channel, the majority of particles released from MCLW propagated westward into the Arctic Ocean, resulting in a larger spreading area than those released from MCLE. Another factor influencing the circulation pathways of particles released along Parry Channel is the southward drift into M'Clintock Channel. The distance between VMS (figure 5.16-c) and VMSE (figure 5.16-d) is approximately 150 km, which are located east and west of M'Clintock Channel, respectively. The majority of particles released from VMS followed the southward drift into M'Clintock Channel, whilst those released from VMSE exhibited a more direct eastward outflow exiting the CAA. The latter resulted in more particles entering Baffin Bay approximately 2 months after release, whilst only a smaller amount of particles from VMS entered Baffin Bay, approximately 20 months after release. The most typical example from the southern CAA releases is from LSS (figure 5.16-e) and SRB (figure 5.16-f). Located approximately 200 km apart, the particles released from LSS exhibited significantly larger area with high velocity than the SRB releases. This was caused by the isolation of Saint Roch Basin and its short sea-ice free period. The Baffin Bay releases also exhibited significantly different circulation pathways. A typical example is found from particles released from offshore and nearshore southern Baffin Bay (figure 5.16-g and h, respectively). The distances between the two release sites is 75 km. Released nearshore, particles exhibited a direct southward flow with Baffin Island Current. However, when released further offshore, a significant portion joined the northward West Greenland Current. Therefore, we found that the circulation pathways were extremely sensitive to the initial seeding location.

The limitations of this study arise when considering the behaviour of oil in the Arctic Ocean. In this study, we focused on the pollutant infested water, *i.e.* the product of the initial weathering processes weeks after the spill. However, the pollutant does not remain inactive during the simulation period. Processes such as sedimentation and emulsification can occur months after the spill (Afenyo *et al.*, 2016). Furthermore, this study only focused on the oceanic advection. In the Arctic environment, the other main transport process is encapsulation, *i.e.* oil being trapped and drifting with sea ice, which would occur when sea ice concentration exceeds 60% (Venkatesh *et al.*, 1990). In order to overcome these limitations, one direction for future work is to use an active particle tracking scheme, representing the most typical composition of ship fuel, to model the weathering processes in the Arctic environment. Furthermore, we believe that encapsulation can be simulated via tuning the integration scheme of ARIANE to include the dynamics of sea ice.

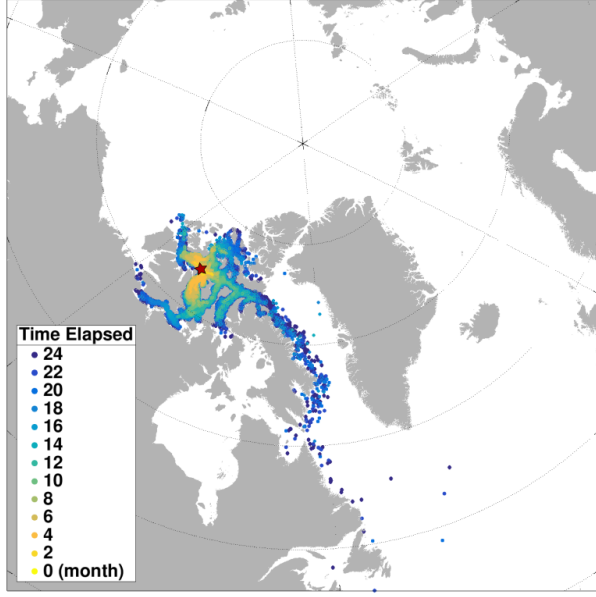
(a)



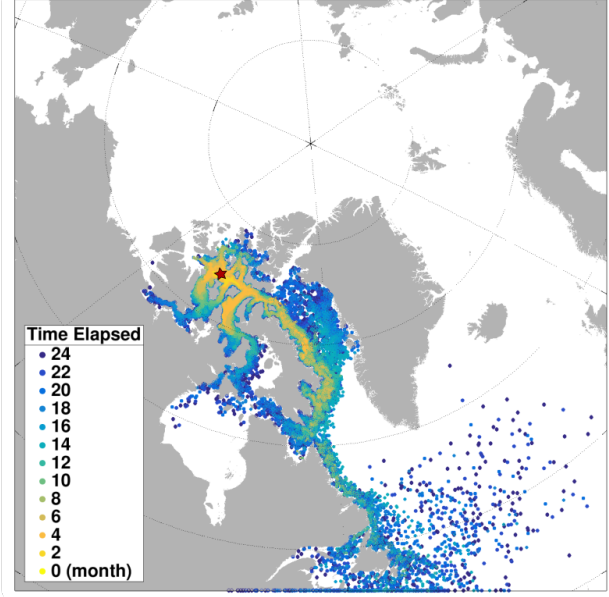
(b)



(c)



(d)



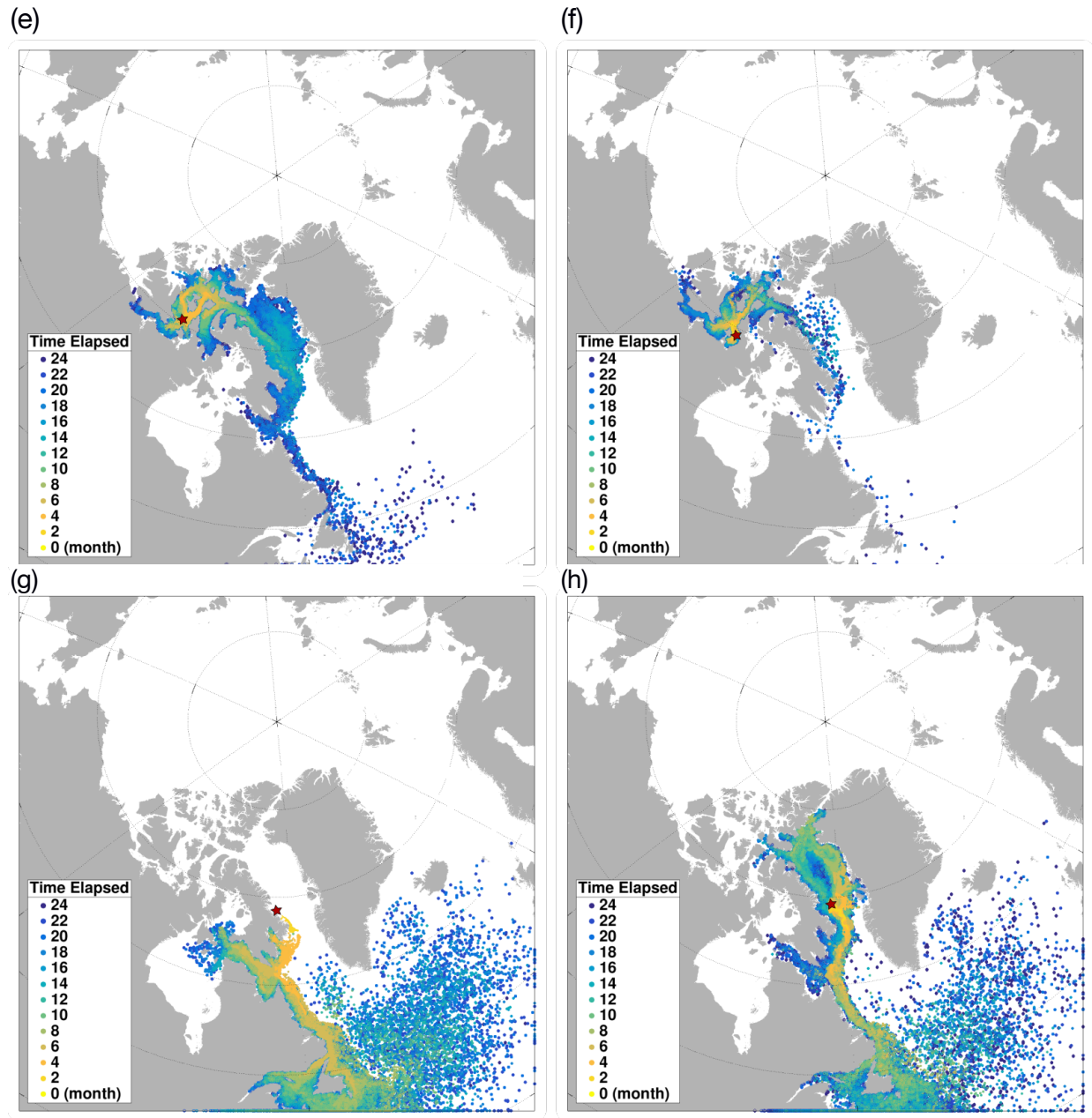


Figure 5.16: propagation of particles released in June 1st, 2010 from western and eastern M'Clure Strait (a and b), western and eastern Viscount Melville Sound (c and d), Lason Sound (e), St Roch Basin (f), nearshore (g) and offshore (h) southern Baffin Bay.

5.5. Conclusion

In this study, we examined the role of oceanic advection in the circulation pathways of pollutant spilt along the NWP in the Canadian Arctic. We found that particles followed three distinctive circulation pathways: (1) released in Canadian Beaufort Sea and the western edge of the CAA, the majority of particles followed the anti-cyclonic BG and then the TPD; (2) other releases in the CAA followed the eastward outflow into Baffin Bay; and (3) particles released in Baffin Bay traversed Davis Strait and propagated southward into the North Atlantic Ocean. Although we found similarities in the propagation of particles released from each region, the circulation pathways were extremely sensitive to where the particles were seeded initially.

We divided the 25 releases sites into 6 groups with respect to the distinctive feature of in their pathways. We computed and compared the spreading area, distances travelled, and deep spread for each region to determine from where, the spill of pollutant would cause most severe outcome. We found that particles released in Baffin Bay, the particles exhibited largest spreading area as the majority propagated into North Atlantic Ocean with high velocity. Furthermore, Baffin Bay releases exhibited large variability and uncertainty in its circulation pathways, as well as the largest percentage of particles with depth over 90 metres. Therefore, the accidental spill of pollutant in Baffin Bay would result in the most severe consequences due to its rapid vertical mixing and proximity to the open water. The Canadian Beaufort Sea releases pose the second largest threat as the majority of particles propagated into the Arctic Ocean immediately after release. Furthermore, the spread of particles in the Arctic Ocean exhibited the largest level of uncertainty, which is extremely challenging for the following recovery operations.

This study highlighted the role of oceanic advection in the spread of pollutant spilt along the NWP in the Canadian Arctic. We expect this study to provide a oceanographic guideline for the commercial opening of the NWP in the future, and illuminate the sensitive regions for future detailed case studies.

Bibliography

- Afenyo, M., Veitch, B., & Khan, F. (2016). A State-of-the-Art Review of Fate and Transport of Oil Spills in Open and Ice-Covered Water Doi:https://doi.org/10.1016/j.oceaneng.2015.10.014
- Bamber, J., Van, D. B., Ettema, J., Lenaerts, J., & Rignot, E. (2012). Recent Large Increases in Freshwater Fluxes From Greenland Into the North Atlantic. *Geophysical Research Letters*, 39(19) Doi:10.1029/2012GL052552
- Blanke, B., & Raynaud, S. (1997). Kinematics of the Pacific Equatorial Undercurrent: an Eulerian and Lagrangian Approach From GCM Results. *Journal of Physical Oceanography*, 27(6), 1038-1053. Doi:10.1175/1520-0485(1997)027<1038:KOTPEU>2.0.CO;2
- Brigham, L. W., Ellis, B., Arctic Council, & Arctic Council Protection of the Arctic Marine Environment Working Group. (2009). *Arctic Marine Shipping Assessment 2009 Report*. Akureyri, Iceland: Arctic Council, PAME, Protection of the Arctic Marine Environment.
- Dai, A., Qian, T., Trenberth, K. E., & Milliman, J. D. (2009). Changes in Continental Freshwater Discharge From 1948 to 2004. *Journal of Climate*, 22(10), 2773-2792. Doi:10.1175/2008JCLI2592.1
- Dawson, J., Pizzolato, L., Howell, S. E. L., Copland, L., & Johnston, M. E. (2018). Temporal and Spatial Patterns of Ship Traffic in the Canadian Arctic From 1990 to 2015. *Arctic*, 71(1), 15-26. Doi:10.14430/Arctic4698
- Drozdowski, A., Nudds, S., Hannah, C. G., Niu, H., Peterson, I., & Perrie, W. (2011). *Review of Oil Spill Trajectory Modelling in the Presence of Ice*. Canada
- Dukhovskoy, D. S., Myers, P. G., Platov, G., Timmermans, M., Curry, B., Proshutinsky, A., . . . Somavilla, R. (2016). Greenland Freshwater Pathways In The Sub-Arctic Seas From Model Experiments With Passive Tracers. *Journal Of Geophysical Research: Oceans*, 121(1), 877-907. Doi:10.1002/2015JC011290

- Feucher, C., Garcia-Quintana, Y., Yashayaev, I., Hu, X., & Myers, P. G. (2019). Labrador Sea Water Formation Rate and its Impact on the Local Meridional Overturning Circulation. *Journal of Geophysical Research: Oceans*, 124(8), 5654-5670. Doi:10.1029/2019JC015065
- Fissel, D. B., De, M., Álvarez, S., Kulan, N., Mudge, T., & Marko, J. R. (2011). Long-Term Trends for Sea Ice in the Western Arctic Ocean: Implications for Shipping and Offshore Oil and Gas Activities
- Gillard, L. C., Hu, X., Myers, P. G., & Bamber, J. L. (2016). Meltwater Pathways From Marine Terminating Glaciers of the Greenland Ice Sheet. *Geophysical Research Letters*, 43(20), 10,873-10,882. Doi:10.1002/2016GL070969
- Grivault, N., Hu, X., & Myers, P. G. (2018). Impact of the Surface Stress on the Volume and Freshwater Transport Through the Canadian Arctic Archipelago From a High-Resolution Numerical Simulation. *Journal of Geophysical Research: Oceans*, 123(12), 9038-9060. Doi:10.1029/2018JC013984
- Haas, C., & Howell, S. E. L. (2015). Ice Thickness in the Northwest Passage. *Geophysical Research Letters*, 42(18), 7673-7680. Doi:10.1002/2015GL065704
- Howell, S. E. L., Tivy, A., Yackel, J. J., & McCourt, S. (2008). Multi-Year Sea-Ice Conditions in the Western Canadian Arctic Archipelago Region of the Northwest Passage: 1968–2006. *Atmosphere-Ocean*, 46(2), 229-242. Doi:10.3137/Ao.460203
- Howell, S. E. L., Wohlleben, T., Dabboor, M., Derksen, C., Komarov, A., & Pizzolato, L. (2013). Recent Changes in the Exchange of Sea Ice Between the Arctic Ocean and the Canadian Arctic Archipelago. *Journal of Geophysical Research: Oceans*, 118(7), 3595-3607. Doi:10.1002/Jgrc.20265
- Hu, X., Sun, J., Chan, T. O., & Myers, P. G. (2018). Thermodynamic and Dynamic Ice Thickness Contributions in the Canadian Arctic Archipelago in NEMO-LIM2 Numerical Simulations. *The Cryosphere*, 12(4), 1233-1247. Doi:10.5194/Tc-12-1233-2018

- Hu, X., Myers, P. G., & Lu, Y. (2019). Pacific Water Pathway in the Arctic Ocean and Beaufort Gyre in Two Simulations With Different Horizontal Resolutions. *Journal of Geophysical Research: Oceans*, 124(8), 6414-6432. Doi:10.1029/2019JC015111
- Hughes, K. G., Klymak, J. M., Hu, X., & Myers, P. G. (2017). Water Mass Modification and Mixing Rates in a 1/12° Simulation of the Canadian Arctic Archipelago. *Journal of Geophysical Research: Oceans*, 122(2), 803-820. Doi:10.1002/2016JC012235
- Jahn, A., Tremblay, B., Mysak, L. A., & Newton, R. (2010). Effect of the Large-Scale Atmospheric Circulation on the Variability of the Arctic Ocean Freshwater Export. *Climate Dynamics*, 34(2), 201-222. Doi:10.1007/S00382-009-0558-Z
- Kelly, S., Popova, E., Aksenov, Y., Marsh, R., & Yool, A. (2018). Lagrangian Modeling of Arctic Ocean Circulation Pathways: Impact of Advection on Spread of Pollutants. *Journal of Geophysical Research: Oceans*, 123(4), 2882-2902. Doi:10.1002/2017JC013460
- Kwok, R., Spreen, G., & Pang, S. (2013). Arctic Sea Ice Circulation and Drift Speed: Decadal Trends and Ocean Currents. *Journal of Geophysical Research: Oceans*, 118(5), 2408-2425. Doi:10.1002/Jgrc.20191
- Lackenbauer, W., Lajeunesse, A., Canadian Defence and Foreign, Affairs Institute, & University of Calgary School of, Public Policy. (2014). On Uncertain Ice: the Future of Arctic Shipping and the Northwest Passage.
- Lazier, J. R. N., & Wright, D. G. (1993). Annual Velocity Variations in the Labrador Current. *Journal of Physical Oceanography*, 23(4), 659-678. Doi:10.1175/1520-0485(1993)023<0659:AVVITL>2.0.CO;2
- McGarrity, J., & Gloystein, H. (2013, September 27). Big Freighter Traverses Northwest Passage for 1st Time. *Reuters Environment* Retrieved From <https://www.reuters.com/article/us-shipping-coal-arctic/big-freighter-traverses-northwest-passage-for-1st-time-idUSBRE98Q0K720130927>

- Mercator Ocean (2017): Mercator Ocean GLORYS2V3 Reanalysis - Forcing dataset (for MARVL). Australian Ocean Data Network.dataset. <http://catalogue.aodn.org.au/geonetwork/srv/en/metadata.show?uuid=55286d43-8d3c-40e3-a12f-3178a2f734ae>
- Mills, W. J. (2003). *Exploring Polar Frontiers : a Historical Encyclopedia*. Santa Barbara, Calif.: Abc-Clio.
- Münchow, A., Falkner, K. K., & Melling, H. (2015). Baffin Island and West Greenland Current Systems in Northern Baffin Bay Doi:https://doi.org/10.1016/j.pocean.2014.04.001
- Østrem, W., Eger, K. M., Fløistad, B., Jørgensen-Dahl, A., Lothe, L., Mejlænder-Larsen, M., . . . Wergeland, T. (2013). *Shipping In Arctic Waters: A Comparison Of The Northeast, Northwest And Trans Polar Passages*. Dordrecht ; New York: Springer.
- Prowse, T. D., Furgal, C., Chouinard, R., Melling, H., Milburn, D., & Smith, S. L. (2009). Implications of Climate Change for Economic Development in Northern Canada: Energy, Resource, and Transportation Sectors. *Ambio*, 38(5), 272-281. Doi:10.1579/0044-7447-38.5.272 [Doi]
- Ridenour, N. A., Hu, X., Jafarikhasragh, S., Landy, J. C., Lukovich, J. V., Stadnyk, T. A., . . . Barber, D. G. (2019). *Sensitivity of Freshwater Dynamics to Ocean Model Resolution and River Discharge Forcing in the Hudson Bay Complex* Doi:https://doi.org/10.1016/j.jmarsys.2019.04.002
- Serreze, M. C., & Stroeve, J. (2015). Arctic Sea Ice Trends, Variability and Implications for Seasonal Ice Forecasting. *Philosophical Transactions.Series A, Mathematical, Physical, and Engineering Sciences*, 373(2045), 20140159. Doi:10.1098/Rsta.2014.0159
- Smith, G. C., Roy, F., Mann, P., Dupont, F., Brasnett, B., Lemieux, J., . . . Bélair, S. (2014). A New Atmospheric Dataset for Forcing Ice–Ocean Models: Evaluation of Reforecasts Using the Canadian Global Deterministic Prediction System. *Quarterly Journal of the Royal Meteorological Society*, 140(680), 881-894. Doi:10.1002/Qj.2194

- Stroeve, J., Holland, M. M., Meier, W., Scambos, T., & Serreze, M. (2007). Arctic Sea Ice Decline: Faster Than Forecast. *Geophysical Research Letters*, 34(9)
Doi:10.1029/2007GL029703
- Stueck, W. (2013, September 19). Danish Firm Seeks To Be First To Bring Bulk Carrier Through Northwest Passage. *The Globe and Mail* Retrieved From <https://www.theglobeandmail.com/report-on-business/international-business/european-business/bulk-carrier-capitalizes-on-arctic-shortcut/article14405743/>
- Thompson, D. W. J., & Wallace, J. M. (1998). The Arctic Oscillation Signature in the Wintertime Geopotential Height and Temperature Fields. *Geophysical Research Letters*, 25(9), 1297-1300. Doi:10.1029/98GL00950
- Tivy, A., Howell, S. E. L., Alt, B., McCourt, S., Chagnon, R., Crocker, G., . . . Yackel, J. J. (2011). Trends and Variability in Summer Sea Ice Cover in the Canadian Arctic Based on the Canadian Ice Service Digital Archive, 1960–2008 and 1968–2008. *Journal of Geophysical Research: Oceans*, 116 Doi:10.1029/2009JC005855
- Transport Canada and Canadian Coast Guard. Assessment of Proposals Related to Oil Spill Risk for the South Coast of Newfoundland
- Venkatesh, S., El-Tahan, H., Comfort, G., & Abdelnour, R. (1990). Modelling the Behaviour of Oil Spills in Ice-Infested Waters. *Atmosphere-Ocean*, 28(3), 303-329.
Doi:10.1080/07055900.1990.9649380
- Wang, Q., Myers, P. G., Hu, X., & Bush, A. B. G. (2012). Flow Constraints on Pathways Through the Canadian Arctic Archipelago. *Atmosphere-Ocean*, 50(3), 373-385.
Doi:10.1080/07055900.2012.704348
- Williams, G. (2009). Arctic Labyrinth : the Quest for the Northwest Passage. Toronto: Viking Canada.
- Yang, Q., Dixon, T. H., Myers, P. G., Bonin, J., Chambers, D., Van, D. B., . . . Mortensen, J. (2016). Recent Increases in Arctic Freshwater Flux Affects Labrador Sea Convection and

Atlantic Overturning Circulation. *Nature Communications*, 7(1), 10525. Doi:10.1038/
Ncomms10525

Chapter 6

Summary and Conclusion

In this thesis, I studied the role of oceanic advection in the long-term fate and transport pathways of pollutant spilt along shipping routes in the Canadian Arctic. The study region was divided into two parts and individually written in Chapter 4 and 5, focusing on the Hudson Bay Complex and Canadian Arctic Archipelago, respectively.

I used a high-resolution numerical model, NEMO, at its regional configuration, ANHA12, providing a resolution of 1/12 degree, with the highest resolution is less than 2 km in the Canadian Arctic. This model configuration has been used and proven to be capable of representing the ocean and sea ice dynamics in the study area by many published research (*e.g.* Feucher *et al.* (2019), Grivault *et al.*, (2018), Hu *et al.* (2018); Hu *et al.* (2019), Pennelly *et al.* (2018), Ridenour *et al.* (2019-a), and Ridenour *et al.* (2019-b)). I used a Lagrangian particle tracking tool, ARIANE, to calculate the circulation pathways of pollutant with oceanic advection. There are 35 release sites in total, distributed along the two shipping routes in the Canadian Arctic: the Northwest Passages and Arctic Bridge. At each site, I have a primary initial area of 5 km by 5 km, representing the state of pollutant infested water days after release. Furthermore, I have additional release sites with an initial area of 10 km by 10 km to represent a different type of pollutant and with different distance to shore to represent an alternative route on the open ocean. There were 5,000 virtual particles released at each site, and simulations were repeated every 10 days during the projected extent operating season (June 1st to October 30th) for 12 years (2004 to 2015).

Simulation outputs were examined in two steps. Firstly, I plotted the propagation of particles during two years of integration to determine their circulation pathways with a time scale. I found three main circulation pathways: (1) released in the Canadian Beaufort Sea, the majority of particles propagated westward with the outer bound of the anti-cyclonic Beaufort Gyre, and then joined Transpolar Drift within one year after release; (2) particles released in the CAA mainly followed the eastward outflow, with the majority entered the Baffin Bay in 2 to 14 months after released (when released in Lancaster Sound and western M'Clure Strait, respectively); (3) Baffin Bay releases circumnavigated the Baffin Bay, and then / or directly joined the southward Labrador Current; (4) particles released in eastern Hudson Strait directly joined Labrador Current, then spread into the North Atlantic Ocean in 2 to 4 month after release; (5) released in western Hudson Strait, whilst some particles followed the eastward outflow and joined Labrador Current in 4 to 6 months, others entered Foxe Basin and Hudson Bay; and (6) released in Foxe Basin and Hudson Bay, the majority of particles followed the cyclonic circulation within these waterbodies.

Secondly, I conducted numerical analysis calculating the horizontal spreading area, distances travelled, percentage of particles with depth over 90 metres, uncertainty and variability. I was able to determine when and over which region, the spill of the pollutant would have the most severe consequences:

- 1) When released from eastern Hudson Strait, the majority of particles propagated southward with the Labrador Current at a high speed, then broadly spread into the North Atlantic Ocean. Particles released from eastern Hudson Strait resulted in the largest spreading area and percentage in the deep spread, as well as a high level of variability and uncertainty. Eastern Hudson Strait simulations also exhibited significant inter-annual and annual variability. I found that the spread of particles was largest for those released in June, then decreased towards October. The annual variability is linked with the strength of the NAO, with strong negative NAO promotes a larger spreading area.

- 2) Released in the Baffin Bay, some particles circumnavigated the Baffin Bay before joining the Labrador Current. Therefore, its spreading area and deep spread percentage are smaller compared to the eastern Hudson Strait releases.
- 3) The majority of particles released in the Canadian Beaufort Sea immediately joined the anti-cyclonic Beaufort Gyre, resulting in a large spreading area with a significantly high level of uncertainty. Its high level of uncertainty and variability is linked to the strength of the AO. During an AO-, the enhancement of the BG promotes a larger spreading area.

Although some limitations arise with the passive representation of pollutant, this thesis highlights the role of oceanic advection in the spreading of pollutant in the Canadian Arctic. It provides an oceanographic overview to the accidental spills along the Northwest Passages and Arctic Bridge, and illuminates the need for more focused case studies in future.

References

- Feucher, C., Garcia-Quintana, Y., Yashayaev, I., Hu, X., & Myers, P. G. (2019). Labrador Sea Water Formation Rate and its Impact on the Local Meridional Overturning Circulation. *Journal of Geophysical Research: Oceans*, 124(8), 5654-5670. Doi:10.1029/2019JC015065
- Grivault, N., Hu, X., & Myers, P. G. (2018). Impact of the Surface Stress on the Volume and Freshwater Transport Through the Canadian Arctic Archipelago From a High-Resolution Numerical Simulation. *Journal of Geophysical Research: Oceans*, 123(12), 9038-9060. Doi:10.1029/2018JC013984
- Hu, X., Sun, J., Chan, T. O., & Myers, P. G. (2018). Thermodynamic and Dynamic Ice Thickness Contributions in the Canadian Arctic Archipelago in NEMO-LIM2 Numerical Simulations. *The Cryosphere*, 12(4), 1233-1247. Doi:10.5194/Tc-12-1233-2018
- Hu, X., Myers, P. G., & Lu, Y. (2019). Pacific Water Pathway in the Arctic Ocean and Beaufort Gyre in Two Simulations With Different Horizontal Resolutions. *Journal of Geophysical Research: Oceans*, 124(8), 6414-6432. Doi:10.1029/2019JC015111
- Pennelly, C., Hu, X., & Myers, P. G. (2019). Cross-Isobath Freshwater Exchange Within the North Atlantic Subpolar Gyre. *Journal of Geophysical Research: Oceans*, 124(10), 6831-6853. Doi:10.1029/2019JC015144
- Ridenour, N. A., Hu, X., Jafarikhasragh, S., Landy, J. C., Lukovich, J. V., Stadnyk, T. A., . . . Barber, D. G. (2019). *Sensitivity of Freshwater Dynamics to Ocean Model Resolution and River Discharge Forcing in the Hudson Bay Complex* Doi:https://doi.org/10.1016/J.Jmarsys.2019.04.002
- Ridenour, N. A., Hu, X., Sydor, K., Myers, P. G., & Barber, D. G. (2019). Revisiting the Circulation of Hudson Bay: Evidence for a Seasonal Pattern. *Geophysical Research Letters*, 46(7), 3891-3899. Doi:10.1029/2019GL082344

Bibliography

- Aagaard, K., & Carmack, E. C. (1989). The role of sea ice and other fresh water in the arctic circulation. *Journal of Geophysical Research: Oceans*, 94, 14485-14498. doi:10.1029/JC094iC10p14485
- Afenyo, M., Veitch, B., & Khan, F. (2016). A state-of-the-art review of fate and transport of oil spills in open and ice-covered water. *Ocean Engineering*, 119, 233-248. doi:10.1016/j.oceaneng.2015.10.014
- Aksenov, Y., Bacon, S., Coward, A. C., & Holliday, N. P. (2010). Polar outflow from the arctic ocean: A high resolution model study doi://doi.org/10.1016/j.jmarsys.2010.06.007
- Amante, C., & Eakins, B. W. (2009). ETOPO1 global relief model converted to PanMap layer format. Retrieved from <https://doi.org/10.1594/PANGAEA.769615>
- Andrews, J., Babb, D., & Barber, D. G. (2018). Climate change and sea ice: Shipping in hudson bay, hudson strait, and foxe basin (1980–2016). *Elem Sci Anth*, 6(1), 19. doi:10.1525/elementa.281
- Bamber, J., van, d. B., Ettema, J., Lenaerts, J., & Rignot, E. (2012). Recent large increases in freshwater fluxes from greenland into the north atlantic. *Geophysical Research Letters*, 39(19) doi:10.1029/2012GL052552
- Baumert, H., Simpson, J., Sundermann, J., 2005. *Marine turbulence: Theories, Observations, and Models*. Cambridge University Press, New York.
- Blanke, B. & Grima, N. (2008) Tutorial: first steps with ARIANE, sequential version.
- Blanke, B., & Raynaud, S. (1997). Kinematics of the pacific equatorial undercurrent: An eulerian and lagrangian approach from GCM results. *Journal of Physical Oceanography*, 27(6), 1038-1053. doi:10.1175/1520-0485(1997)027<1038:KOTPEU>2.0.CO;2

- Blanke, B., & Raynaud, S. (1997). Kinematics of the pacific equatorial undercurrent: An eulerian and lagrangian approach from GCM results. *Journal of Physical Oceanography*, 27(6), 1038-1053. doi:10.1175/1520-0485(1997)027<1038:KOTPEU>2.0.CO;2
- Blanke, B., & Raynaud, S. (1997). Kinematics of the pacific equatorial undercurrent: An eulerian and lagrangian approach from GCM results. *Journal of Physical Oceanography*, 27(6), 1038-1053. doi:KOTPEU>2.0.CO;2
- Brigham, L. W., Ellis, B., Arctic Council, & Arctic Council Protection of the Arctic Marine Environment Working Group. (2009). Arctic marine shipping assessment 2009 report. Akureyri, Iceland: Arctic Council, PAME, Protection of the Arctic Marine Environment.
- Brigham, L. W., Ellis, B., Arctic Council, & Arctic Council Protection of the Arctic Marine Environment Working Group. (2009). Arctic marine shipping assessment 2009 report. Akureyri, Iceland: Arctic Council, PAME, Protection of the Arctic Marine Environment.
- Buist, I., Belore, R., Dickins, D., Hackenberg, D., Guarino, A., & Wang, Z. (2009). Empirical weathering properties of oil in ice and snow. Paper presented at the Proceedings Arctic and Marine Oilspill Program Technical Seminar, , 32 67-107.
- Carmack, E. C., & MacDonald, R. W. (2002). Oceanography of the canadian shelf of the beaufort sea: A setting for marine life. *Arctic*, 55(2), S29.
- Castro de, I. G., Hu, X., & Myers, P. G. (2015). Potential positive feedback between greenland ice sheet melt and baffin bay heat content on the west greenland shelf. *Geophysical Research Letters*, 42(12), 4922-4930. doi:10.1002/2015GL064626
- Comiso, J. C. (2012). Large decadal decline of the arctic multiyear ice cover. *Journal of Climate*, 25(4), 1176-1193. doi:10.1175/JCLI-D-11-00113.1
- Courtois, P., Hu, X., Pennelly, C., Spence, P., & Myers, P. G. (2017). Mixed layer depth calculation in deep convection regions in ocean numerical models doi:<https://doi.org/10.1016/j.ocemod.2017.10.007>

- Curry, B., Lee, C. M., & Petrie, B. (2011). Volume, freshwater, and heat fluxes through davis strait, 2004–05. *Journal of Physical Oceanography*, 41(3), 429-436. doi:10.1175/2010JPO4536.1
- Dai, A., Qian, T., Trenberth, K. E., & Milliman, J. D. (2009). Changes in continental freshwater discharge from 1948 to 2004. *Journal of Climate*, 22(10), 2773-2792. doi:10.1175/2008JCLI2592.1
- Dawson, J., Pizzolato, L., Howell, S. E. L., Copland, L., & Johnston, M. E. (2018). Temporal and spatial patterns of ship traffic in the canadian arctic from 1990 to 2015. *Arctic*, 71(1), 15-26. doi:10.14430/arctic4698
- DeCola, Robertson, Fletcher, Susan Harvey, 2006. Offshore Oil Spill Response in Dynamic Ice Conditions: A Report to WWF on Considerations for the Sakhalin II Project. Nuka Research and Planning Group.
- Defossez, M., Saucier, F. J., Myers, P. G., Caya, D., & Dumais, J. -. (2012). Comparing winter and summer simulated estuarine circulations in foxe basin, canada. *Atmosphere-Ocean*, 50(3), 386-401. doi:10.1080/07055900.2012.693256
- DRAKKAR, Barnier, B., L., B., J., L. S., J.-M., M., T., P., S., T., M., T. A., G., M., A., B., C., B., J., D., S., G., R., B. B., J., C., G., G., S., A., A., C., de Cuevas B., A., N., K., H., G., S., S., D., W., H., C., S. & P., M. 2007 Eddypermitting ocean circulation hindcasts of past decades. *CLIVAR Exchanges* 12 (3), 8–10.
- Drozdowski, A., Nudds, S., Hannah, C. G., Niu, H., Peterson, I., & Perrie, W. (2011). Review of oil spill trajectory modelling in the presence of ice. Canada
- Dukhovskoy, D. S., Myers, P. G., Platov, G., Timmermans, M., Curry, B., Proshutinsky, A., . . . Somavilla, R. (2016). Greenland freshwater pathways in the sub-arctic seas from model experiments with passive tracers. *Journal of Geophysical Research: Oceans*, 121(1), 877-907. doi:10.1002/2015JC011290
- Feucher, C., Garcia-Quintana, Y., Yashayaev, I., Hu, X., & Myers, P. G. (2019). Labrador sea water formation rate and its impact on the local meridional overturning

- circulation. *Journal of Geophysical Research: Oceans*, 124(8), 5654-5670. doi:10.1029/2019JC015065
- Fichefet, T., & Maqueda, M. A. M. (1997). Sensitivity of a global sea ice model to the treatment of ice thermodynamics and dynamics. *Journal of Geophysical Research: Oceans*, 102, 12609-12646. doi:10.1029/97JC00480
- Fissel, D. B., De, M., Álvarez, S., Kulan, N., Mudge, T., & Marko, J. R. (2011). Long-term trends for sea ice in the western arctic ocean: Implications for shipping and offshore oil and gas activities
- Fratantoni, P. S., & McCartney, M. S. (2010). Freshwater export from the labrador current to the north atlantic current at the tail of the grand banks of newfoundland doi:<https://doi.org/10.1016/j.dsr.2009.11.006>
- Garcia-Quintana, Y., Courtois, P., Hu, X., Pennelly, C., Kieke, D., & Myers, P. G. (2019). Sensitivity of labrador sea water formation to changes in model resolution, atmospheric forcing, and freshwater input. *Journal of Geophysical Research: Oceans*, 124(3), 2126-2152. doi:10.1029/2018JC014459
- Gillard, L. C., Hu, X., Myers, P. G., & Bamber, J. L. (2016). Meltwater pathways from marine terminating glaciers of the greenland ice sheet. *Geophysical Research Letters*, 43(20), 10,873-10,882. doi:10.1002/2016GL070969
- Grivault, N., Hu, X., & Myers, P. G. (2018). Impact of the surface stress on the volume and freshwater transport through the canadian arctic archipelago from a high-resolution numerical simulation. *Journal of Geophysical Research: Oceans*, 123(12), 9038-9060. doi:10.1029/2018JC013984
- Guy, E., & Lasserre, F. (2016). Commercial shipping in the arctic: New perspectives, challenges and regulations. *Polar Record*, 52(3), 294-304. doi:10.1017/S0032247415001011
- Haas, C., & Howell, S. E. L. (2015). Ice thickness in the northwest passage. *Geophysical Research Letters*, 42(18), 7673-7680. doi:10.1002/2015GL065704

- Howell, S. E. L., Tivy, A., Yackel, J. J., & McCourt, S. (2008). Multi-year sea-ice conditions in the western canadian arctic archipelago region of the northwest passage: 1968-2006. *Atmosphere-Ocean*, 46(2), 229-242. doi:10.3137/ao.460203
- Howell, S. E. L., Wohlleben, T., Dabboor, M., Derksen, C., Komarov, A., & Pizzolato, L. (2013). Recent changes in the exchange of sea ice between the arctic ocean and the canadian arctic archipelago. *Journal of Geophysical Research: Oceans*, 118(7), 3595-3607. doi:10.1002/jgrc.20265
- Hu, X., Myers, P. G., & Lu, Y. (2019). Pacific water pathway in the arctic ocean and beaufort gyre in two simulations with different horizontal resolutions. *Journal of Geophysical Research: Oceans*, 124(8), 6414-6432. doi:10.1029/2019JC015111
- Hu, X., Sun, J., Chan, T. O., & Myers, P. G. (2018). Thermodynamic and dynamic ice thickness contributions in the canadian arctic archipelago in NEMO-LIM2 numerical simulations. *The Cryosphere*, 12(4), 1233-1247. doi:10.5194/tc-12-1233-2018
- Hughes, K. G., Klymak, J. M., Hu, X., & Myers, P. G. (2017). Water mass modification and mixing rates in a 1/12° simulation of the canadian arctic archipelago. *Journal of Geophysical Research: Oceans*, 122(2), 803-820. doi:10.1002/2016JC012235
- Hurrell, J. W., Kushnir, Y., Ottersen, G., & Visbeck, M. (2003). The north atlantic oscillation: Climatic significance and environmental impact doi:10.1029/GM134
- Jahn, A., Tremblay, B., Mysak, L. A., & Newton, R. (2010). Effect of the large-scale atmospheric circulation on the variability of the arctic ocean freshwater export. *Climate Dynamics*, 34(2), 201-222. doi:10.1007/s00382-009-0558-z
- Jones, E. P., & Anderson, L. G. (1994). Northern hudson bay and foxe basin: Water masses, circulation and productivity. *Atmosphere-Ocean*, 32(2), 361-374. doi:10.1080/07055900.1994.9649502
- Karcher, M., Smith, J. N., Kauker, F., Gerdes, R., & Smethie Jr., W. M. (2012). Recent changes in arctic ocean circulation revealed by iodine-129 observations and modeling. *Journal of Geophysical Research: Oceans*, 117 doi:10.1029/2011JC007513

- Kelly, S., Popova, E., Aksenov, Y., Marsh, R., & Yool, A. (2018). Lagrangian modeling of arctic ocean circulation pathways: Impact of advection on spread of pollutants. *Journal of Geophysical Research: Oceans*, 123(4), 2882-2902. doi:10.1002/2017JC013460
- Kwok, R., Spreen, G., & Pang, S. (2013). Arctic sea ice circulation and drift speed: Decadal trends and ocean currents. *Journal of Geophysical Research: Oceans*, 118(5), 2408-2425. doi:10.1002/jgrc.20191
- Lackenbauer, W., Lajeunesse, A., Canadian Defence and Foreign Affairs Institute, & University of Calgary School of Public Policy. (2014). On uncertain ice: The future of arctic shipping and the northwest passage. Retrieved from <http://www.deslibris.ca/ID/245170>;
- Lazier, J. R. N., & Wright, D. G. (1993). Annual velocity variations in the labrador current. *Journal of Physical Oceanography*, 23(4), 659-678. doi:10.1175/1520-0485(1993)023<0659:AVVITL>2.0.CO;2
- Lu, Y., Higginson, S., Nudds, S., Prinsenber, S., & Garric, G. (2014). Model simulated volume fluxes through the canadian arctic archipelago and davis strait: Linking monthly variations to forcing in different seasons. *Journal of Geophysical Research: Oceans*, 119(3), 1927-1942. doi:10.1002/2013JC009408
- Madec Gurvan, Romain Bourdallé-Badie, Pierre-Antoine Bouttier, Clément Bricaud, Diego Bruciaferri, Daley Calvert, ... Martin Vancoppenolle. (2013, February 11). NEMO ocean engine (Version v3.4-patch). Notes Du Pôle De Modélisation De L'institut Pierre-simon Laplace (IPSL). Zenodo. <http://doi.org/10.5281/zenodo.1475234>
- Madec, G., & Imbard, M. (1996). A global ocean mesh to overcome the north pole singularity. *Climate Dynamics*, 12(6), 381-388. doi:10.1007/BF00211684
- McGarrity, J., & Gloystein, H. (2013, September 27). Big freighter traverses northwest passage for 1st time. Reuters Environment Retrieved from <https://www.reuters.com/article/us-shipping-coal-arctic/big-freighter-traverses-northwest-passage-for-1st-time-idUSBRE98Q0K720130927>

- Mercator Ocean (2017): Mercator Ocean GLORYS2V3 Reanalysis - Forcing dataset (for MARVL). Australian Ocean Data Network.dataset. <http://catalogue.aodn.org.au/geonetwork/srv/en/metadata.show?uuiid=55286d43-8d3c-40e3-a12f-3178a2f734ae>
- Mertz, G., Narayanan, S., & Helbig, J. (1993). The freshwater transport of the labrador current. *Atmosphere-Ocean*, 31(2), 281-295. doi:10.1080/07055900.1993.9649472
- Mills, W. J. (2003). *Exploring polar frontiers : A historical encyclopedia*. Santa Barbara, Calif.: Abc-Clio. Retrieved from <http://www.loc.gov/catdir/toc/ecip048/2003019362.html>
- Münchow, A., Falkner, K. K., & Melling, H. (2015). Baffin island and west greenland current systems in northern baffin bay doi:<https://doi.org/10.1016/j.pocean.2014.04.001>
- Murray, R. J. (1996). Explicit generation of orthogonal grids for ocean models doi://doi.org/10.1006/jcph.1996.0136
- Mussels, O., Dawson, J., & Howell, S. (2017). Navigating pressured ice: Risks and hazards for winter resource-based shipping in the canadian arctic. *Ocean and Coastal Management*, 137, 57-67. doi:10.1016/j.ocecoaman.2016.12.010
- Østreg, W., Eger, K. M., Fløistad, B., Jørgensen-Dahl, A., Lothe, L., Mejlnder-Larsen, M., . . . Wergeland, T. (2013). Shipping in arctic waters: A comparison of the northeast, northwest and trans polar passages doi:10.1007/978-3-642-16790-4
- Parkinson, C. L. (2014). Spatially mapped reductions in the length of the arctic sea ice season. *Geophysical Research Letters*, 41(12), 4316-4322. doi:10.1002/2014GL060434
- Pennelly, C., Hu, X., & Myers, P. G. (2019). Cross-isobath freshwater exchange within the north atlantic subpolar gyre. *Journal of Geophysical Research: Oceans*, 124(10), 6831-6853. doi:10.1029/2019JC015144
- Pizzolato, L., Howell, S. E. L., Dawson, J., Laliberté, F., & Copland, L. (2016). The influence of declining sea ice on shipping activity in the canadian arctic. *Geophysical Research Letters*, 43(23), 12-12,154. doi:10.1002/2016GL071489

- Popova, E. E., Yool, A., Aksenov, Y., & Coward, A. C. (2013). Role of advection in arctic ocean lower trophic dynamics: A modeling perspective. *Journal of Geophysical Research: Oceans*, 118(3), 1571-1586. doi:10.1002/jgrc.20126
- Prinsenber, S. J. (1986). In Martini I. P. (Ed.), Chapter 12 on the physical oceanography of foxe basin Elsevier. doi:[https://doi.org/10.1016/S0422-9894\(08\)70905-X](https://doi.org/10.1016/S0422-9894(08)70905-X)
- Prowse, T. D., Furgal, C., Chouinard, R., Melling, H., Milburn, D., & Smith, S. L. (2009). Implications of climate change for economic development in northern canada: Energy, resource, and transportation sectors. *Royal Swedish Academy of Sciences, 38(Ambio: Climate Impacts on Northern Canada)*, 272-281.
- Reed, M., Johansen, Ø, Brandvik, P. J., Daling, P., Lewis, A., Fiocco, R., . . . Prentki, R. (1999). Oil spill modeling towards the close of the 20th century: Overview of the state of the art doi:[https://doi.org/10.1016/S1353-2561\(98\)00029-2](https://doi.org/10.1016/S1353-2561(98)00029-2)
- Ridenour, N. A., Hu, X., Jafarikhasragh, S., Landy, J. C., Lukovich, J. V., Stadnyk, T. A., . . . Barber, D. G. (2019a). Sensitivity of freshwater dynamics to ocean model resolution and river discharge forcing in the hudson bay complex doi:<https://doi.org/10.1016/j.jmarsys.2019.04.002>
- Ridenour, N. A., Hu, X., Sydor, K., Myers, P. G., & Barber, D. G. (2019b). Revisiting the circulation of hudson bay: Evidence for a seasonal pattern. *Geophysical Research Letters*, 46(7), 3891-3899. doi:10.1029/2019GL082344
- Saucier, F., Senneville, S., Prinsenber, S., Roy, F., Smith, G., Gachon, P., . . . Laprise, R. (2004). Modelling the sea ice-ocean seasonal cycle in hudson bay, foxe basin and hudson strait, canada. *Climate Dynamics*, 23(3), 303-326. doi:10.1007/s00382-004-0445-6
- Serreze, M. C., & Barry, R. G. (2014). *The arctic climate system* (Second ed.). Cambridge: Cambridge University Press. Retrieved from <https://doi.org/10.1017/CBO9781139583817>

- Serreze, M. C., & Stroeve, J. (2015). Arctic sea ice trends, variability and implications for seasonal ice forecasting. *Philosophical Transactions of the Royal Society A: Mathematical, Physical and Engineering Sciences*, 373(2045), 20140159. doi:10.1098/rsta.2014.0159
- Shasby, Mark, and Smith, Durelle, 2015, USGS Arctic science strategy, 2015–2020: U.S. Geological Survey Fact Sheet 2015-3049, 2 p., <https://dx.doi.org/10.3133/fs20153049>.
- Smith, G. C., Roy, F., Mann, P., Dupont, F., Brasnett, B., Lemieux, J., . . . Bélair, S. (2014). A new atmospheric dataset for forcing ice–ocean models: Evaluation of reforecasts using the canadian global deterministic prediction system. *Quarterly Journal of the Royal Meteorological Society*, 140(680), 881-894. doi:10.1002/qj.2194
- Sørstrøm, S. E., Brandvik, P. J., Buist, I., Daling, P., Dickins, D., Faksness, L., . . . Singaas, I. (2010). Joint industry program on oil spill contingency for arctic and ice-covered waters : Summary report. (). Trondheim
- Stewart, E. J., Howell, S. E. L., Draper, D., Yackel, J., & Tivy, A. (2009). Sea ice in canada's arctic: Implications for cruise tourism. *Arctic*, 60(4) doi:10.14430/arctic194
- Straneo, F., & Saucier, F. (2008a). The outflow from hudson strait and its contribution to the labrador current doi:<https://doi.org/10.1016/j.dsr.2008.03.012>
- Straneo, F., & Saucier, F. J. (2008b). The Arctic–Subarctic exchange through hudson strait. In R. R. Dickson, J. Meincke & P. Rhines (Eds.), *Arctic–Subarctic ocean fluxes: Defining the role of the northern seas in climate* (pp. 249-261). Dordrecht: Springer Netherlands. doi:10.1007/978-1-4020-6774-7_11 Retrieved from https://doi.org/10.1007/978-1-4020-6774-7_11
- Stroeve, J., Holland, M. M., Meier, W., Scambos, T., & Serreze, M. (2007). Arctic sea ice decline: Faster than forecast. *Geophysical Research Letters*, 34(9)
- Stueck, W. (2013, September 19). Danish firm seeks to be first to bring bulk carrier through northwest passage. *The Globe and Mail* Retrieved from <https://>

www.theglobeandmail.com/report-on-business/international-business/european-business/bulk-carrier-capitalizes-on-arctic-shortcut/article14405743/

Stueck, W. (2013, September 19). Danish firm seeks to be first to bring bulk carrier through northwest passage. *The Globe and Mail* Retrieved from <https://www.theglobeandmail.com/report-on-business/international-business/european-business/bulk-carrier-capitalizes-on-arctic-shortcut/article14405743/>

Thompson, D. W. J., & Wallace, J. M. (1998). The arctic oscillation signature in the wintertime geopotential height and temperature fields. *Geophysical Research Letters*, 25(9), 1297-1300. doi:10.1029/98GL00950

Tivy, A., Alt, B., Howell, S., Wilson, K., & Yackel, J. (2007). Long-range prediction of the shipping season in hudson bay: A statistical approach. *Weather and Forecasting*, 22(5), 1063-1075. doi:10.1175/WAF1038.1

Tivy, A., Howell, S. E. L., Alt, B., McCourt, S., Chagnon, R., Crocker, G., . . . Yackel, J. J. (2011). Trends and variability in summer sea ice cover in the canadian arctic based on the canadian ice service digital archive, 1960–2008 and 1968–2008. *Journal of Geophysical Research: Oceans*, 116 doi:10.1029/2009JC005855

Transport Canada and Canadian Coast Guard. Assessment of proposals related to oil spill risk for the south coast of newfoundland

van Sebille, E., Griffies, S. M., Abernathey, R., Adams, T. P., Berloff, P., Biastoch, A., . . . Zika, J. D. (2018a). Lagrangian ocean analysis: Fundamentals and practices doi:<https://doi.org/10.1016/j.ocemod.2017.11.008>

Venkatesh, S., El-Tahan, H., Comfort, G., & Abdelnour, R. (1990). Modelling the behaviour of oil spills in ice-infested waters. *Atmosphere-Ocean*, 28(3), 303-329. doi:10.1080/07055900.1990.9649380

Wagner, P., Rührs, S., Schwarzkopf, F. U., Koszalka, I. M., & Biastoch, A. (2019). Can lagrangian tracking simulate tracer spreading in a high-resolution ocean general circulation

- model? *Journal of Physical Oceanography*, 49(5), 1141-1157. doi:10.1175/JPO-D-18-0152.1
- Wang, Q., Myers, P. G., Hu, X., & Bush, A. B. G. (2012). Flow constraints on pathways through the canadian arctic archipelago. *Atmosphere-Ocean*, 50(3), 373-385. doi:10.1080/07055900.2012.704348
- Williams, G. (2009). *Arctic labyrinth : The quest for the northwest passage*. Toronto: Viking Canada.
- Yang, J. (2009). Seasonal and interannual variability of downwelling in the beaufort sea. *Journal of Geophysical Research*, 114 doi:10.1029/2008JC005084
- Yang, Q., Dixon, T. H., Myers, P. G., Bonin, J., Chambers, D., van, d. B., . . . Mortensen, J. (2016). Recent increases in arctic freshwater flux affects labrador sea convection and atlantic overturning circulation. *Nature Communications*, 7(1), 10525. doi:10.1038/ncomms10525
- Yashayaev, I., & Greenan, B. (2010). Environmental conditions in the labrador sea in 2009.